THE UNIVERSITY *of* EDINBURGH

Post-glacial Fluvial Dynamics of the British Isles

Anya Heather Towers

Doctor of Philosophy

THE UNIVERSITY OF EDINBURGH

2024

Declaration

I declare that this thesis was composed by myself, that the work contained herein is my own except where explicitly stated otherwise in the text, and that this work has not been submitted for any other degree or professional qualification except as specified.

Anya Towers

November 2024

Abstract

Throughout the Quaternary, ice sheets and glaciers episodically expanded to cover up to 30 percent of the Earth's surface. Many of these areas are now ice-free due to climatic warming after approximately 14.5 ka. Rivers are the main erosional agents and drivers of landscape evolution in post-glacial landscapes; however, their response to past glaciations is notoriously complex. Key challenges associated with understanding fluvial processes in post-glacial landscapes originate from the glacial modification of hillslopes and channels, such as decoupling of hillslopes from channels due to the over-deepening and widening of valleys by glaciers, or extensive glacial sediment drapes (e.g., till, moraines, paraglacial terraces) which influence sediment supply and transport capacity. Additionally, Glacial Isostatic Adjustment (GIA) results in considerable spatial and temporal variations in relative sea-levels, which set the base-levels of rivers. Rivers communicate changes in base-level to the rest of the landscape by the upstream propagation of transient signals. Relatively little research has quantified geomorphic processes in post-glacial landscapes in post-orogenic regions. Much geomorphological research has focused on unglaciated landscapes and glaciated landscapes in tectonically active regions.

In the first part of this thesis, I explore the controls on erosion rates in the post-glacial Feshie basin, Scotland. Erosion rates are inferred from the concentration of *in-situ* cosmogenic radionuclides (CRN) measured in river sands. When erosion rates are calculated based on the common assumption of basin-wide homogeneity of erosion, I counter-intuitively find no correlation between erosion rates and topographic metrics (e.g. slope). To explain the concentrations, I suggest that sediment is sourced from both the 'background' hillslopes and paraglacial terraces. I test this hypothesis with a mixing model, which indicates that the observed distribution of CRN concentrations can be explained if terrace escarpments have cm-scale retreat rates during large flood events. These results highlight the on-going glacial legacy on landscape evolution.

In the second part of this thesis, I explore controls of fluvial grain sizes in Scotland. I document river surface grain sizes at 300 locations through a citizen science survey. I then investigate whether grain sizes can be correlated and predicted from environmental variables (e.g., basin slope, flow distance from headwaters) through Spearman's correlation statistics and random forest regression modelling. In contrast to other studies that have primarily focused on non-glaciated landscapes, we find no apparent controls on surface grain sizes in channels across Scotland. I suggest that Scotland's post-glacial legacy drives the lack of sedimentological trends, which aligns with the interpretations from the first research chapter.

In the third part of this thesis, I explore the response of rivers to base-level rise (which is largely driven by GIA) and coastal erosion in Southern England. Emerging research suggests that coastal erosion can initiate the formation of migrating knickpoints. Through topographic analysis, I find that some rivers have migrating knickpoints in Southern England. I then investigate the fluvial and coastal factors influencing these knickpoints at the regional scale, as outlined by previous research. I find a clear lithological control: channels underlain by more resistant rocks consistently incise at their outlets, compared to less resistant rocks, for a given drainage area ($<$ 25km^2). However, I find no drainage area or coastal erosion rate control.

Overall, this thesis contributes to the growing body of research quantifying landscape evolution in regions affected by glaciation. Importantly, I find that post-glacial landscapes in post-orogenic terrains are largely influenced by the glacial legacy more than 10 ka after deglaciation. Moreover, I find that past glaciations influence river processes in regions that have not been glaciated through base-level rise from GIA.

Lay Summary

This thesis explores how landscapes across the British Isles have evolved since the Last Glaciation, which ended 12,000 years ago. During glacial cycles, ice reshaped topography by removing and depositing material. After the ice (i.e., the Holocene epoch), rivers cut into bedrock and transported material from mountain ranges to seas. Due to ongoing Glacial Isostatic Adjustment, land in Scotland has been uplifting, while in Southern England, land has been subsiding. In the British Isles, relatively little is known about the response of rivers to past glaciations.

First, I study the sources and transport of modern river sands in the Scottish mountain ranges. Understanding how rivers move and carry sediment is essential and useful for solving problems in ecology and river management. Using geochemical tracing methods, I find that sands in rivers are sourced from bedrock and glacial deposits. This indicates that glaciers have a long-lasting impact on sediment supply in formerly glaciated regions. Next, I explore controls on the size of sediments in Scottish rivers. Sediment grain sizes provide information on sediment sources and influence river transport conditions. In contrast to other studies that have primarily focused on landscapes with little past or present glacial influence, I find no apparent controls on grain size in Scotland. I suggest that Scotland's post-legacy drives the lack of geomorphic trends. Finally, I investigate the response of rivers to coastal erosion and sea level rise (i.e., land subsidence) in Southern England. I find that some rivers become more erosive as they flow towards the coast, which has implications for landscape evolution over geological timescales. Overall, the findings from this thesis highlight the long-lasting impact of the glacial legacy on landscape processes, with implications for sediment transport, erosion, and the evolution of landscapes.

Acknowledgements

Wow, what a journey—30,000 pebbles measured, and I have submitted!

First, thank you to my supervisors, Simon Mudd and Mikael Attal, for their enthusiasm, support, and feedback throughout the PhD. It has been such a rewarding learning experience! Thank you also to Fiona Clubb for your valuable contributions and for all the fun field trips, both in Scotland and Nepal. Thank you to Hugh Sinclair for encouraging me to do a PhD and for being such a friendly and approachable character. Thanks to Andy Dugmore, Andy Hein, and Anthony Newton for the many Drummond hallway chats, teaching experiences, and general geomorphic enthusiasm. A special thank you to Roberto Martinez and the geomorphic team from SEPA for their support throughout my PhD. Thank you to NERC and SEPA for funding my research.

A huge thank you to the Drummond PhD community for the friendship throughout my PhD years. Morag, thank you for the constant chatter, cups of tea, cake supply, and for simply being the best! Nick, a special thanks for being such a great field trip buddy (I hope Hugh cooks you a 'veggie' risotto without chicken one day!). Thank you to Marina for the many coffee breaks, writing/hillwalking holidays, and free shoes. Thank you to everyone else (I apologise for all the sand and snowsuits that I filled the office with!): Polly, Louis, Ashrika, Prakash, Bronwyn, Saraswati, Leam, Ryan, Harry, Clara, Eliana, Anthony, Carla, Hannah, and Qiuyang.

Thank you also to my non-geoscience friends, family, and Eliot for the love and support. Eliot, thank you so much for your endless enthusiasm, positivity, scientific discussions, adventures and for helping me get through the tough times.

Contents

Figures and Tables

Figures

Tables

Chapter 1

Introduction

1.1 Overview

Variations in the Earth's climate have driven cyclic global glaciations (Lisiecki and Raymo, 2005). Throughout the Quaternary, ice sheets and glaciers episodically expanded to cover up to 30 percent of the Earth's surface (Ehlers et al., 2018). Many of these areas are now ice-free due to climatic warming after 14.5 ka (e.g., Ehlers et al., 2018; Lisiecki and Raymo, 2005). Such areas represent a significant fraction of global land (e.g., most of the UK, Scandinavia, North America) and their extent will inevitably grow as a result of glacial retreat driven by climate change.

Rivers are the main archives of change in post-glacial landscapes. Rivers drive landscape evolution by setting the base level for hillslope processes through incision into bedrock, and by transporting material from its source region (e.g. mountain ranges) to sedimentary sinks (Attal et al., 2015; Howard and Kerby, 1983; Sklar and Dietrich, 2006; Whipple, 2002; Whittaker, 2012). Rivers communicate variations in external drivers of landscape change, such as climate, sea-level and tectonics, to the rest of the landscape by the upstream propagation of transient signals. These transient signals are referred to as knickpoints (or knickzones) and are marked by a change in the steepness of channel profiles (Stock and Montgomery, 1999; Whipple and Tucker, 1999).

The fluvial response to past glaciations is notoriously complex. Key challenges associated with understanding geomorphic processes in post-glacial landscapes include the decoupling of hillslopes from channels due to the over-deepening and widening of valleys by glaciers, and extensive glacial and paraglacial sediment drapes (e.g., till, moraines, terraces) acting as sediment stores along rivers (Ballantyne, 2019;

Whitbread et al., 2015). A key area of research is therefore understanding the long-term adjustment of post-glacial landscapes. However, relatively little work has focused on understanding post-glacial landscape processes in tectonically quiescent regions due to their complexity. A significant portion of geomorphological research has concentrated on unglaciated landscapes in active tectonic margins. Emerging research suggests that post-glacial landscapes in post-orogenic terrains are largely influenced by the glacial legacy more than 10 ka after deglaciation (e.g., Ballantyne, 2002; Church and Ryder, 1972; Johnson et al., 2022; Mason and Polvi, 2023; Reid et al., 2022). For example, by quantifying valley shape, Prasicek et al. (2015) found that, in contrast to rapidly uplifting regions such as Taiwan, where glacially modified topography is rapidly replaced by fluvial topography, the glacial imprint lasts for millions of years in tectonically quiescent regions. These preliminary studies therefore indicate that underlying geomorphic principles are ill-equipped for understanding post-glacial landscapes.

The British Isles have been in a phase of glacial isostatic adjustment since the disappearance of the British-Irish Ice Sheet and complete deglaciation following the Loch Lomond Stadial/Younger Dryas around 12 ka ago (Ballantyne, 2019; Clark et al., 2018; Firth and Stewart, 2000; Shennan et al., 2009). Relative sea-levels have largely been falling in Scotland, and rising in Southern England. Studies have shown that base-level fall has driven the formation of retreating bedrock knickpoints in Scotland (Castillo et al., 2013; Jansen et al., 2011). These knickpoints are clustered around Scotland's coastlines, implying that the fluvial response to high uplift rates has not yet been transmitted to the central Scottish mountain ranges. The extent and timescales of the post-glacial legacy remain poorly quantified in Scotland and relatively little is known about the rates and controls on denudation and sediment budgets. Understanding the delivery of sediments through river basins is important because sediments influences river morphology, hazards (e.g., flood risk), habitat value (e.g., spawning of salmonids) and landscape response to climatic and tectonic forcings (Attal and Lavé, 2006; Finnegan et al., 2017; Sklar and Dietrich, 2006; Thapa et al., 2024).

Studies have shown that knickpoints are generated in regions where relative base-levels are rising, or where there is no relative base-level change (Limber and Barnard, 2018; Snyder et al., 2002). In coastal settings, waves that cut into the channel bed at the river mouth can lead to the initiation of a hanging waterfall (i.e. a knickpoint) that discharges directly into the ocean. Channel incision then erodes the landscape vertically and can translate the knickpoint upstream. In Southern England, where sea-levels have been rising throughout the Holocene, relatively little is known about the response of rivers to coastal erosion (Shadrick et al., 2022; Shennan et al., 2000). This research is important because it explores the relationships between coastal erosion and fluvial processes.

In the first part of this thesis (Chapter 2), I explore the controls on erosion rates in the Feshie basin, which is located in post-glacial Cairngorm Mountains. I measure the concentration of detrital cosmogenic radionuclides (CRN) in stream sediments, which, in recent decades, have been widely used to quantify catchment average denudation rates over millennial timescales (e.g. Bierman, 1994; Brown et al., 1995; Granger et al., 1996; von Blanckenburg, 2005). Rates derived from CRNs typically reflect the weathering, erosion and fluvial transport of hillslope sediments which have been linked to climatic and/or tectonic controls in active orogenic settings (e.g. Bookhagen and Strecker, 2012; Godard et al., 2014; Safran et al., 2005; Scherler et al., 2014). To understand these wider controls of climate and/or tectonics on landscape evolution, studies have correlated CRN-derived erosion rates to upstream catchment characteristics, such as channel steepness and uplift rates (e.g. Cyr et al., 2010; Delunel et al., 2020,1; Harel et al., 2016; Wittmann et al., 2007). In the first research chapter, I test two hypotheses. The first hypothesis is that apparent erosion rates positively correlate with topographic metrics, such as channel steepness, and uplift rates to the first order in the Feshie basin. The second hypothesis is that CRN concentrations represent a mix of 'background' hillslope sediment and paraglacial terrace sediment. I consider these two scenarios as end-member hypotheses: one in which rivers have incised through the glacial drape and adjusted to regional uplift rates, and the other where sediment is recycled from paraglacial deposits with little modification of the underlying bedrock.

In the second research chapter (Chapter 3), I will continue to investigate the controls on sediment characteristics in post-glacial landscapes. Here, I will document and explore the controls on fluvial surface grain sizes across Scotland. Grain sizes are a key characteristic for understanding fluvial environments. For example, grain sizes influence river transport conditions, provide information on sediment sources, control rates of bedrock incision (e.g., Sklar and Dietrich, 2004) and the width of channels (e.g. Baynes et al., 2020; Finnegan et al., 2005; Li et al., 2020a). The grain sizes of sediments in channels have been linked to landscape characteristics, such as flow distance from headwaters, topographic relief, lithology and climate, in landscapes with little past or present glacial influence. Few studies have explored the controls on sediment characteristics in formerly glaciated landscapes. In this chapter, I will document river surface grain sizes across Scotland through a citizen science survey. I will then investigate whether grain sizes can be correlated and predicted from environmental variables, that have been suggested to control grain sizes in landscape with little past or present glacial influence.

In the third part of this thesis, I explore the response of rivers to base-level rise (which is largely driven by GIA) and coastal erosion in Southern England. Emerging research has shown that coastal erosion can initiate the formation of migrating knickpoints (e.g., Limber and Barnard, 2018; Mackey et al., 2014; Snyder et al., 2002). Waves that cut into the channel bed at the river mouth can lead to the initiation of a hanging waterfall that discharges directly into the ocean (Emery and Kuhn, 1982; Mackey et al., 2014; Snyder et al., 2002; Wolinsky and Murray, 2009). Rivers can then translate these waterfalls upstream as migrating knickpoints. Through topographic analysis, I test if channels in Southern England incise at their outlets. I then explore the controls on knickzones, such as drainage area, lithology and coastal erosion rates.

Below I present the overarching research questions which this thesis will aim to address:

1. What controls sediment characteristics in post-glacial and post-orogenic regions such as Scotland ?
    (a) What controls denudation rates and CRN concentrations in Scottish mountain ranges ?
    (b) What controls the grain size of river sediments in Scotland ?

2. How do rivers respond to coastal erosion and sea-level rise in Southern England ?

Below, I present a broad introduction to each of these topics and outline the scope of the central chapters of this thesis.

1.2 Theoretical Background

1.2.1 Pleistocene glaciations

The Quaternary Period comprises the Pleistocene Epoch (2.59 Ma to 11.7 ka) and the Holocene Epoch (11.7 ka to the present, (Lisiecki and Raymo, 2005)). The Quaternary was characterised by extreme climatic shifts. These caused the alternation between glacial stages, when much of the UK experienced climates of arctic severity, and interglacial stages, when warmer and more temperate conditions prevailed (Ballantyne et al., 2021). During these glacial cycles, most of the UK was covered in ice except much of the land south of the River Thames in southern England (Figure 1.1).

Whilst the main topographic features of the UK were established before the Quaternary, such as the spatial organisation of drainage basins, successive glacial cycles modified the landscape through erosion and deposition (Linton, 1949). Glacial erosion is largely controlled by the basal thermal regime, which influences the rates of both abrasion and plucking (e.g., Hallet, 1979; Hallet et al., 1996; Herman et al., 2021). A glacier is classified as cold-based, in which the basal ice is frozen to the bed, or warm-based, in which the basal ice is at the pressure melting point, or polythermal. It is typically assumed that glacial erosion occurs exclusively below warm-based glaciers: basal sliding is limited under cold-based glaciers because ice is largely frozen to the bed, whereas warm-based glaciers can actively slide along the bed, and thus erode via abrasion and plucking (Benn and Evans, 2014; Hallet, 1979; Hallet et al., 1996). Erosion by warm-based glaciers is far more efficient than fluvial erosion and can significantly outpace rock uplift rates, creating "U" shaped valleys which have steep sides and wide valley floors (Figure 1.1). Widespread glaciogenic deposits (e.g., moraines, till) form following the removal and re-distribution of rock mass by ice.

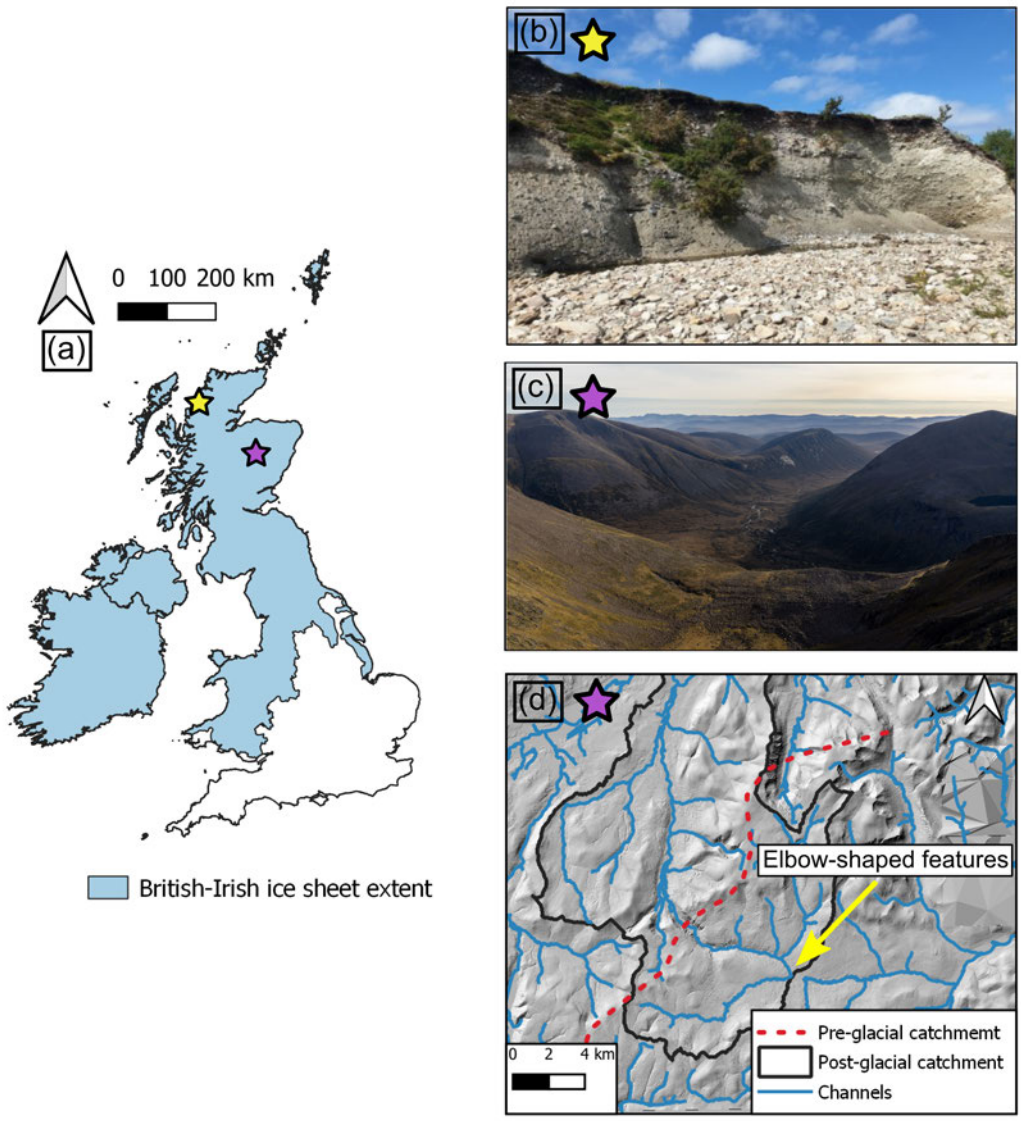

Figure 1.1: (a) Map of the maximum land ice extent during the Last British-Irish Ice Sheet. Ice extent shapefiles were sourced from Clark et al. (2018). **(b-c)** Photographs of post-glacial geomorphic landforms, such as glaciogenic deposits (photograph **b**; River Strathain, North-west Highlands) and U-shaped valleys (photograph **c**; Lairig Ghru, Cairngorm Mountains, sourced from Ryan Ing). Scarp in **(b)** is approximately 10 m high. **(d)** Example of glacially-modified drainage networks. Map is of the western Cairngorms with modern channel network marked in blue. The pre-glacial (as hypothesised by Linton (1949)) and post-glacial drainage basin of the Feshie river is marked in red and black, respectively. Many rivers exhibit anomalous, elbow-shaped features which are indicative of glacially-modified topography. The stars marked on **(b-d)** correspond to the location of the stars on **(a)**. River network was sourced from the Ordnance Survey (2021).

1.2.2 Glacial isostatic adjustment and Holocene sea level change

The growth and retreat of ice sheets throughout the Quaternary raised and lowered sea levels (Chappell et al., 1996; Lea et al., 2002; Spratt and Lisiecki, 2016). Vertical land motion, which is primarily driven by glacial isostatic adjustment (GIA) and eustatic sea-level change, has resulted in considerable spatial and temporal variations in the relative sea-level (RSL) change rate of the British Isles. GIA is defined as the visco-elastic reaction of the solid Earth to the glaciation and deglaciation of its surface (Stockamp et al., 2016). Figure 1.2 shows a reconstruction of present-day rates of RSL change and vertical land motion by Bradley et al. (2023). Present-day RSLs are generally falling in Scotland and rising in Southern England. Rates of RSL change peaked during deglaciation, with base-level fall rates of up to 30 mm/yr in the western Highlands (Shennan et al., 2000).

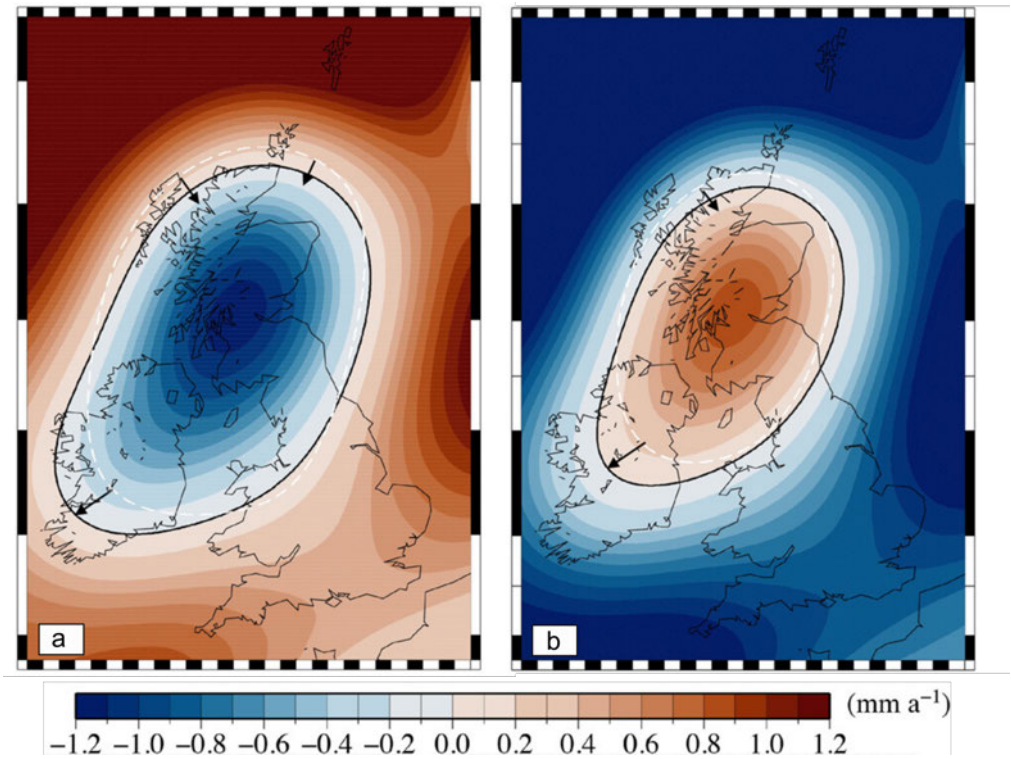

Figure 1.2: Illustration of the present-day rates (mm/yr) of RSL change (a) and vertical land motion (b). These reconstructions are taken directly from Bradley et al. (2023). The black line marks the zero-contour line.

1.2.3 Post-glacial landscapes

The withdrawal of glacier ice exposes landscapes that are unstable and consequently liable to rapid and extensive environmental change. In their seminal paper, Church and Ryder (1972) defined such systems as paraglacial, which describes "nonglacial processes that are directly conditioned by glaciation". A core theme of the paraglacial concept is the overall long-term decline in sediment fluxes. Ballantyne (2002) presented this idea as a conceptual sediment exhaustion curve, whereby sediment flux is related to the amount of remaining 'available' sediment by a negative exponential function (Figure 1.3). Ballantyne (2002) further classified paraglacial landscapes as 'primary' or 'secondary' depending on whether sediments are sourced from in-situ glacigenic sediment (e.g., slope failure from deglacial stress release), and/or the reworking of paraglacial sediment stores from further upstream, respectively. The reworking of sediment can result in 'waves' of sediment travelling through basins, creating a more complex sediment exhaustion curve with secondary peaks. Similarly, extrinsic drivers (e.g., extreme precipitation) of sediment release and incision will result in episodic sediment yields (Figure 1.3).

The post-glacial response is largely governed by climate, tectonics and topography before, during and after glaciation (Adams and Ehlers, 2018). Following the recent development of quantitative geomorphic tools (e.g., CRN erosion rates, DEMs), studies have tested the conceptual post-glacial landscape evolution processes discussed above. Studies have shown that fluvial systems in post-orogenic regions can be dominated by post-glacial processes > 10 ka after glaciation. For example, Reid et al. (2022) showed that glacial landscape configuration influences channel response to flooding in the Guichon basin, British Columbia, Canada, approximately 10 ka years after glaciation. Through analysis of aerial and satellite imagery, they demonstrated that channel planform instability was significantly higher downstream of reaches that received large volumes of sediment from glaciofluvial terraces. This contrasted to reaches that did not receive material from glaciofluvial terraces where no major changes in channel widths were observed. Mason and Polvi (2023) also suggested that the Pleistocene glacial legacy dominated present-day geomorphic processes in their study area in Fennoscandia, northern Sweden. Unlike non-glacial landscapes, they found that rivers showed very little self-organisation at the reach-scale. Specifically, no associations were found between channel width, slope and sediment grain size. For example, boulders were rarely clustered into bedforms, such as step-pool sequences,

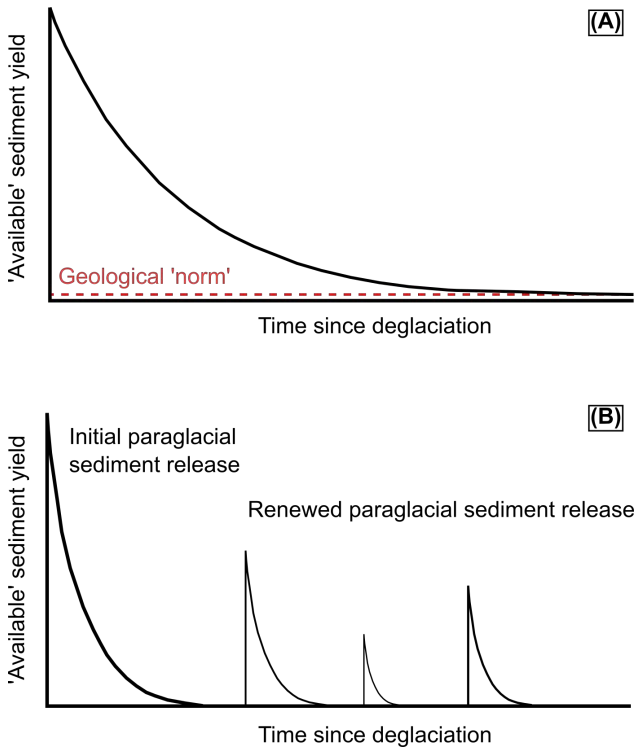

Figure 1.3: (A) shows a schematic diagram of the simple paraglacial sediment exhaustion model, modified from Ballantyne (2002). Sediment yields are shown to decline towards a conceptual 'geological norm', which is assumed to represent steady-state pre-glacial conditions. (B) shows paraglacial sediment release as a function of external perturbations, such as extreme rainfall, which triggers pulses of renewed sediment release.

which are typical of boulder-bed mountain rivers in non-glaciated landscapes (e.g., Church and Zimmermann, 2007; Montgomery and Buffington, 1997). By estimating the volume of sediment stored in catchments through LiDAR and seismic profiles, Johnson et al. (2022) suggested that the post-glacial legacy dominates landscape evolution in the Teton range, Wyoming, USA. Whilst the estimated hillslope sediment production rates (0.17 mm/yr) were found to be similar to the uplift rates, the fluvial denudation rates were significantly lower (0.004 mm/yr). They concluded that the flattening of valley floors by glaciers results in highly inefficient fluvial systems, with reduced stream power and sediment transport capacity.

The above discussion suggests that fluvial systems in post-orogenic regions can be dominated by post-glacial processes >10 ka years after glaciation. In contrast to these studies, other studies have suggested that late Holocene geomorphic processes in some post-glacial regions are largely not governed by the glacial modification of topography due to the styles of glaciation (i.e., lack of modification by glaciers) and/or post-glacial tectonics (i.e., rapid uplift). For example, by quantifying valley shape, Prasicek et al. (2015) found that glacial topography is rapidly replaced by fluvial topography in Earth's most rapidly uplifting regions, such as Taiwan. Adams and Ehlers (2018) found that CRN-derived erosion rates match rock uplift rates in the post-glacial Olympic Mountains, USA. Moreover, they found that erosion rates correlate with topographic metrics, such as channel steepness, similar to observations from non-glaciated landscapes, and that erosion rates do not show any discernible trends with the estimated Pleistocene glacial imprint. They suggested that past glaciations have not radically altered the topography enough to drastically change the pattern of erosion.

The extent and timescales of the post-glacial legacy remain poorly quantified in Scotland. Relatively little is known about the rates and controls on post-glacial denudation rates and sediment budgets.

1.2.4 Quantifying landscape denudation rates

Sediment delivery to river networks influences their morphology and dynamics. For example, increased sediment deposition can reduce the capacity of channels to contain floodwaters which can lead to an increase in flood hazard (Raven et al., 2009; Slater et al., 2015; Stover and Montgomery, 2001). Through flood modelling, Thapa et al. (2024) demonstrated that the estimated flood inundation extent for the Kathmandu Valley, Nepal, is up to 50% higher when sediment is included. Quantifying denudation rates and sediment delivery into rivers is therefore important.

In recent decades, detrital cosmogenic radionuclides (CRN) in stream sediments have been widely used to quantify catchment average denudation rates over millennial timescales (e.g. Bierman, 1994; Brown et al., 1995; Granger et al., 1996; von Blanckenburg, 2005). In fact, there are now more than 4000 published CRN-derived denudation rates (Codilean et al., 2022). Rates derived from long-lived isotopes, such as ^{10}Be (half-life of $\approx$ 1.39 Myr, Chmeleff et al. (2010)), reflect the weathering, erosion and fluvial transport of hillslope sediments which have been linked to climatic and/or tectonic controls in active orogenic settings (e.g. Bookhagen and Strecker, 2012; Godard et al., 2014; Safran et al., 2005; Scherler et al., 2014). Cosmogenic nuclides are produced when secondary cosmic rays interact with the upper 1-2 meters of the Earth's surface. This means that the measured concentrations record an integrated denudation history while material passes through this depth interval. Moreover, the integration timescales are calculated by dividing the denudation rate by the absorption depth scale (Lal, 1991). For example, the characteristics integration timescales of ^{10}Be-derived erosion rates vary between 10^2 years for mountainous regions located in active margins, and 10^5 years for post-orogenic, low-relief landscapes (von Blanckenburg, 2005). To understand these wider controls of climate and/or tectonics on landscape evolution, studies have correlated CRN-derived erosion rates to upstream catchment characteristics, such as channel steepness, temperature and uplift rates (e.g. Cyr et al., 2010; Delunel et al., 2020,1; Harel et al., 2016; Wittmann et al., 2007).

Studies on post-glacial fluvial incision rates in Scotland have largely focused on bedrock knickpoints. Changes in the steepness of channel profiles are referred to as knickpoints or knickzones and are extensive in transient landscapes (Knopf, 1924; Whipple and Tucker, 1999). The upstream propagation of knickpoints is an important mechanism for channel incision and it communicates changes in external drivers such

as climate, sea level and tectonics throughout a landscape. Castillo et al. (2013), Bishop et al. (2005) and Jansen et al. (2010) showed that glacio-isostatic rebound during the Holocene has driven the formation of retreating bedrock knickpoints. These knickpoints remain largely clustered around Scotland's coastlines, which implies that the high rates of isostatic uplift have not been transmitted to the central Scottish ranges. By cosmogenic exposure dating of strath terrace surfaces, Jansen et al. (2011) demonstrated that the retreat rates of knickpoints associated with base-level fall in western Scotland peaked in the early to mid Holocene (maximum knickpoint retreat rate of 790 mm/yr), and have since decreased by two orders of magnitude (< 20 mm/yr). Similar trends were also observed from inferred vertical incision rates from strath terraces and channel bed sites, with Late Holocene rates between 0.07 - 0.24 mm/yr. The location of these knickpoints has been shown to depend on drainage area. For example, the location of knickpoints in small drainage basins (10^7 m^2) is currently 100m inland, whereas in larger drainage basins (10^8 m^2), knickpoints are located 1000m inland (Jansen et al., 2011). Jansen et al. (2011) inferred the observed slowing of post-glacial knickpoint retreat and vertical incision in western Scotland to the depletion of paraglacial sediment supply over the Holocene, leading to a deficiency in sediment "tools" for bedrock erosion. Relatively little is known about the rates and processes controlling denudation in Scotland's central mountain ranges.

1.2.5 The role of sediment grain size

Bedload grain sizes are a key characteristic for understanding fluvial environments. Sediment grains can act as abrasive tools that enable rivers to incise through the underlying bedrock (the 'tools effect') but in large amounts, sediment can cover bedrock and thus insulate the bed from erosive forces (the 'cover effect', Sklar and Dietrich, 1998, 2001; Whipple and Tucker, 2002). Positive and negative feedbacks link grain size and topographic evolution. For example, rivers supplied with coarser particles and larger sediment volumes must be steeper to both transport the imposed sediment load and incise into the underlying bedrock (e.g., Cook et al., 2013; Finnegan et al., 2017; Sklar and Dietrich, 2004). Sediments therefore play a fundamental role in mediating the relief of river basins, which, in turn, affects local climate and erosional processes that control sediment production on hillslopes (i.e., a positive feedback effect).

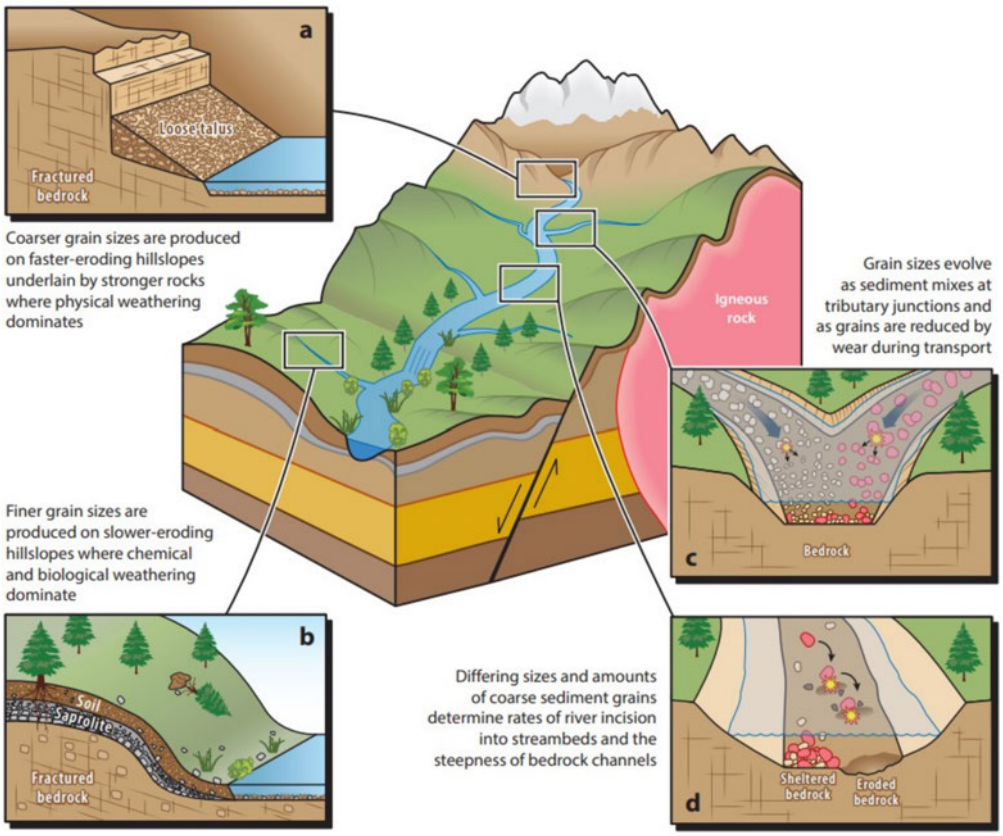

Figure 1.4: Schematic diagram illustrating grain size dynamics in erosional landscapes. Diagram is taken directly from Sklar (2024).

Initial hillslope grain size distributions delivered to rivers are controlled by fragmentation, weathering and rock mass structure (e.g., Sklar, 2001; Sklar et al., 2017; Wells et al., 2008). Individual sediment particles then reduce in size, primarily by abrasion, during downstream fluvial transport (Sternberg, 1875). The distributions of fluvial grain sizes have therefore been correlated to the longitudinal flow distance along a channel (e.g., Gomez et al., 2001; Moussavi-Harami et al., 2004; Rice and Church, 1998; Sklar et al., 2006). Downstream fining trends can be offset by variations in the supply of sediment (e.g., sediment input from landslides and tributaries) and the transport ability of a channel (e.g., Attal and Lavé, 2006; Attal et al., 2015; Sklar et al., 2006).

A handful of studies have further explored the effects of landscape characteristics, such as topography, lithology and climate, on the size distributions of channel sediments at the local-scale through field observations and topographic analysis. For example, hillslope gradient has been shown to be one of the most important topographic controls on grain sizes (Sklar et al., 2017), and several studies have shown fluvial grain sizes to increase with hillslope steepness (e.g., Attal et al., 2015; Purinton and Bookhagen, 2021; Whittaker et al., 2010). Attal et al. (2015) found hillslope grain sizes increase with hillslope steepness and erosion rates in the Feather River basin, Northern California. They showed an increase in the channel sediment grain sizes to arise from an increase in the flow competence (i.e., ability of a river to transport sediment) and changes in hillslope sediment sources from soil-mantled to mass-wasting processes (e.g., landslides, debris flows). A similar trend was documented by Whittaker et al. (2010) in the Appenine Mountains of Italy, whereby coarser fluvial grain sizes were measured in landslide-dominated areas. Likewise, the importance of lithology in controlling bedload characteristics, including grain sizes, has been demonstrated by several studies (e.g., Mueller and Pitlick, 2013; Purinton and Bookhagen, 2021; Sklar et al., 2020). For example, Mueller and Pitlick (2013) showed that more erodible rock types, such as sedimentary rocks, were associated with higher sediment yields in comparison to more resistant rocks, such as granitic rocks, in the Rocky Mountains, USA.

Studies have tested the predictability and controls of fluvial grain sizes and sediment substrate cover at large spatial scales by documenting sediment characteristics across multiple basins with gradients in topography, lithology, climate and hydrology (Abeshu et al., 2021; Haddadchi et al., 2018; Mugodo et al., 2006; Snelder et al., 2011). Given the large spatial extent of these studies, they have focused on applying data-driven machine learning techniques, such as a random forest regressor. These empirical models have used readily available environmental variables that broadly reflect each locality's upstream network structure and sediment source characteristics, such as flow distance, basin slope, lithology and precipitation indices. Snelder et al. (2011) found that surface grain sizes could be reasonably well predicted for rivers across France which, outside high mountain environments, have largely not been glaciated. Their study found an r^2 value of 0.52 between the observed and predicted values, and identified channel slope, basin averaged slope and rock hardness to be the most important variables controlling the modelled grain sizes.

Research into controls on bedload grain sizes has largely focused on landscapes with no past or present glacial influence. A key research avenue therefore includes exploring the applicability of global predictive grain size models, such as that proposed by Snelder et al. (2011) which was tested in a largely non-glaciated landscape, to post-glacial landscapes.

1.2.6 The role of coastal erosion and sea-level rise on channel incision

Migrating knickpoints are commonly associated with base-level fall, which occurs from a drop in base-level and/or an increase in the rate of rock uplift (e.g., Castillo et al., 2013; Crosby and Whipple, 2006; Jansen et al., 2011; Whipple and Tucker, 1999; Whittaker, 2012). As discussed, studies have shown that glacio-isostatic rebound during the Holocene has driven the formation of retreating bedrock knickpoints in Scotland (Castillo et al., 2013; Jansen et al., 2011). Knickpoints can also form due to changes in lithology, such as a channel cutting across a lithological contact from less to more resistant rock (Forte et al., 2016; Haviv et al., 2010; Stock and Montgomery, 1999).

Coastal erosion, which is more prevalent in regions where relative base-levels are rising (Shadrick et al., 2022), can also initiate the formation of migrating knickpoints (e.g., Hackney et al., 2015; Leyland and Darby, 2009; Limber and Barnard, 2018; Mackey et al., 2014; Snyder et al., 2002). These knickpoints have received comparatively little study, however. Waves that cut into the channel bed at the river mouth can lead to the initiation of a hanging waterfall that discharges directly into the ocean (Emery and Kuhn, 1982; Mackey et al., 2014; Snyder et al., 2002; Wolinsky and Murray, 2009). Channel incision erodes a landscape vertically and can translate the waterfall upstream as a migrating knickpoint.

The nearshore channel slope is a fundamental control on knickpoint formation; when the land is steep, wave erosion can create cliffs (Limber and Barnard, 2018; Snyder et al., 2002). The nearshore channel slope can be expressed by basic fluvial geomorphometry laws (Flint, 1974; Limber and Barnard, 2018; Snyder et al., 2002). It has long been established that rivers tend to evolve towards an equilibrium, charac-

terised in locations with uniform lithology by a channel gradient that decreases with increasing drainage area (Flint, 1974). Recent studies have thus related the occurrence of knickpoints generated through coastal erosion to specific river geometries (Limber and Barnard, 2018; Snyder et al., 2002). If there is sufficient wave energy, coastal erosion can erode the outlets of small channels because they are inherently steeper, creating cliffs with waterfalls. These waterfalls may then migrate upstream as knickpoints (Limber and Barnard, 2018). Overall, relatively little is known about the large-scale applicability of this model to channels in Southern England. Studies have instead focused on understanding the effects of coastal erosion and sea-level rise at the local scale (Leyland and Darby, 2009; Quinn et al., 2013).

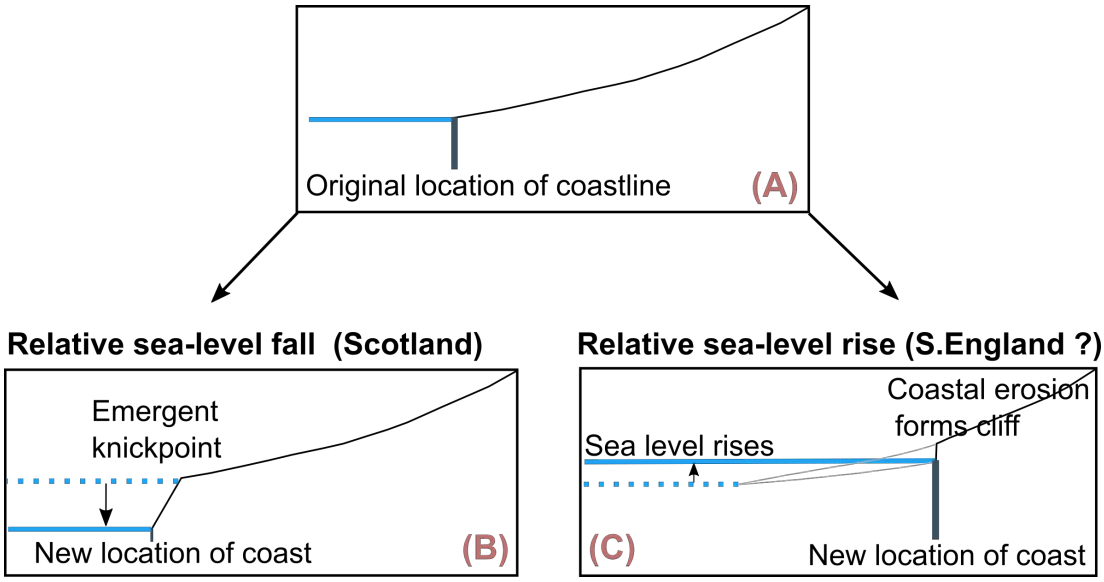

Figure 1.5: Schematic showing sea-level change and knickpoint formation. Panel (A) shows a longitudinal channel profile (black line) that flows to the sea (blue line). In a scenario where relative seal-level falls, a knickpoint develops (Panel B). Knickpoints from base-level fall have been observed in Scotland (Castillo et al., 2013; Jansen et al., 2011). Knickpoints can also develop from coastal erosion, which is associated with sea-level rise (Panel (C), Limber and Barnard (2018); Shadrick et al. (2022); Snyder et al. (2002)). Diagrams are not to scale.

1.3 Research objectives and thesis outline

The main chapters of this thesis (Chapters 2- 4) are written in the form of research papers that have either been, or shortly will be, submitted to journals. As such, each of these chapters serve as stand-alone documents covering separate topics, but each contributing to addressing the overarching aim of this thesis. That is, to investigate geomorphic processes in tectonically quiescent landscapes influenced by past glaciations. Chapters 2 and 3 explore sediment sources and transport in post-glacial landscapes. Chapters 2 and 4 explore how base-level change, which is largely driven by the glacial isostatic adjustment, influences the evolution of fluvial systems in Britain.

1. Chapter 2 explores the controls on Holocene denudation rates and sediment storage dynamics inferred from *in situ* ^{14}C concentrations in the Feshie basin, Scotland

2. Chapter 3 explores the controls on fluvial sediment grain sizes across Scotland.

3. Chapter 4 investigates the response of rivers to coastal erosion and sea-level rise in Southern England

4. Chapter 5 discusses the findings of the previous chapters and places them in the context of the wider body of research in geomorphology.

The contributions I have made to each of these documents is clearly outlined at the start of each chapter.

Chapter 2

Denudation rates and Holocene sediment storage dynamics inferred from in-situ ^{14}C concentrations in the Feshie basin, Scotland

Sediment samples for ^{14}C analysis were collected by Anya Towers, Simon Mudd, Mikael Attal and Fiona Clubb. Sample preparation and ^{14}C extraction was performed at the University of Cologne, Germany, and ETH Zürich, Switzerland, by Steven Binnie, Tibor Dunai and Negar Haghipour. I conducted the data analysis (e.g., DEM analysis, flood modelling, terrace mixing model) and led the writing of the manuscript. Simon Mudd wrote the code and text for calculating erosion rates (i.e., CAIRN) and ^{14}C concentrations of terrace columns.

This chapter has been published in *Earth Surface Processes and Landforms* (http://dx.doi.org/10.1002/esp.70043).

Abstract

Scotland's Highlands are tectonically quiescent but have experienced high rates of isostatic uplift in response to deglaciation. To understand the effects of both deglaciation and regional uplift on landscape evolution, we measured the concentration of cosmogenic *in situ* ^{14}C in river sands collected in Glen Feshie (Cairngorms). Like other terrestrial cosmogenic radionuclides, *in situ* ^{14}C can be used to calculate basin-wide denudation rates over millennial timescales. ^{14}C has a short half-life relative to other *in situ* cosmogenic radionuclides, giving it an advantage in post-glacial landscapes: very little ^{14}C will be inherited from exposure before glaciation of the landscape, meaning that concentrations will reflect sediment production and transport in the Holocene. When we calculate denudation rates based on the common assumption of basin-wide homogeneity of erosion, we find no correlation between topographic metrics such as the normalised channel steepness index and inferred denudation rates, which range between 0.175 and 1.356 mm/yr. Based on field and remote sensing observations, we suggest that ^{14}C becomes diluted downstream due to sediment supply from paraglacial terrace material, and develop a mixing model to test this hypothesis. We identify the terraces that are likely to contribute sediment to the channels through flood modelling, geomorphic mapping and remote sensing observations. Our mixing model indicates that the observed distribution of ^{14}C concentrations can be explained if terrace escarpments have basin-averaged migration distances of 8 to 30 cm during large flood events. This interpretation is consistent with remotely sensed images of channel activity and terrace bank retreat within the catchment. Our results show that paraglacial sediment stores contribute to sediment fluxes in the late Holocene and highlight the on-going glacial legacy on landscape evolution.

2.1 Introduction

Sediment delivery to river networks influences their morphology and dynamics. For example, increased sediment deposition can reduce the capacity of channels to contain floodwaters which can lead to an increase in flood hazard (Raven et al., 2009; Slater et al., 2015; Stover and Montgomery, 2001). In recent decades, detrital cosmogenic radionuclides (CRN) in stream sediments have been widely used to quantify catchment average denudation rates over millennial timescales (e.g. Bierman, 1994;

Brown et al., 1995; Granger et al., 1996; von Blanckenburg, 2005). Rates derived from long-lived isotopes, such as ^{10}Be (half-life of $\approx$ 1.39 Myr, Chmeleff et al. (2010)), reflect the weathering, erosion and fluvial transport of hillslope sediments which have been linked to climatic and/or tectonic controls in active orogenic settings (e.g. Bookhagen and Strecker, 2012; Godard et al., 2014; Safran et al., 2005; Scherler et al., 2014). To understand these wider controls of climate and/or tectonics on landscape evolution, studies have correlated CRN-derived erosion rates to upstream catchment characteristics, such as channel steepness, temperature and uplift rates (e.g. Cyr et al., 2010; Delunel et al., 2020,1; Harel et al., 2016; Wittmann et al., 2007).

Research into controls on denudation has mainly focused on non-glaciated landscapes, however, which are typically less complex than formerly glaciated landscapes. Key challenges associated with understanding geomorphic processes in low-relief, post-glacial landscapes originate from the preservation of glacially modified topography. In these landscapes, hillslopes can be decoupled from channels due to the over-deepening and widening of valleys by glaciers, and extensive glacial sediment drapes (e.g. till, moraines, paraglacial terraces) influence sediment supply and transport capacity (Ballantyne, 2019; Whitbread et al., 2015). In many Scottish river basins, channel erosion has exposed dramatic paraglacial terraces that appear to be contributing large quantities of sediment to modern rivers (e.g. Ballantyne, 2019). Scotland has been in a phase of glacial isostatic rebound since the disappearance of the British-Irish Ice Sheet and complete deglaciation following the Loch Lomond Stadial/Younger Dryas around 12 ka ago (Ballantyne, 2019; Clark et al., 2018; Firth and Stewart, 2000; Shennan et al., 2009). Uplift rates are spatially variable across Scotland, with the highest uplift rates in the central and western Highlands ($>$1 mm/yr average over the last 1000 years, Shennan et al. (2009)). Base-level signals propagating inland from the North Sea do not appear to have transmitted this high uplift rate to the central Scottish ranges, however, as knickpoints presumed to be caused by the isostatic rebound are clustered around Scotland's coastlines (Bishop et al., 2005; Castillo et al., 2013). Relatively little is known about the rates and processes controlling denudation in these central ranges.

In addition to geomorphic complexity, denudation rates are also much more challenging to measure in low-relief, post-glacial landscapes such as Scotland. The use of long-lived isotopes such as ^{10}Be in these settings is problematic, because repeated phases of shielding and exposure during past glacial, interglacial and interstadial periods can lead to ^{10}Be concentrations that are difficult to interpret. For example, in the high-relief, glacial and post-glacial European Alps, where the median ^{10}Be derived denudation rate is 0.414 mm/yr (Delunel et al., 2020), denudation rates derived from ^{10}Be typically integrate over millennial timescales. The integration timescales are calculated by the absorption depth scale, which is generally accepted to be the top 60 cm of Earth's surface, divided by the denudation rate (e.g. Lal, 1991). Moreover, inferred denudation rates can be corrected for cosmogenic shielding by snow and ice (e.g. Mudd et al., 2016) from late Holocene glacial inventories and snow cover maps. In Scotland, which has a lower relief compared to the European Alps, one would expect lower denudation rates (e.g. von Blanckenburg, 2005) meaning that ^{10}Be erosion rates would integrate over longer timescales (e.g., a denudation rate of 0.05 mm/yr would integrate over 12000 years). This means that low denudation rates derived from ^{10}Be may integrate over glacial, interglacial and interstadial cycles (e.g., Lateglacial Interstade $\approx$ 14.7 - 12.9 ka, Middle Devinsian before the expansion of the last British-Irish Ice Sheet $\approx$ 35 ka, Ballantyne et al. (2021)). This leads to the potential for large amounts of uncertainty in ^{10}Be derived denudation rates. Furthermore, the recycling of sediment as well as transport of sediment across topographic divides during multiple phases of glaciation will have occurred in post-glacial landscapes such as Scotland (Linton, 1949). As a result, sediment grains sampled at a given location will likely have experienced complex and different histories, making quantification of the inherited component of the ^{10}Be concentrations impossible.

In contrast to ^{10}Be, cosmogenic *in situ* ^{14}C has a short half-life ($\approx$ 5700 years, (International Atomic Energy Agency, 2024)), which means that inferred denudation rates from ^{14}C atoms in stream sediments will mainly reflect post-glacial, Holocene erosion. For example, approximately 90 % of ^{14}C will have decayed after 20,000 years of complete burial. This technique therefore provides a new opportunity to understand landscape evolution and rates of erosion in formerly glaciated regions.

Applying ^{14}C to infer catchment-averaged erosion rates remains limited, however, because of challenges associated with constraining ^{14}C production rates and analytical methods, such as sample extraction (see Hippe (2017) for a review). Following recent advancements in the extraction techniques and scaling of ^{14}C production rates (e.g. Lifton et al., 2014,2; Lupker et al., 2015), studies have used ^{14}C alongside ^{10}Be to identify complex erosional histories (Hippe et al., 2021; Kober et al., 2019; Slosson et al., 2022). An exciting application of ^{14}C is the ability to detect short-lived sediment routing and storage events (100s to 1000s of years) which would not be detectable in catchments with relatively little sediment storage and/or where erosion rates are derived from longer-lived isotopes such as ^{10}Be (Hippe, 2017; Slosson et al., 2022; Wittmann et al., 2011). For example, Slosson et al. (2022) suggested lower concentrations of ^{14}C in stream sediments relative to ^{10}Be concentrations are caused by sediment shielding and storage in highly dynamic hillslope talus deposits in the Argentine Andes.

In this study, we report the first Scottish ^{14}C-derived erosion rates in the post-glacial catchment of Glen Feshie, a braided, gravel-bedded river with an abundant sequence of paraglacial terraces and local bedrock sections located in the Cairngorm mountains of Scotland. We use a nested approach with samples along the main stem and at the mouth of tributaries to assess the contributions of various geomorphic domains and the controls on erosion rates. In contrast with tectonically active landscapes with coupled channels-hillslopes where erosion rates tend to correlate with topographic metrics such as channel steepness, and uplift rates to the first order (e.g., Harel et al., 2016; Kirby and Whipple, 2012), we expect that a significant portion of the fluvial sediment will be sourced from paraglacial sediment stores in our study area (e.g. Ballantyne, 2002; Church and Ryder, 1972), which will affect ^{14}C concentrations. We may consider these two scenarios as end-member hypotheses: one in which rivers have incised through the glacial drape and adjusted to regional uplift rates, and the other where sediment is recycled from paraglacial deposits with little modification of the underlying bedrock.

To test which of these two scenarios is more consistent with our measured detrital ^{14}C concentrations, we explore the relationships between CRN-derived sediment fluxes and basin-averaged topographic parameters, such as channel steepness. We hypothesise that if landscape denudation is driven by active bedrock incision, CRN-

derived denudation rates should positively correlate with landscape steepness. We then explore the influence of paraglacial sediment supply on CRN-derived denudation rates by presenting a mixing model which mixes 'background' sediment (i.e., sediment sourced from basin-wide erosion) with terrace sediment with various ^{14}C concentrations. We assess the impact of the remobilization of terrace sediment by first identifying the terraces that are coupled to the channel during high flows. In the model, we then vary terrace migration distances and terrace ^{14}C concentrations across a realistic range based on the constraint we have on terrace ages and historical terrace migration. We assess the sensitivity of the results to these parameters, and combine these modelling results with our observations to constrain rates and processes of sediment production in Glen Feshie.

2.2 Study area

The River Feshie is a tributary of the River Spey in the post-glacial western edge of the Cairngorm Mountains (Figure 2.1). The main channel flows $\approx$ 39 km mainly northwards and has a catchment area of $\approx$ 231 km^2. The land is managed for mostly moorland and woodland, with commercial forestry and farming in the lower reaches. The catchment typically floods throughout the year and discharges peak during the winter and spring (maximum annual discharges regularly exceed 40 m^3/s at the gauging station upstream of the confluence with the Spey). The underlying bedrock geology is composed of Moinian Schist with a small proportion of Cairngorm Granite which underlies the higher ground in the northeast (BGS, 2021). Both of these lithologies have high concentrations of quartz, making the Feshie basin an ideal setting for studying the concentrations of *in situ* ^{14}C. The Feshie is thought to have been deglaciated at the end of the Late Devensian $\approx$13,000 yr B.P. (Young, 1975). However, it is unknown whether the catchment was glaciated during the Loch Lomond Stadial/Younger Dryas (12,900 -11,700 B.P., Chandler et al. (2019); Sissons (1974)). The area subsequently experienced isostatic uplift which is estimated to be $>$1 mm/yr over the past 1000 years (Shennan et al., 2009). The aftermath of the last glaciation can be observed from features such as the wide, trough-like valleys and paraglacial outwash terraces.

In comparison to other UK rivers, the Feshie is exceptionally dynamic due to its abundant sediment supply and flashy flow regime (Rumsby et al., 2008; Williams et al., 2020).

Studies have suggested the Feshie's paraglacial terraces represent an initial phase of net sediment deposition by meltwater streams during glacial retreat (Ballantyne, 2019; Robertson-Rintoul, 1986; Young, 1976). These thick valley fills were incised throughout the Holocene leading to terrace formation. Robertson-Rintoul (1986) mapped the Feshie terraces and assigned the terraces to 5 groups on the basis of soil-stratigraphic evidence. Robertson-Rintoul (1986) suggested the older, higher terraces (Groups 1 and 2) formed at 15.6 cal ka BP and 11.5 cal ka BP from soil-stratigraphic comparisons and assumed deglaciation ages. Furthermore, a radiocarbon age of 4.1 - 3.7 cal ka BP was obtained by Robertson-Rintoul (1986) for charcoal fragments within a horizon of buried soil in a lower-level terrace (Group 3) in the Lorgaidh basin (see Figure 2.1 for location of Lorgaidh basin) suggesting the lower-level terraces are of Late Holocene age (i.e. post-4000 years). The buried soil layer in this terrace (95 cm below terrace surface) suggests episodes of sediment aggradation then incision during the Late Holocene (Robertson-Rintoul, 1986). All radiocarbon ages reported here were re-calibrated using the IntCal20 calibration curve and Calib version 8.2 (Reimer et al., 2020). Calibration ranges for individual radiocarbon dates represent $\pm 2\sigma$ (95.4% probability). Ages are calibrated to BP 1950.

Whilst the modern-day dynamics of the terraces remain relatively unconstrained and there is little quantitative data on the lateral migration of the channel into these terraces, field observations and satellite imagery confirm the active nature of the channel braid plain and that terrace erosion plays a key role in providing sediment to the channels (Figure 2.2). For example, Figure 2.3 shows tens of meters of bank erosion between 2006 and 2019 for the downstream braided reach that is located upstream of the confluence with the Spey.

Measurements of terrace heights and valley-fill depths suggest that the Feshie's valley is glacially over-deepened. In the upper braided reach downstream of the Lorgaidh confluence, a seismic refraction survey recorded a minimum sedimentary fill depth of 30 m below the modern-day floodplain (survey carried out by Bronwyn Matthews and Dr. Mark Naylor from the University of Edinburgh at CRN sample location FLOD

using an array of wired seismic nodes and a known source consisting of a hammer and plate). Downstream of the Garbhlach confluence, a borehole survey taken from a 5 m high terrace (relative to the channel) reported a fill depth of 14.5 m before intersecting with bedrock (BGS, 2021). In contrast to the main valley alluvial fill, the Feshie basin also contains steep-sided, narrow, high-relief valleys with little sediment accommodation space such as the Garbhlach basin where the hillslopes are characterised by talus and debris flows (Figure 2.2). The Feshie basin also contains bedrock knickzones, such as the one labelled in Figure 2.2. Bedrock knickzones are a legacy of glacial erosion and are a common feature of post-glacial landscapes (Whitbread et al., 2015).

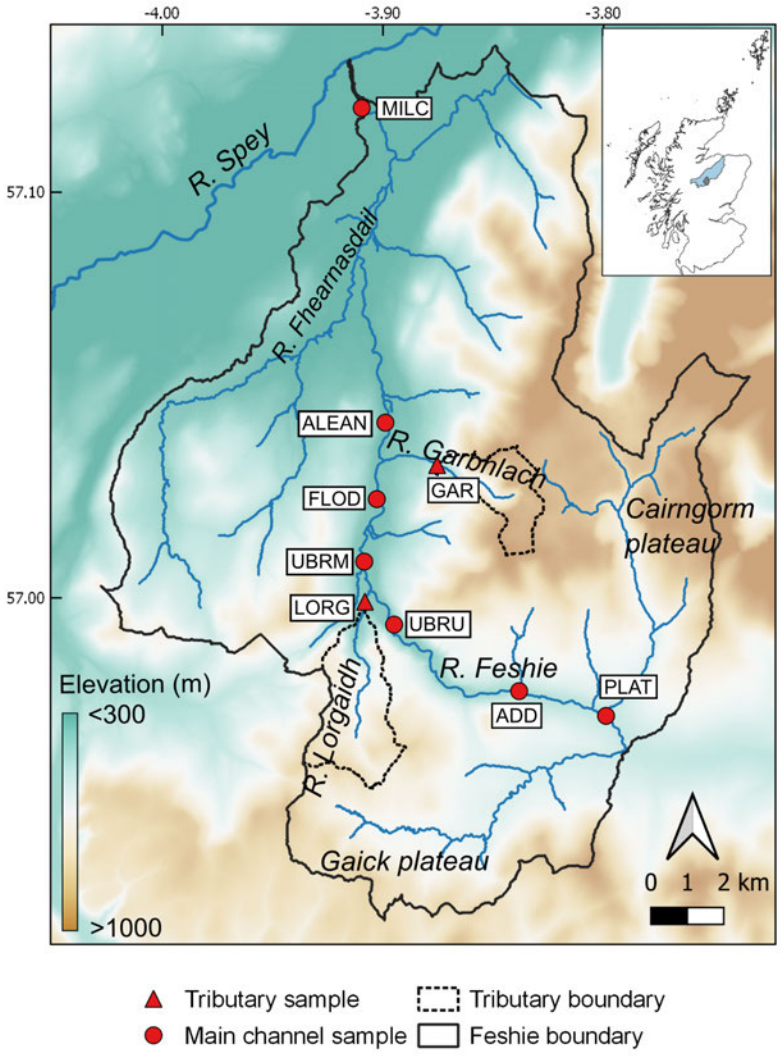

Figure 2.1: Elevation map of Glen Feshie with CRN sample locations. Red dots mark samples collected along the main river channel and red triangles represent samples collected in tributaries. Inset map shows a map of Scotland with the Spey basin coloured in blue and Feshie in grey. 5 m Digital Terrain Model was sourced from the Ordnance Survey (Ordnance Survey, 2021).

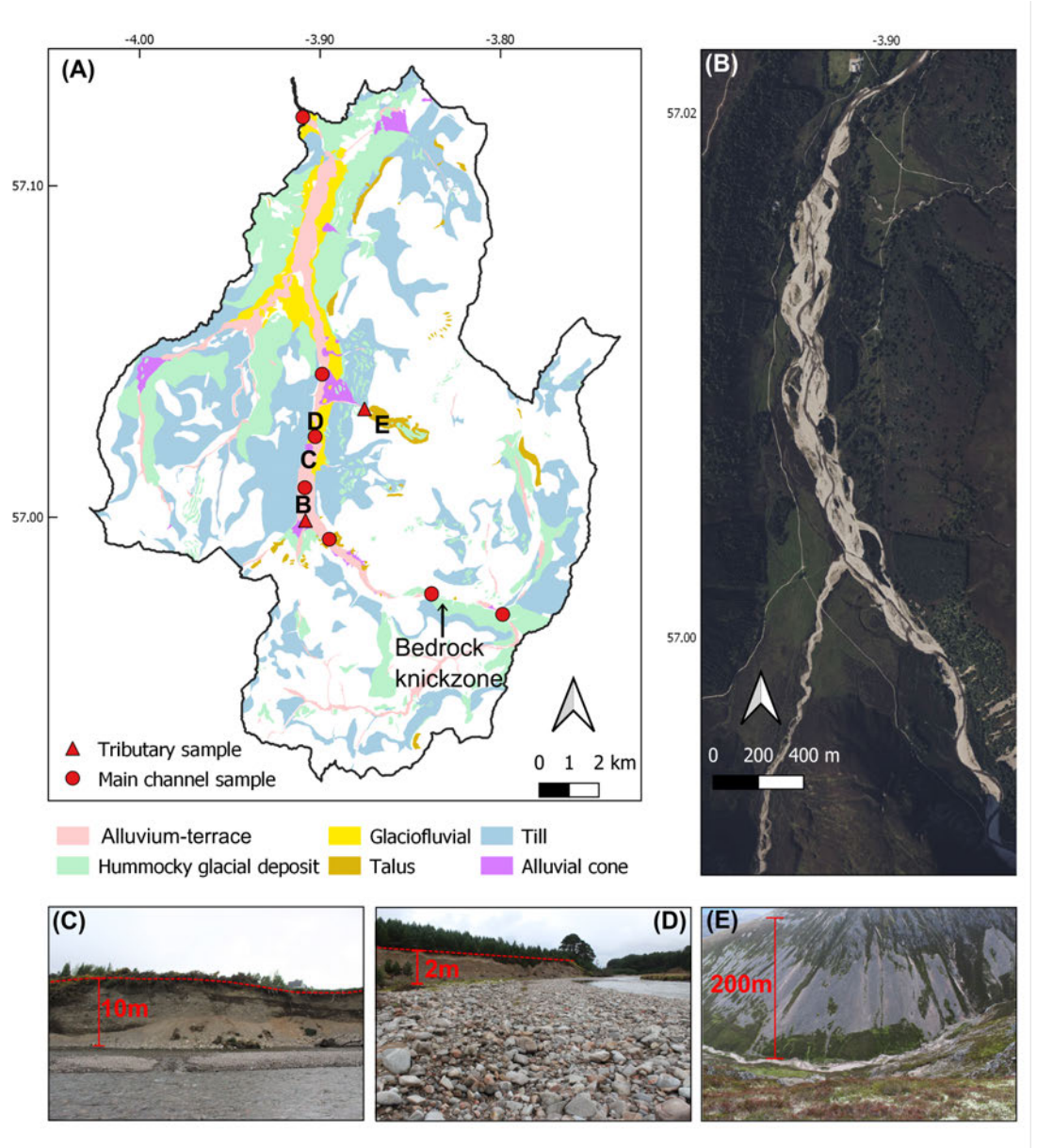

Figure 2.2: Figure (A) shows key lithological groups in Glen Feshie (lithological groups obtained from the British Geological Survey (BGS, 2021)). ≈3 km-long bedrock knickzone is marked along the main channel. “Alluvium-terrace" represents material that has been incised and reworked by channels during the Holocene, whereas “Glaciofluvial" represents material that was deposited by glacial meltwater streams and appears mostly disconnected from the modern-day channel network. Red symbols mark CRN sample locations: red dots mark samples collected along the main river channel and red triangles represent samples collected in tributaries. The locations of Figures B, C, D and E are marked on Figure A. Figure (B) shows an aerial image highlighting the characteristic braided nature of the Feshie (Bing Maps, 2023). Figures (C) and (D) show terraces which are actively feeding material into the channel. Both terraces appear paraglacial and are poorly bedded and unsorted (i.e. contain a wide range of grain sizes and angular to sub-rounded clasts with no preferential orientation direction in places). The surface of the terraces in (C) and (D) is marked by a red dashed line and their approximate heights are also shown. Figure (E) is a photograph of the steep, high-relief Garbhlach basin where the hillslopes are characterised by bedrock and talus deposits.

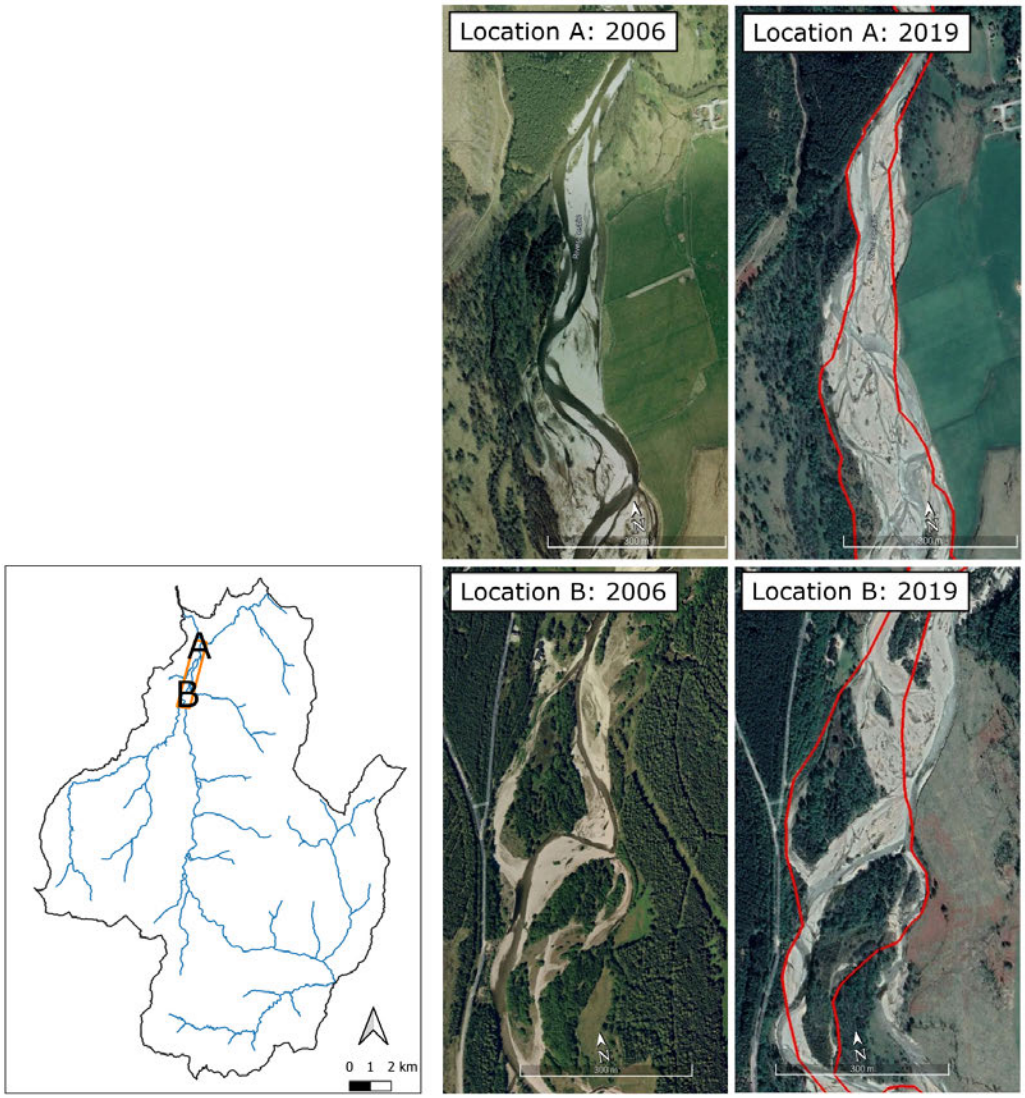

Figure 2.3: Evidence of meter-scale channel change from Google Earth Imagery (Google Maps, 2023) between 2006 and 2019 in the downstream braided reach (orange box on inset map). Red line on 2019 imagery marks the approximate extent of the 2006 bankfull channel. Tens of meters of bank migration is observed, especially at location B, which could have been enhanced by the felling of plantation woodland. Imagery dates were selected following the limited availability of clear, cloud free images.

2.3 Materials and methods

2.3.1 ^{14}C sediment sampling and processing

In this section, we describe the sampling strategy, sample preparation and ^{14}C extraction, and the procedure for calculating denudation rates based on the ^{14}C concentrations.

Sampling strategy

Nine quartz-rich sand samples were taken from modern gravel bars in August 2021. Samples were collected with the objective of constraining the contribution of different geomorphic domains on Holocene denudation rates in a post-glacial setting (see Section 2.2 for a detailed geomorphic description of the catchment). For example, sample GAR (see Figure 2.1 for sample names) was collected to understand the influence of a high-relief, steep landscape with relatively little valley fill on sediment fluxes. In contrast, sample PLAT was collected to isolate the influence of a low-relief setting with abundant valley fills on erosion rates. The remainder of the samples were collected downstream along the main valley-fill sequence to understand sediment source to sink fluxes.

Sample preparation and ^{14}C extraction

Sample preparation and ^{14}C extraction was performed at the University of Cologne, Germany, and ETH Zürich, Switzerland. Samples were sieved and the 250-500 μm fraction was retained for *in situ* ^{14}C preparation. Samples were etched in $\approx$18 % HCl (technical grade) on a shaking table for 24 hours. For the ensuing froth flotation, to remove feldspar and mica, samples were activated with 1 %HF and processed with 1% AERO65 frother and Laurylamine (0.03 % v/v) using a laboratory flotation machine (MN 935/5, Humboldt Wedag). AERO65 is a completely water-soluble polyglycol type frother that produces a closely knit and persistent froth. Polyglcols are synthesized from ethylene oxide, the latter is a petrochemical product (Bailey FE and Koleske JV, 1990), thus free from ^{14}C (petroleum is older than $>$50 kyr, thus all ^{14}C has decayed). The resulting enriched quartz was etched twice in 5 % HF/HNO_3 on a shaking table for 24 hours and twice in 1 % HF/HNO_3 in an ultrasonic bath for 24 hours to obtain pure quartz (Kohl and Nishiizumi, 1992) free of organic residues from froth flotation

agents (Nichols and Goehring, 2019). Due to the perfect solubility of polyglycol in water, it will be rinsed out in in the repeated decanting rinsing during post-flotation etching; besides it contains no ^{14}C from the production process.

The pure quartz samples (≈4 g each) were extracted subsequently for gas-source accelerator mass spectrometer (AMS) analysis in a custom build extraction line at the University of Cologne following the procedure described in Fülöp et al. (2015). As per Fülöp et al. (2015), carbonate was added before processing. Blanks were analysed at the Cologne AMS facility (Schiffer et al., 2020) and samples for this study at the ETH Zürich (Lupker et al., 2019; Wacker et al., 2013). As is common practice since the onset of AMS technology in the 1980s, both AMS facilities are calibrated with standard materials. Both laboratories participate in international laboratory inter-comparisons (Scott et al., 2018). Both facilities use NBS-Ox II standard material for calibration. The background measurement from full processed blanks, which was obtained by the repeated extraction of synthetic quartz (Schiffer et al., 2020), is 38000 ± 10000 atoms ^{14}C (± 1δ, n=26; measurements since 2020).

We refer the reader to Table A.S3 in Appendix A for information on the blank measurements.

Denudation rate calculations

Catchment-averaged denudation rates were calculated from each sample's ^{14}C concentration using the CAIRN (Catchment-averaged denudation Rates from cosmogenic Nuclides) method (Mudd et al., 2016). CAIRN calculates analytical solutions of a statement of conservation of nuclide concentration through time t:

$$\frac{dC_j}{dt} = P_j - \lambda_j C_j \tag{2.1}$$

where C_j is the concentration of nuclide j (in this case ^{14}C) in units atoms per gram, P_j is the nuclide production rate in units atoms per gram per year, and λ_j is the nuclide decay coefficient (in units 1/yr). This approach is similar to that of Parker (1991), but after applying simplifying assumptions, solutions to this equation reduce to more widely used derivations such as Lal (1991) and Granger and Smith (2000).

Production can be a function of latitude, altitude (or atmospheric pressure), geomagnetic field strength and shielding by rock, soil, water or snow (e.g. Balco et al., 2008). Production of the nuclide can be caused by both neutrons and muons (e.g. Gosse and Phillips, 2001). CAIRN calculates production following the relatively simple approach of an approximation using four summed exponential functions, similar to a number of authors (Braucher et al., 2009; Granger and Smith, 2000; Schaller et al., 2009; Vermeesch, 2007):

$$P_j(d) = P_{j,SLHL} \sum_{i=0}^{3} S_{i,j} F_{i,j} e^{\frac{-d}{\Lambda_j}} \tag{2.2}$$

where $P_{j,SLHL}$ is the total surface production rate (atoms g^{-1} yr^{-1}) at sea level and high latitude, $F_{i,j}$ is a dimensionless scaling that relates the relative production of neutron spallation and muon production, $S_{i,j}$ is a dimensionless scaling factor that combines the effects of production scaling and shielding of cosmic rays, d is a mass per unit area which represents the mass overlying a point under the surface (typically reported in g cm^{-2}), and Λ_j is the attenuation length for reaction type j (g cm^{-2}). The reaction types are $i = 0$ for neutrons and $i = 1 - 3$ for muons.

The depth d, called shielding depth, is related to depth below the surface as:

$$d = \int_{\zeta-\eta}^{\zeta} \rho(z)\,\mathrm{d}z \tag{2.3}$$

where ζ (cm) is the elevation of the surface, η (cm) is the depth in the subsurface of the sample, z (cm) is the elevation in a fixed reference frame and ρ (g cm^{-3}) is the material density, which may be a function of depth. The shielding depth is typically reported in g cm^{-2}. For a constant density, $d = \rho\eta$.

Combining equation (2.1) and equation (2.2) results in a partial differential equation that can be solved analytically.

One simple scenario is when the denudation rate, ε, (g cm^{-2} yr^{-1}) is constant in time. The general solution for this scenario for the concentration of a nuclide at depth d and time t that had a starting position at depth d_0 and an initial concentration C_0 at time t_0 is:

$$C(t) = C_0 e^{-(t-t_0)\lambda_i} + P_0 \left[\sum_{i=0}^{3} \frac{S_i F_i \Lambda_i}{\varepsilon + \Lambda_i \lambda} e^{\frac{-d_0}{\Lambda_i}} \left(e^{\frac{\varepsilon(t-t_0)}{\Lambda_i}} - e^{-(t-t_0)\lambda} \right) \right] \tag{2.4}$$

We have dropped the subscript j indicating the nuclide for simplicity; subsequent equations apply to any nuclide. Equation (2.4) is the same as equation (11) in Mudd et al. (2016). We can use equation (2.4) to derive more complex erosion scenarios that might occur in a transient landscape.

For computing the apparent erosion rate, CAIRN further assumes constant erosion rates beginning at infinite depth and infinite time ($t_0 = 0$ and $t = \infty$, $d_0 = \infty$), reducing the equation to:

$$C(d) = P_{SLHL} \sum_{i=0}^{3} \frac{S_i F_i \Lambda_i e^{-d/\Lambda_i}}{\varepsilon + \lambda \Lambda_i} \tag{2.5}$$

where ε is the denudation rate (g cm^{-2} yr^{-1}). If we set $d = 0$ (that is, we solve for material being eroded from the surface, with no distributed mass loss via chemical weathering), equation (2.5) reduces to equation (6) from Granger and Smith (2000) for denudation only (i.e., no burial or exposure), and reduces to equation (8) of Lal (1991) if production is due exclusively to neutrons.

CAIRN does include modules for topographic shielding, but DiBiase (2018) demonstrated that the shorter attenuation length from steep slopes cancels topographic shielding so we do not reduce production from topographic shielding to calculate denudation rates. CAIRN then calculates the production rate for each pixel based on an effective attenuation depth following the approach of Vermeesch (2007). We calculate the surface production scaling, S_{tot}, using the scaling of Lal (1991) and Stone (2000). It should be noted that the Lal/Stone (LSt) scaling is time invariant. Nuclide production is, however, known to vary with the intensity of Earth's geomagnetic field, which is taken into account in other scaling schemes such as the Lifton/Sato/Dunai (LSD) which take into account time-varying production rates Lifton et al. (2014). The recent studies of Charreau et al. (2019) and Stübner et al. (2023) have shown that failing to account for time-varying production can lead to large changes in inferred erosion rates using ^{10}Be. However, the difference between the LSt scaling and LSD scaling is relatively low at high latitude sites such as ours ($<$10%) and where erosion rates

vary by less than an order of magnitude (Charreau et al., 2019; Stübner et al., 2023). Neither of these two studies explored the effect on ^{14}C, but the higher production rates of ^{14}C lead us to expect the differences would be even smaller at high latitude for this nuclide.

The scaling terms for individual production mechanisms, S_i, may vary depending on elevation, shielding, sample thickness, or denudation rates. For example, muogenic pathways will contribute relatively more to production when there is more shielding since muogenic reactions penetrate deeper than spallation. Following Vermeesch (2007) we calculate a single surface production rate, S_{tot}, that combines production scaling and topographic shielding, and then partition this total production to individual scaling terms by employing a virtual attenuation length, Λ_v, in units of g cm^{-2}:

$$S_i = e^{\frac{-\Lambda_v}{\Lambda_i}} \tag{2.6}$$

We then calculate Λ_v based on S_{tot}. S_{tot} is calculated using the Lal/Stone scaling, but this is calculated using the spallation production rate reported by Borchers et al. (2016) and dividing this by the fraction of production from spallation from Lupker et al. (2015), i.e. 12.24 atoms/g/yr divided by F_0 = 0.788 to arrive at a P_{SLHL} of 15.533 atoms/g/yr. We then calculate the individual production mechanisms such that:

$$S_{tot} = \sum_{i=0}^{3} S_i F_i \tag{2.7}$$

In equation (2.7), S_{tot} and F_i are known, whereas S_i are functions of Λ_v. We thus iterate upon Λ_v, calculating S_i using equation (2.6) using Newton's method until equation (2.7) converges on a solution for Λ_v.

We can then calculate the production of atoms of ^{14}C at every pixel in our DTM using equation (2.5). We make an initial guess at the denudation rate, ε, based on simple denudation rate estimates from Lal (1991), and then we use Newton-Raphson iteration to converge on the observed concentrations in a given basin by changing the ε value. The full method is described in Mudd et al. (2016). The parameter values used for the scaling and production are shown in Table 2.1.

We report uncertainties on the denudation rates by calculating denudation rates from the reported ^{14}C concentrations $\pm$ the blank-corrected uncertainty values. We refer the reader to Table A.S1 in Appendix A for a glossary of all the symbols outlined in this section.

Parameter	Value
$P_{0,SLHL}$	15.533 atoms/g/yr
F_0	0.788
F_1	0.212

Table 2.1: Parameters used in CRN calculations. The length scales for spallation and muogenic production are 160 g/cm^2 and 1500 g/cm^{2}for F_0, F_1, respectively. The relative scaling parameters are from Lupker et al. (2015). The total production rate at high latitude and sea level is calculated using the production from the Lal/Stone scaling reported for spallation in Borchers et al. (2016) divided by the spallation scaling, F_0. The decay coefficient is 1.2158^{-4} yr^{-1}.

2.3.2 Basin-averaged topographic parameters

As described in the Introduction, studies in mountainous landscapes have found that denudation rates tend to correlate with topographic metrics such as channel steepness and elevation (e.g. Cyr et al., 2010; Delunel et al., 2020,1; Harel et al., 2016; Wittmann et al., 2007). For example, Delunel et al. (2010) found a correlation between denudation rates and mean basin elevation in the Western French Alps, from which they suggested frost-shattering to be the main driver of denudation rates in their study area. For each sample, we determine the upstream contributing basin area, and then calculate basin-averaged topographic metrics from the 5 m Digital Terrain Model (DTM) from the Ordnance Survey (Ordnance Survey, 2021). Basin area, elevation (proxy for temperature), slope and channel steepness were derived from the DTM in LSDTopoTools (Mudd et al., 2023). We calculate the normalised channel steepness index, k_{sn}, which is the channel slope normalised to drainage area and typically reflects the erosive ability of a channel (Flint, 1974; Wobus et al., 2006). We use the algorithms from Mudd et al. (2014) to calculate k_{sn}, using a concavity index of 0.45 (Mudd et al., 2014). A map of channel steepness across the Feshie basin is available in Figure A.S1 in Appendix A.

2.3.3 Terrace mixing model

Erosion rates derived from ^{14}C concentrations in catchments with little valley-fill (e.g. Garbhlach tributary) can be reasonably assumed to represent catchment-wide denudation rates. However, as described in Section 2.2, the Feshie contains an abundant sequence of paraglacial terraces along the main channel, and along the Lorgaidh and Fhearnasdail tributaries. To test whether these terraces are contributing significant quantities of sediment to the modern channel and affecting the detrital ^{14}C concentrations, we present a mixing model which mixes the 'background' sediment with terrace sediment. The 'background' erosion rate reflects sediment sourced 'basin-wide' from erosion of channels and hillslopes with no contribution from transient sediment stores. In this section, we first present the model, followed by the methodologies to obtain terrace bank heights, lengths and ages which will all influence the output of the mixing model.

Description of model and assumptions

We hypothesise that samples along the main channel and River Lorgaidh will provide faster apparent catchment-averaged erosion rates than they should because they will contain sediment with background ^{14}C concentrations mixed with lower concentration material from terraces bordering the channels. We hypothesise that the terrace material has lower CRN concentrations because: (1) the production of CRN in terrace materials decreases with depth (see cartoon diagram in Figure 2.4) and (2) terrace materials have remained buried until the last phase of major incision, and were therefore largely shielded from cosmic rays (i.e., 'fill-cut' terraces, see Section 2.3.3 for further discussion).

To test our overarching hypothesis of low ^{14}C concentration terrace material mixing with high ^{14}C concentration 'background' material, we perform a mass balance calculation for each sample (except GAR which is from a catchment that is largely devoid of terrace material) which calculates a drainage basin's ^{14}C outlet concentration, C_{Basin}, by mixing the 'background' sediments with terrace sediments. Our approach is similar to the theoretical model outlined by Wittmann and von Blanckenburg (2009), who proposed a method to detect sediment storage and transfer in depositional basins from

^{14}C. Our model assumes that both terrace sediments and 'background' sediments have similar concentrations of quartz, and that there have been no differences in the chemical depletion rates amongst sediment sources.

Assuming all sediments are well-mixed, the concentration of ^{14}C in the collected sediments, C_{basin}, is equal to the number of atoms supplied to the sampling site divided by the mass of sediment supplied. We assume the sample is composed of atoms (α) and masses (M) of ^{14}C supplied by background erosion (α_{bg}, M_{bg}) and terrace erosion (α_f, M_f). The timing and frequency of terrace erosion is largely unknown in the catchment. For example, terraces could erode progressively through time (i.e. low magnitude, high frequency scenario), or only erode during major flood events (high magnitude, low frequency scenario). Field observations suggest both scenarios are likely: we observe sloped sediment deposits at the base of terraces, indicating a more progressive system, but also observe undercut terraces, suggesting flood events drive geomorphic change. For the purpose of this study and the mixing model proposed, we assume terrace sediment was sourced from the last major flood event before sample collection, the details of which are outlined in Section 2.3.3. Also supporting this assumption is the fact that, when observed, the accumulations of debris at the toe of terrace scarps (which testify to progressive terrace erosion) tend to be disconnected from the active channel, i.e., not in contact with the flowing water at low flow. This sediment may therefore become incorporated only during major floods, even if it has progressively accumulated between two major floods.

C_{basin}, in atoms per gram, is given by:

$$C_{Basin} = \frac{\alpha_{bg} + \alpha_f}{M_{bg} + M_f} \tag{2.8}$$

The mass supplied in the last flood event from the terraces is the sediment density times the volume transferred to the channel. For convenience, we use units of g/m^3 for density, which allows us to match unit conventions for measuring CRN concentrations and distances. The units of density in these equations cancel as they appear in both top and bottom terms of the fraction in equation (2.8), so they are, in practice, arbitrary. The volume from the terraces is the product of the migration distance (D_T in meters),

the height of the terrace bank relative to the channel (H_T in meters) and the length of the eroded terrace (L_T in meters). The model assumes that the terrace walls are vertical (see Figure 2.4). The number of atoms supplied is this mass times the concentration of ^{14}C in the terrace (C_T, in atoms/gram). The mass of the sediment supplied from the 'background' at the sampling point is the erosion rate (E_{bg}, units m/yr) times the time since the last flood, ΔT, times the upstream area (A in m^2), times the sediment density (g/m^3). The number of atoms supplied from the 'background' at the sampling point are this mass times the concentration in the background (C_{bg}). Note that all these terms include the density, which we assume to be the same for both the 'background' and terrace sediment, so these terms cancel, resulting in:

$$C_{Basin} = \frac{C_{bg}E_{bg}A\Delta T + C_T L_T H_T D_T}{E_{bg}A\Delta T + L_T H_T D_T} \tag{2.9}$$

In equation (2.9) the numerator is in units atoms m^3/g and the denominator is in units m^3, so the units of C_{basin} are atoms/g. To calculate the background concentration, C_{bg}, we need to assume a given background erosion rate; we then use CAIRN to solve for the concentration at the sampling point. We note at the this stage that the sample GAR could be a good candidate for this assumed background erosion rate, as its upstream area is relatively devoid of terraces (Figures 2.1 and 2.2) and ^{14}C concentrations will likely represent catchment-wide denudation rates, as will be discussed. The methods for obtaining terrace bank heights, lengths and concentrations are outlined in Section 2.3.3. Terrace migration distances are largely an unknown, so we model a range of migration distances and discuss these in relation to terrace concentrations in Section 2.4.3. Variations in terrace bank migration distances, ages and heights are expected to cause differences in ^{14}C concentrations (and apparent denudation rates) between sites that have recorded a paraglacial terrace signal.

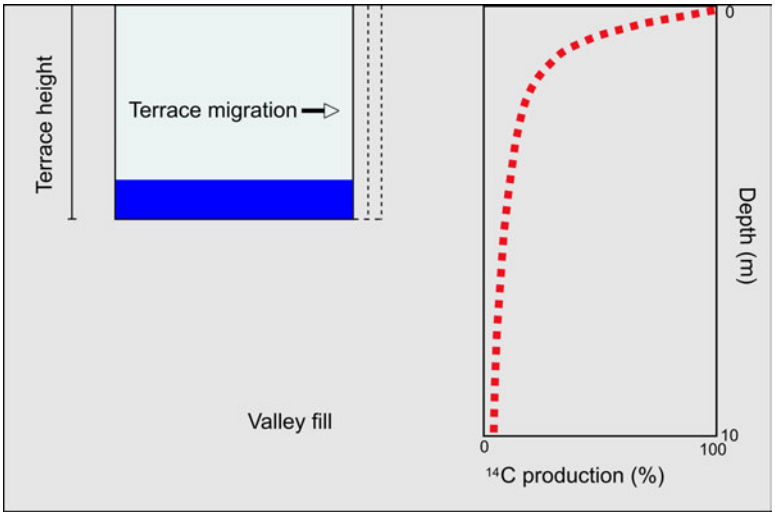

Figure 2.4: 2D cartoon diagram showing the terrace components of our model, modified from Wittmann and von Blanckenburg (2009). The production of ^{14}C is shown to decrease with surface depth (red dashed line, decay curve taken from Hippe (2017)). Terrace height H_T, terrace migration distance in the time period considered D_T, and terrace length L_T (not shown because our cartoon is 2D) control the concentration of the terrace material entering the river in our model. Valley fill depth is not to scale because it is largely unknown and likely to be spatially variable.

Methods for obtaining terrace bank heights and lengths

As highlighted above, we assume sediment was sourced and transported from the terraces during the last major flood event before sample collection. To obtain the lengths (L_T) and heights (H_T) of the terrace banks connected to the channel network during this flood event, we create a flood extent map. The following section describes the flood modelling and terrace extraction methodology.

To document flood trends prior to sample collection, we download discharge and rainfall data from UKCEH (https://nrfa.ceh.ac.uk/data/station/peakflow/8013) for the gauging station at Feshiebridge (located near MILC sample in Figure 2.1, also marked on Figure 2.9). The discharge time-series (Figure 2.5) shows that the last major flood event (February 2021, 86.99 m^3/s) had occurred 6 months before sample collection in August 2021. This flood event is equivalent to a $\approx$ 1 in 5 year flood event (see Figure A.S2 in Appendix A). We simulate the flood extent

associated with this discharge in HAIL-CAESAR on the 5 m DTM. HAIL-CAESAR is a hydrodynamic landscape evolution model which is derived from the CAESAR-Lisflood model (Coulthard et al., 2013).

We run the model in “catchment mode" which requires the input of rainfall to generate runoff. Rainfall data was unavailable for the February 2021 flood event so we use rainfall data from a flood event in September 2009 when a similar discharge of 86.6 m^3/s was recorded. We run the model with rainfall 20 days prior to the flood event with a Manning's roughness value of 0.04 which represents mountain rivers with gravels, cobbles and boulders (Chow, 1959). We set the topmodel m value, which controls the peak and duration of flood events, to 0.001 which represents high infiltration rates for high, flashy flood peaks (Beven, 1997). With these parameters, including a high topmodel m value, the simulated peak discharge was 62 m^3/s, which highlights the potential of spatially heterogeneous rainfall. Because we are interested in mapping the flood extent associated with a 86.6 m^3/s flood, rather than replicating the precise flow dynamics, we increased the rainfall by 30 $\%$, which produced a simulated discharge of 82 m^3/s which is very close to our target discharge. We refer the reader to Appendix A for the simulated flood hydrograph (Figure S3).

To obtain the height of the terrace banks relative to the channel, we create a 10 m buffer around the modelled flood extent and sample this 10 m buffer every 5 m to create nodes. We then clip the nodes to the BGS alluvium/terrace dataset (BGS, 2021). We choose a buffer distance of 10 m to account for sloped sediment deposits between the terraces and the edge of the simulated flood extent, based on satellite and field observations (Figure 2.6). Many of the exposed terrace faces along the river are near vertical (see Figure 2.2), but we use a 10 m buffer to ensure that we capture the top of the terrace surfaces reliably. For example, even for a 45 degree terrace scarp we would still capture a 10 m high terrace. We then compare the elevation of each 5 m terrace bank node to the nearest channel's elevation (which was derived from the DEM) using the steepest descent flow routing algorithm presented by Clubb et al. (2017). We will refer to this height as terrace height in the rest of the paper.

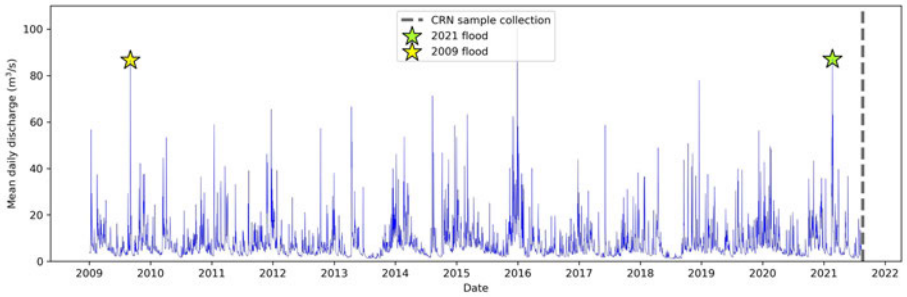

Figure 2.5: Mean daily discharge recorded at the Feshiebridge gauging station (near MILC sampling point, also marked on Figure 2.9). Discharge data (and rainfall) was sourced from the UKCEH (https://nrfa.ceh.ac.uk/data/station/peakflow/8013). The green star shows the most recent major flood event prior to sample collection which is a $\approx$ 1 in 5 year flood event. The flood modelling in this study is based on the 2009 event (yellow star) because no rainfall was available for the 2021 event (see Figure S4 in Appendix A for available rainfall data).

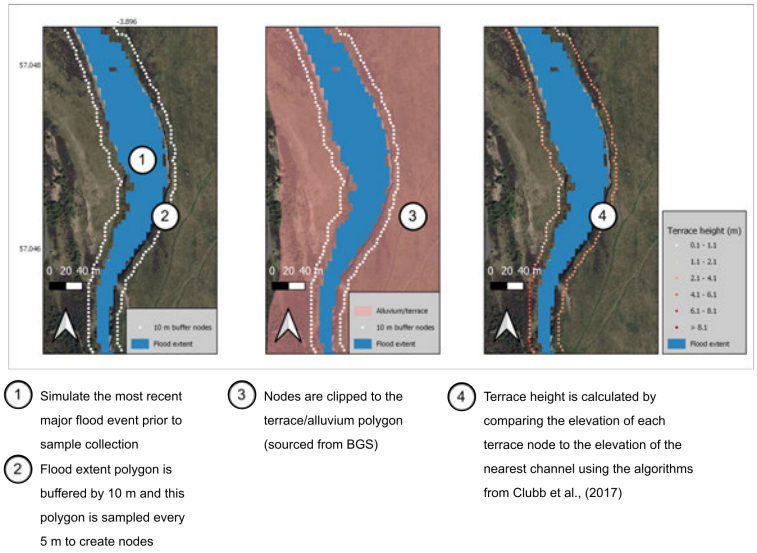

Figure 2.6: Flood modelling methodology used to infer the approximate height of terrace banks bordering the channel in the Feshie basin. We simulate a 1 in 5 year flood event (shown by the blue 'Flood extent' polygon) in HAIL-CAESAR which represents the approximate return period of the last major flood event prior to sample collection. This flood extent is then buffered by 10 m and the resulting polygon is sampled every 5 m to create nodes ('10 m buffer nodes'). These nodes are then clipped to the terrace/alluvium polygon which was sourced from the BGS (see Figure 2.2 for the alluvium/terrace extent of the Feshie catchment, BGS (2021)). To obtain the height of the terrace banks, the elevation of the terrace nodes are compared to the elevation of the nearest channel using the algorithms from Clubb et al. (2017).

Methods for obtaining terrace concentrations

The mixing model presented in equation (2.9) requires terrace concentrations, C_T, to model a basin's outlet concentration, C_{basin}. The concentration of ^{14}C in terraces is mostly a function of the exposure time to cosmic rays. We explore an end-member scenario, whereby the sediment in the terraces has been shielded before exposure as the fill-cut terraces were formed. In this experiment, we assess whether incorporation of terrace material with the lowest ^{14}C concentration possible could explain the observations. ^{14}C inheritance in the terraces may be spatially variable and there is no data regarding these concentrations, hence the choice of this conservative scenario.

The timing of late Holocene major incision events and thus lower-level terrace (exposure) ages are largely unknown. To our knowledge, only one terrace date in the Feshie basin has been published: a radiocarbon age of 4.1 - 3.7 cal ka BP was obtained by Robertson-Rintoul (1986) for a lower-level terrace (Group 3) in the Lorgaidh basin, suggesting that the lower-level terraces are of Late Holocene age (post-4000 years). Robertson-Rintoul (1986) also inferred a younger terrace group of 900 cal ka BP to exist from soil stratigraphic mapping (Group 4). Both of these terrace groups (1000 and 4000 years) were interpreted to border the modern-day channel in the mapped extent which focused on the upper braided reach and Lorgaidh basin (location B in Figure 2.2). These results imply the channel receives sediment from terraces aged at both 1000 and 4000 years. Based on these findings, we tentatively model our terrace bank migration distances with terrace ages of 1000 and 4000 years and discuss the implications in Section 2.4.3.

We simulate the concentration of ^{14}C in terraces using a column model available in LSDTopoTools (Mudd et al., 2023). This model follows the same governing equation as equation (2.4), but in this case we simulate ^{14}C concentrations as a function of depth over a fixed duration ($t - t_0 = t_t$, where t_t is the age of the terrace) such that the governing equation reduces to:

$$C(t_t, d) = C_0 e^{-t_t \lambda_i} + P_0 \left[\sum_{j=0}^{3} \frac{S_i F_i \Lambda_i}{\varepsilon + \Lambda_i \lambda} e^{\frac{-d}{\Lambda_i}} \left(e^{\frac{\varepsilon t_t}{\Lambda_i}} - e^{-t_t \lambda} \right) \right] \tag{2.10}$$

We therefore assume minimal denudation over the age of the terrace ($e \sim 0$) in the column model. The scaling and production parameters for this component of the study are shown in Table 2.1. The column model is evolved from the particle-based model presented in Mudd (2017), but includes the more rigorous production and scaling mechanisms from Mudd et al. (2016).

The mixing model presented in equation (2.9) assumes that the total height of a terrace column, D_T, collapses into the river during a flood event. We therefore sample the column's ^{14}C concentration every 0.05 m, following which we calculate a depth-averaged concentration (C_T in equation (2.9)). The column model assumes there is no mixing or bioturbation within the terrace deposits. This assumption is supported by the fact that, when observed, terraces in the Feshie appear paraglacial and are largely composed of unsorted gravels, with very little soil relative to the total terrace height (Figure 2.2). Moreover, if mixing is present within a thin soil layer, then the depth-averaged ^{14}C concentration of a terrace is likely to resemble that of an unmixed terrace profile (Hippe, 2017).

We set the elevation and height of the column to the average elevation and height of the terraces in the Feshie as defined in the terrace bank extraction method section (Section 2.3.3). We also perform a sensitivity analysis to test the influence of terrace elevations (i.e. production rates of ^{14}C) on the terrace concentrations.

As discussed, we assume there is no initial ^{14}C concentration, on the basis that the material was buried deep enough before the formation of the terrace such that all pre-existing ^{14}C had decayed. This latter assumption may not perfectly reflect reality: terraces will have accumulated a small percentage of ^{14}C during their burial phases from deep production by muons (see Figure 2.4). For example, the total *in situ* ^{14}C concentration at 10 m depth is $<5\%$ of the surface nuclide production (Figure 2.4, Hippe (2017)). Moreover, Robertson-Rintoul (1986) documented a buried soil layer (95 cm below the terrace surface) with a radiocarbon age of 4.1–3.7 cal ka BP, suggesting sediment aggradation above previous floodplain levels. As a result, it is likely that the terrace sediment may not have been completely shielded until terrace formation. We do not add an initial concentration to the terrace column model because

we largely do not know the ^{14}C concentrations and burial history of the terraces. Any antecedent ^{14}C will increase the concentration of ^{14}C derived from the terraces, so terrace migration rates estimated from our model will be minimum rates

2.3.4 Methods for calculating erosion rates from sediment fluxes

Erosion rates derived from ^{14}C concentrations in catchments with abundant paraglacial terraces are not expected to represent true 'basin-wide' denudation rates. To further understand the relationships between denudation rates and the isostatic uplift rate in these basins, we calculate erosion rates from sediment fluxes. That is, we test whether the erosion rate from sediment fluxes is, in fact, comparable to the isostatic uplift rate in basins with paraglacial terraces when both the 'background' erosion of hillslopes and the erosion of paraglacial material are considered. The erosion rate from sediment flux, E_{flux}, is the sum of the 'background' erosion rate (E_{bg}, units m/yr) and of the terrace volume that collapses into the river during a large flood event divided by the sample's drainage area (A in m^2). The latter represents the equivalent erosion rate had the volume of material from the terrace been sourced from uniform erosion upstream of the sample. The volume of sediment from the terraces is the product of the migration distance (D_T in meters), the height of the terrace bank relative to the channel (H_T in meters) and the length of the eroded terrace (L_T in meters; see Section 2.3.3 for a full description of these parameters). For the purpose of this study, we assume that terrace collapse occurs during large annual flood events. The erosion rate from sediment flux, in units m/yr, is given by:

$$E_{flux} = E_{bg} + \frac{L_T H_T D_T}{A} \tag{2.11}$$

2.4 Results

2.4.1 Overview of inferred denudation rates

The following section presents catchment-averaged denudation rates inferred from concentrations of ^{14}C in detrital sediments. We say “inferred" because these denudation rates are based on the assumption that concentrations result from steady, spatially homogeneous denudation. We report rates in mm/yr, as these rates are perhaps more intuitive than a mass-based denudation rate which represent an equivalent bedrock lowering with a density of 2650 kg/m^3 in the parent material. The denudation rates reported below are calculated using CAIRN (Mudd et al., 2016), which is described in detail in Section 2.3.1. We also calculate denudation rates using CRONUS (Balco et al., 2008), which vary by approximately 10 percent from the CAIRN-derived erosion rates (see Table 3.1).

Overall, the inferred denudation rates are similar for seven out of the nine sampled sites, with rates between 0.442 and 0.612 mm/yr. The denudation rate calculated for the high-elevation, low-relief Gaick plateau is 0.478 mm/yr (PLAT). Downstream of this sample, the river flows through a bedrock knickzone (Figure 2.2) downstream of which the inferred denudation rate is similar to that from the Gaick plateau (sample ADD, 0.442 mm/yr). Around 4.5 km downstream, the Feshie then enters the main glacial trough where the main valley-fill sequence begins and debris flows enter the channel. Here, the inferred catchment-averaged denudation rate increases to 0.612 mm/yr (UBRU). Further downstream, the denudation rates show little change where the river passes the confluence with the Lorgaidh and flows through the uppermost braided section (UBRM, 0.582 mm/yr; FLOD, 0.582 mm/yr). The Lorgaidh (LORG), which displays evidence of Holocene hillslope failure (e.g. talus deposits, debris flows) and contains terraces which the river is laterally migrating into, has a slightly lower inferred denudation rate of 0.457 mm/yr.

The steep, high-relief Garbhlach tributary has the lowest inferred denudation rate in the entire catchment (GAR, 0.175 mm/yr). Downstream of the confluence with the Garbhlach, an inferred denudation rate of 0.523 mm/yr is calculated from sample ALEAN which is similar to the sample upstream of the Garbhlach’s confluence along the main channel (FLOD, 0.582 mm/yr). Finally, our downstream-most sample, MILC, which is $\approx$ 1.5 km upstream of the Feshie’s confluence with the Spey, displays the

highest erosion rate recorded in this study, 1.356 mm/yr. Overall, the catchment-averaged denudation rates are, on average, significantly lower than the isostatic uplift rates predicted for the Feshie basin of $>$1 mm/yr (Shennan et al., 2009).

Error bars are shown on the CAIRN-derived erosion rates on Figure 2.7. Error values represent erosion rates calculated from the reported ^{14}C concentrations $\pm$ the blank-corrected uncertainty values. The key findings discussed above remain the same when these errors are considered. That is, we find the lowest inferred denudation in the steep, high-relief Garbhlach tributary, and the highest apparent denudation rate at our downstream-most sample near the Spey, MILC. These key findings are also consistent with the denudation rates and uncertainties derived from CRONUS (see Table 3.1 and Figure 2.7, Balco et al. (2008)). We refer the reader to Table A.S3 in Appendix A for information on blank measurements and uncertainties.

Sample	River name	Lat.	Long.	Basin area (km^2)	Sample elevation (m)	Sample ^{14}C (atoms g^{-1})	Uncertainty $\pm$ (atoms g^{-1})	CAIRN-derived erosion rate (mm yr^{-1})	CRONUS-derived erosion rate (mm yr^{-1})
GAR	Garbhlach	57.03407	-3.8729	4.47	438	100440	2570	0.175	0.167
ADD	Feshie	56.9786	-3.83459	73.13	450	52500	2450	0.442	0.389
LORG	Lorgaidh	57.00016	-3.9047	7.26	376	49050	2500	0.457	0.421
PLAT	Feshie	56.97275	-3.79523	33.57	513	47130	2520	0.478	0.434
ALEAN	Feshie	57.04437	-3.89655	126.57	324	45100	2520	0.523	0.470
FLOD	Feshie	57.02548	-3.89996	116.12	343	42480	2510	0.582	0.514
UBRM	Feshie	57.01004	-3.90527	100.76	358	41290	2510	0.582	0.541
UBRU	Feshie	56.9946	-3.8914	91.65	380	40860	2510	0.612	0.550
MILC	Feshie	57.12184	-3.90915	232.28	229	24260	2520	1.356	1.03

Table 2.2: ^{14}C sample details, $\pm$ blank-corrected ^{14}C concentrations, and modelled erosion rates from CAIRN and CRONUS. We refer the reader to Table A.S4 and Table A.S5 in Appendix A for more detailed descriptions of the ^{14}C concentrations and erosion rates.

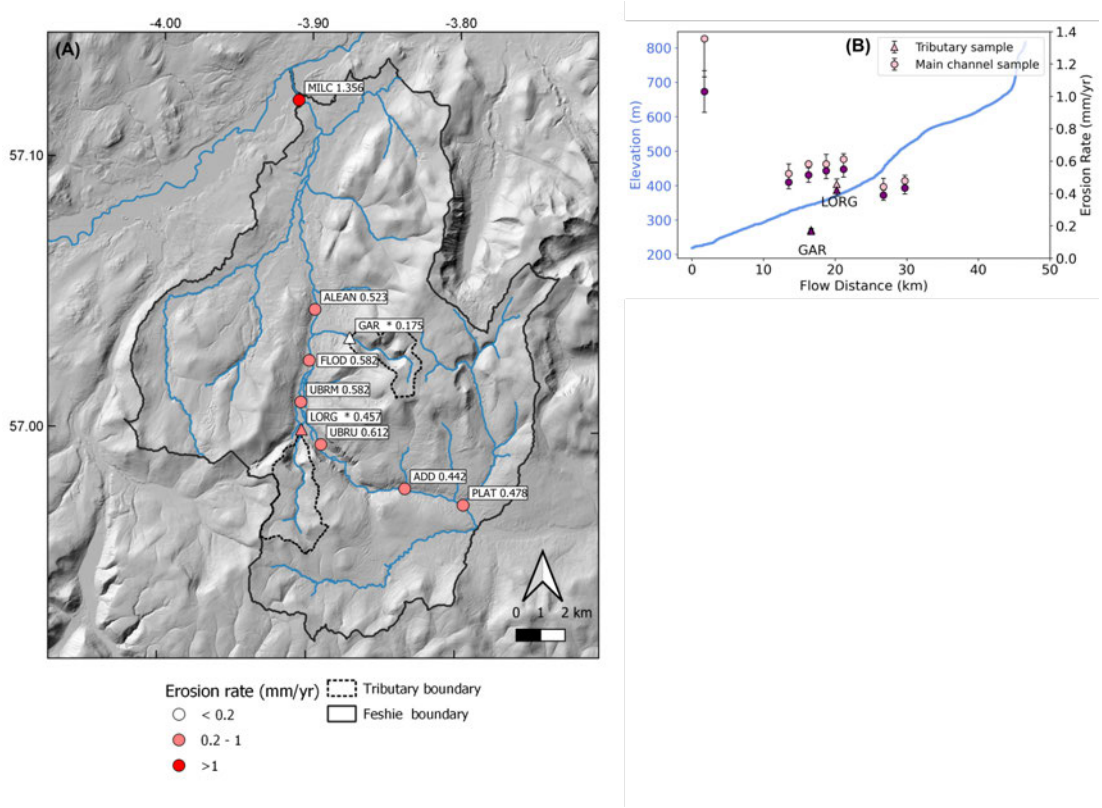

Figure 2.7: (A) Map of the Feshie with sample names and ^{14}C-derived erosion rates. (B) Plot of main river profile (blue line) and erosion rates calculated through both CAIRN (pink markers) and CRONUS (purple markers). CAIRN error values represent erosion rates calculated from the reported ^{14}C concentrations $\pm$ the blank-corrected uncertainty values. CRONUS error values represent both measurement uncertainty and production rate uncertainty.

2.4.2 Relationships between apparent erosion rates and basin-averaged topographic parameters

Many studies have correlated denudation rates to basin-averaged topographic parameters to understand the wider controls of climate and/or tectonics on landscape evolution (e.g. Cyr et al., 2010; Delunel et al., 2010; Hack et al., 1957; Harel et al., 2016; Wittmann et al., 2007). In this study, we counter-intuitively find negative correlations between the apparent erosion rates and upstream basin-averaged slope, normalised channel steepness and elevation (proxy for temperature, Figure 2.8). We find the highest inferred denudation rate of 1.356 mm/yr at the most downstream sample, MILC, and the lowest inferred denudation rate of 0.175 mm/yr in the steepest tributary catchment, the Garbhlach basin (GAR). Furthermore, we cannot explain our erosion rates from any apparent geological controls, as the bedrock geology is

relatively homogeneous in the catchment (BGS, 2021). Similarly, vegetation does not appear to exert a primary control on the erosion rates. Commercial forestry dominates the lower areas of the catchment near the confluence with the Spey, and new native forest and moorland occupy much of the upper basin. It is important to note that we find the lowest denudation rate in the Garbhlach tributary, a catchment that is very steep and largely devoid of terrace materials. This result supports our hypothesis that a significant portion of the sediment transported by the main stem river is sourced from low-concentration terrace materials. In the following section, we use our mixing model to test this hypothesis.

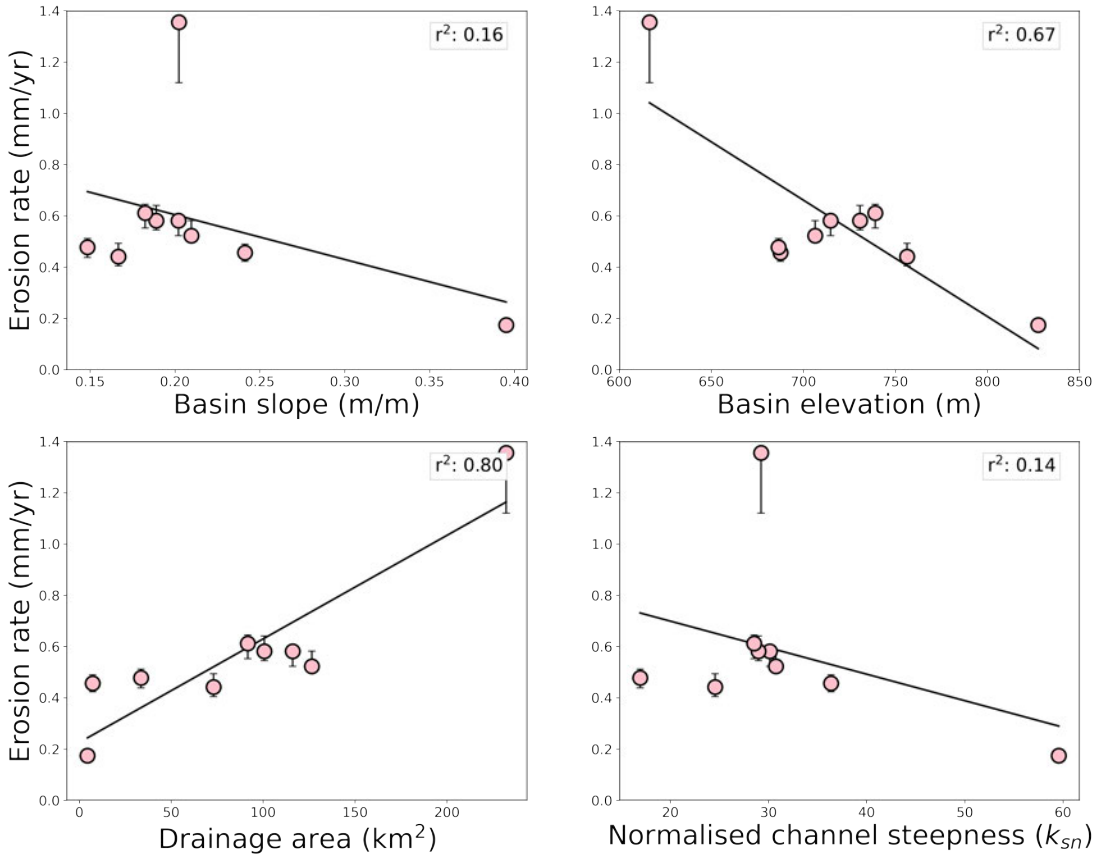

Figure 2.8: Relationship between denudation rates and catchment-averaged topographic parameters including mean basin slope, elevation, drainage area and normalised channel steepness. R^2 linear regression values are shown for each plot.

2.4.3 Terrace mixing model results

To run our mixing model, we need a 'background' denudation rate that is representative of catchment-wide denudation. In the absence of other reliable catchment-wide denudation rates, we assume that the Garbhlach's denudation rate of 0.175 mm/yr represents this background denudation rate. We note that this is likely an upper bound and that the real background denudation rate may be lower, as the Garbhlach is one of the steepest tributaries in the catchment. Using the GAR value of 0.175 mm/yr as the background denudation rate, we use CAIRN to calculate the expected ^{14}C concentration for all the other samples. We then use the mixing model to simulate the impact of introducing lower concentration material from the upstream terraces, as explained in the methods. The dilution proceeds iteratively. For example the sample near the Spey (MILC) features the lowest ^{14}C concentration and the highest apparent erosion rate (1.356 mm/yr). This means that sediments with relatively low ^{14}C concentrations must

have been supplied between MILC and ALEAN. The model assumes these lower concentration sediments have been supplied by terraces. The height and age of the terrace will affect the ^{14}C concentrations in the terrace material that is remobilised. For example, erosion of higher and/or younger terraces will lead to the introduction of material with lower average ^{14}C concentrations. The terrace migration rate will affect the ratio of background material to terrace material in the river sediment: the greater the migration rate, the greater the dilution of the background sediment with low ^{14}C concentration sediment from the terraces. We examine each of these possibilities in the following discussion.

Terrace height results

Figure 2.9 shows a map and longitudinal river profile of the left and right terrace heights in the Feshie basin. Terrace heights, derived from the 10 m buffer zone, average 2.2 m above the channel for the entire basin (see Figure A.S5 in Appendix A for distribution of terrace heights). There is no obvious downstream trend in terrace heights, although terraces in the headwaters (upstream of flow distance 35 km) tend to be not as high as further downstream. Localised reaches with higher terraces above $\approx$5 m are observed at locations such as the Garbhlach confluence and upstream of sample UBRU (flow distance between 20 and 25 km). Terrace heights do not appear to increase between sample ALEAN and MILC, and average between 2 and 2.5 m, suggesting that terrace height does not account for the higher erosion rate (lower concentration) near the Spey. There do not appear to be any high terraces feeding the tributary channels between ALEAN and MILC.

Terrace age results

Figure 2.10 shows the relationship between terrace ages and depth-averaged ^{14}C concentrations for the average terrace height of 2.2 m and average terrace elevation of 420 m in the Feshie basin, simulated by our terrace column model. As the average terrace age increases, the depth-averaged terrace ^{14}C concentration increases.

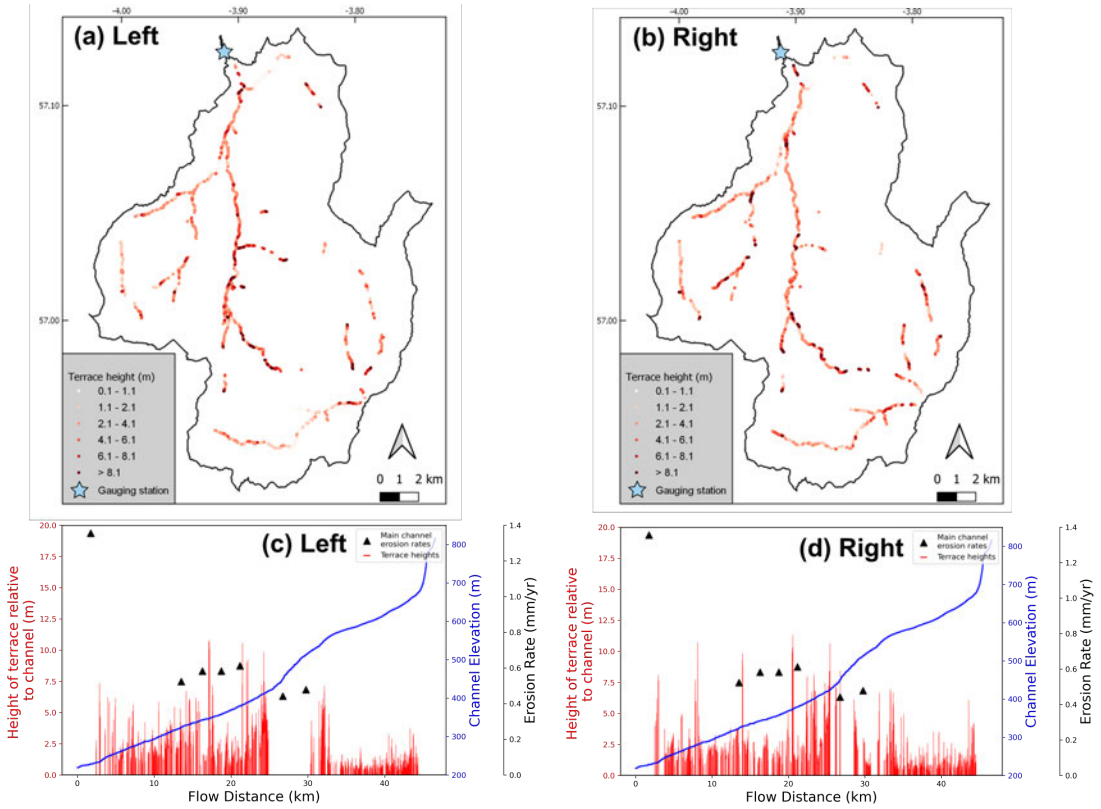

Figure 2.9: (A) and (B) Maps of left (A) and right (B) terrace heights (m) derived from the 2009 flood with a 10 m buffer. (C) and (D) Long profile plot of the main Feshie River with left (C) and right (D) terrace heights marked in red. Main channel erosion rates are shown by the black triangles.

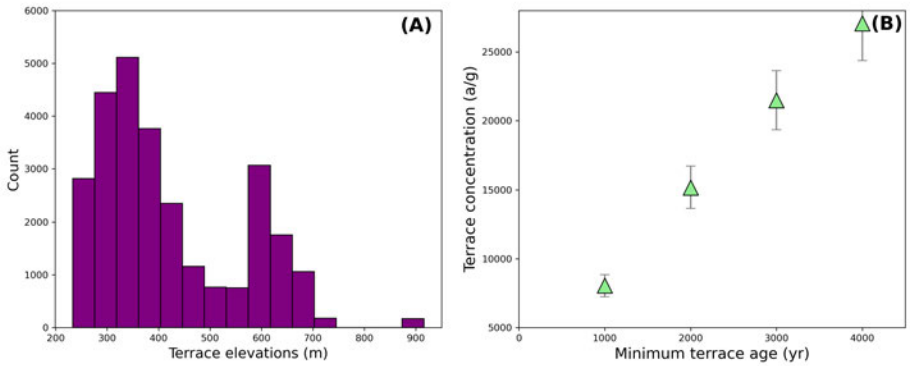

Figure 2.10: (A) Histogram of the terrace elevations derived from the 10 m buffer method for the entire Feshie catchment. (B) Relationship between terrace age and depth-averaged terrace ^{14}C concentration using our average terrace height of 2.2 m and elevation of 420 m. 10 % error bars represent uncertainty associated with the production rates from terrace elevation (i.e. an increase in elevation of 200 m increases the terrace ^{14}C concentration by approximately 10 % for the same terrace scarp height).

Terrace elevations mostly range between 230 m and 600 m, which is ≈200 m below and above the mean elevation of 420 m in the Feshie basin. With regards to the influence of elevation on ^{14}C production rates, a change in terrace elevation of 200 m changes the final terrace concentration by 10 % for our average terrace height of 2.2 m. Error bars on Figure 2.10 represent this 10 % uncertainty (see Table A.S2 in Appendix A for full sensitivity analysis). Latitude makes a negligible difference to the modelled terrace concentrations due to the catchment size. The uncertainty from elevation on terrace ages is discussed in more detail alongside the terrace migration results in Section 2.4.3.

As discussed in Section 2.3.3, Robertson-Rintoul (1986) interpreted the lower level terraces in the Feshie basin to have formed 1000 and 4000 years ago, from radiocarbon dating and geomorphic mapping. These ages correspond to depth-averaged terrace ^{14}C concentrations of approximately 8000 atoms/g and 27000 atoms/g, respectively. Therefore we tentatively model each samples' ^{14}C basin outlet concentration with terrace migration distances associated with these depth-averaged terrace concentrations and discuss the implications in Section 2.4.3.

Terrace migration distance results

We first present results using a range of catchment-averaged terrace migration distances per flood event (D_T in equation (2.9)), that is, all terraces upstream of each sampling point are assumed to migrate at the same rate. We perform the calculation for each sampling point. The results for ALEAN and MILC (sample near Spey) are shown in Figure 2.11. The remainder of the samples yield similar results to ALEAN and are shown in Figure A.S6 in Appendix A. If the terraces that are contributing sediment to the modern channel have been exposed to cosmic rays for 1000 years throughout the Feshie basin, then we can explain MILC's lower sampled concentration with higher terrace migration distances during a flood event. This result remains valid even when we take into account the uncertainty from terrace elevation-derived production rates (see shaded lines on Figure 2.11). For example, if the average terrace concentrations in the Feshie equate to 8000 atoms/g (i.e. exposed to cosmic rays for 1000 years), then we can explain ALEAN's observed basin outlet concentration with catchment-averaged terrace migration distances of 0.08 m/flood event. To explain the highest apparent erosion rate from the MILC sample (with the lowest measured ^{14}C concentration) downstream near the Spey, catchment-averaged terrace migration distances must be significantly higher (0.3 m/flood event) for the same terrace concentration of 8000 atoms/g.

The terrace migration values presented above are catchment-averaged. However, we know that the sediment sampled at ALEAN has a ^{14}C concentration that is nearly twice that at MILC further downstream, implying that a significant change in terrace dynamics occurs in the nested basin between ALEAN and MILC. Major rivers within this nested basin include both the section of the main Feshie channel between the two sampling locations and the Fhearnasdail tributary (see Figure 2.1 for location). To calculate the required migration distances in this nested basin, we run our sediment mixing model (equation (2.9)) and set the terrace migration distances upstream of ALEAN to 0.08 m/flood event (e.g. 1000 year scenario). We then model the required nested basin's terrace migration distances to obtain MILC's outlet concentration. For example, if the terraces upstream of ALEAN have a migration rate of 0.08 m/flood event, we find that the nested basin requires migration distances of around 0.5 m/flood event if terraces have been exposed to cosmic rays for 1000 years.

Another hypothesis is that the terraces in the Feshie basin have been exposed to cosmic rays for 4000 years, and thus have an approximate depth-averaged ^{14}C concentration of 27000 atoms/gram (see Section 2.4.3). In this scenario, terraces upstream of ALEAN require a basin-averaged retreat rate of approximately 0.2 m/flood event. Our results suggest that it may be possible to yield MILC's lower basin outlet concentration with basin-averaged retreat rates of 5 m/flood event when considering terrace production rate uncertainties. However, we know that, in this scenario (i.e., terraces exposed to cosmic rays for 4000 years), the required migration distances upstream of ALEAN are 0.2 m/flood event. When we calculate the required terrace migration rates in the nested basin between MILC and ALEAN, we find that even a terrace migration rate of 1000 m/flood event, which is unrealistic, cannot yield the measured outlet concentration at MILC. We therefore cannot explain MILC's basin outlet concentration if all terraces that are feeding material into the modern channel have relatively high ^{14}C concentrations (i.e., 27000 atoms/gram).

An alternative hypothesis to the lower concentration recorded at MILC is the possibility of younger terraces between MILC and ALEAN that are inputting lower concentration material into the river. Our basin-averaged terrace model suggests that the lower basin outlet concentration at MILC could be explained if MILC has younger catchment-averaged terraces than ALEAN, whilst the terrace migration rates remain the same (Figure 2.11). That is, if terraces upstream of ALEAN have been exposed to cosmic rays for 4000 years, then a terrace migration rate of 0.2 m/flood event is required. Likewise, if terraces in the entire MILC basin have been exposed to cosmic rays for 1000 years, then a similar terrace migration rate of 0.2 m/flood event can explain the lower basin outlet concentration. However, we know that, in this scenario, terraces upstream of ALEAN have a depth-averaged ^{14}C concentration of 27000 atoms/gram (i.e., exposed to cosmic rays for 4000 years), which means that the nested basin between ALEAN and MILC is where a change in terrace concentrations must occur if the retreat rates remain the same. If we run our mixing model and set the terraces upstream of ALEAN to 27000 atoms/gram, we find that even if the terraces in the nested basin have a ^{14}C concentration of 0 atoms/gram, then MILC's basin outlet concentration cannot be obtained. Therefore, younger terrace ages alone cannot account for MILC's basin outlet concentration as it is not possible to obtain the outlet concentration at MILC with the same migration distances as ALEAN.

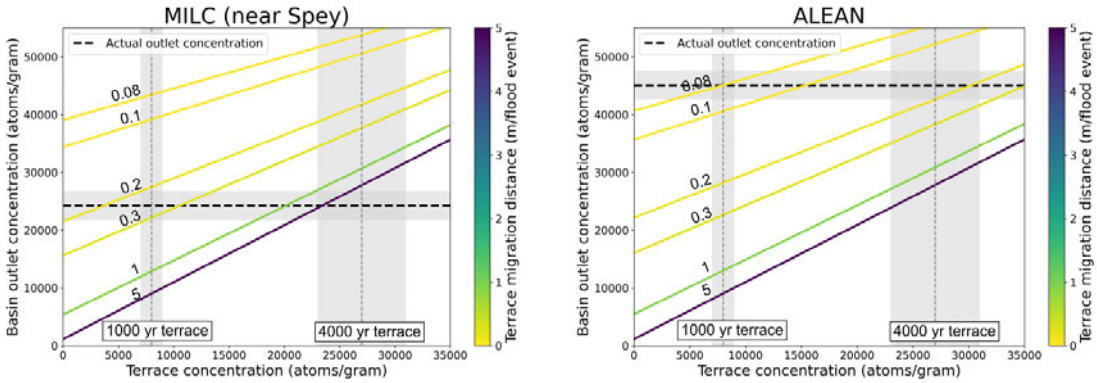

Figure 2.11: Results of the mixing model for MILC (downstream site near Spey) and ALEAN. This model considers catchment-averaged terrace migration rates, that is, all terraces upstream of each sampling location migrate at the same rates. The measured ^{14}C concentration at these sites ('actual outlet concentration') is shown by the black horizontal dashed line. Blank-corrected analytical uncertainties are shown by the grey shaded error bars on the 'actual outlet concentration'. The influence of various terrace migration distances per flood event (0.08, 0.1, 0.2, 0.3, 1, 5 m) on the predicted ^{14}C concentration at these sites is shown by the coloured lines with their corresponding terrace concentrations. Grey vertical lines represent concentrations for terrace with ages of 1000 (8000 atoms/g) and 4000 years (27000 atoms/g), with shaded 10 $\%$ error bars. These error bars represent uncertainty from terrace elevation-derived ^{14}C production rates (see Section 2.3.3). See Figure S6 in Appendix A for results at other sample sites.

2.4.4 Erosion rates from sediment fluxes

Here, we present overall sediment volumes sourced from both paraglacial terraces and 'background' material on annual timescales. Specifically, we assume that terrace material is sourced from large annual flood events, and that the 'background' denudation rate is that of the Garbhlach's, 0.175 mm/yr, for the entire Feshie basin. The volume of sediment from the terraces is the product of the migration distance (D_T), the height of the terrace banks relative to the channel (H_T) and the length of the eroded terraces (L_T). Regarding the terrace migration distances, we use the basin-averaged migration distances associated with a 1000-year-old terrace for each sample (see Section 2.4.3). We use this scenario because we can obtain realistic terrace migration rates when we mix the 'background' sediment with 1000-year-old

terraces that, importantly, have low ^{14}C concentrations. We do not use migration rates associated with 4000-year-old terraces because the modelled concentrations in these terraces are higher and require unrealistic migration rates (see Figure 2.11).

The total volume of sediment sourced from paraglacial terraces during large annual flood events is slightly lower than the 'background' sediment volume for most samples. MILC, which is the sample located near the confluence with the Spey and has the lowest basin outlet ^{14}C concentration, has a significantly higher terrace volume relative to the 'background' volume. That is, to explain MILC's low outlet concentration, we need to dilute the 'background' concentration with a larger volume of low concentration terrace material compared to the other samples which require smaller terrace volumes (due to their higher basin outlet concentrations).

We calculate erosion rates from sediment fluxes in basins with abundant paraglacial terraces (i.e., all samples except GAR). Similar to the inferred erosion rates from CAIRN, we find that these erosion rates are significantly lower than the isostatic uplift rates for the Feshie basin.

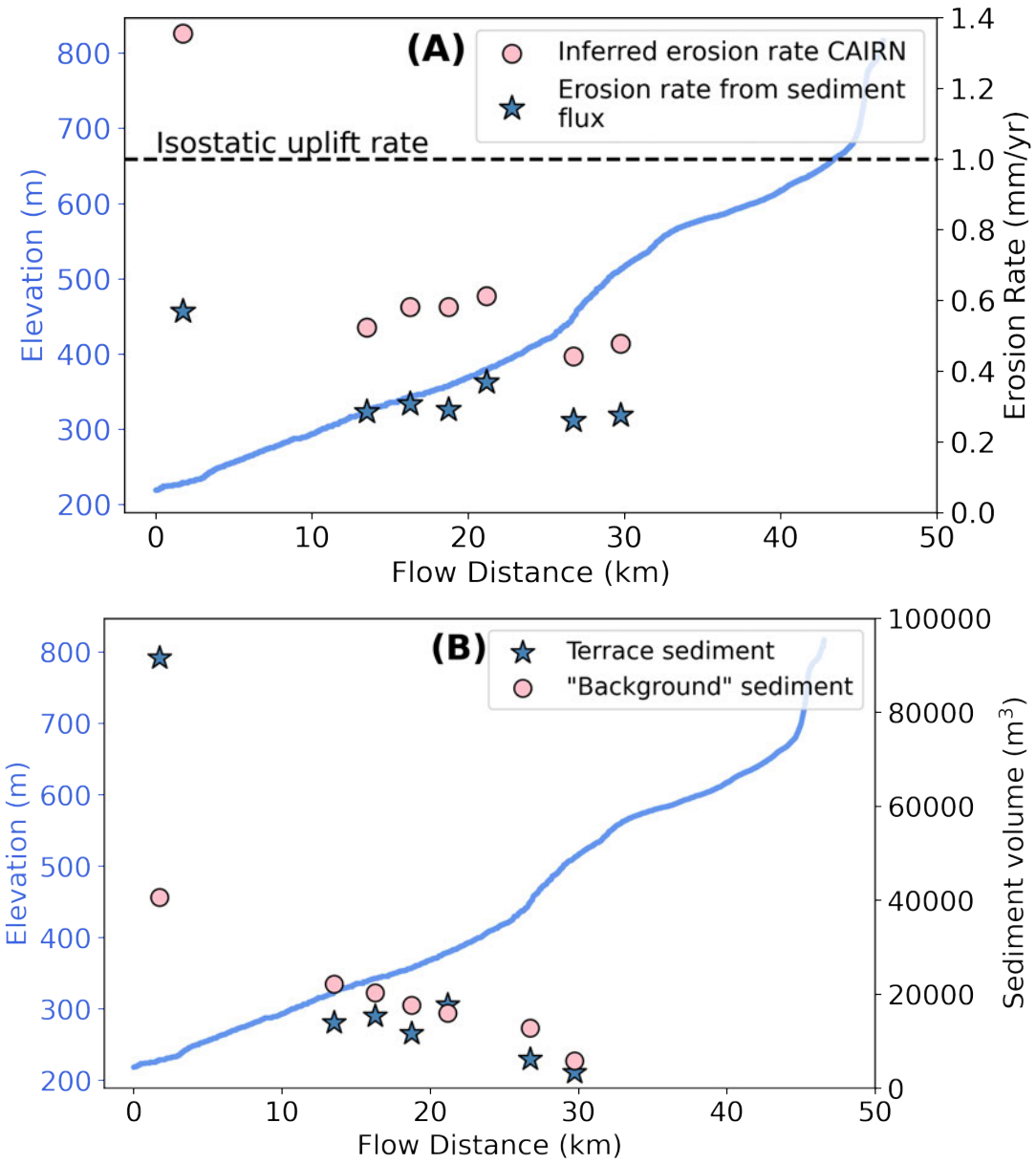

Figure 2.12: (A) CAIRN erosion rates and sediment flux erosion rates for main channel samples. Sediment flux erosion rates represent the sum of the 'background' erosion rates and the terrace erosion rates. The approximate isostatic uplift rate is marked by a black dashed line (Shennan et al., 2009). (B) Paraglacial terrace and 'background' sediment volumes for main channel samples. The background denudation rate (from CAIRN) for the Garbhlach basin, 0.175 mm/yr, was used to calculate the 'background' sediment volumes and sediment flux derived erosion rates shown in these plots. Terrace migration rates associated with a terrace age of 1000 years were used to calculate terrace volumes and erosion rates from sediment fluxes.

2.5 Discussion

2.5.1 Relationships between uplift, denudation and slope

We interpret the Garbhlach's denudation rate of 0.175 mm/yr to be representative of the true catchment-wide denudation because unlike the remainder of our sampled basins, the Garbhlach is largely devoid of transient sediment stores and the hillslopes in the Garbhlach basin appear to be connected to the channel, as shown by the "V" shaped valley. The Garbhlach's denudation rate is near the upper bound of previously reported Late Holocene bedrock incision rates in upland rivers in Scotland. Jansen et al. (2011) and Kim (2004) inferred present-day vertical incision rates of 0.07 - 0.24 mm/yr by measuring ^{10}Be concentrations of bedrock surfaces along knickpoint reaches that are assumed to be caused by base-level fall. The Garbhlach is also the steepest catchment in the Feshie basin which supports the idea that 0.175 mm/yr is likely to be an upper bound and that the real background denudation rate in the Feshie may be lower. Nonetheless, the Garbhlach's denudation rate is an order of magnitude lower than the glacial isostatic uplift rates predicted for the Feshie basin of $>$1 mm/yr (Shennan et al., 2009). We also find that erosion rates calculated from sediment fluxes, which represent the sum of the 'background' and terrace erosion rates and vary between 0.2 - 0.6 mm/yr, are lower than the isostatic uplift rate. These results support studies which have proposed that base-level signals propagating inland from the coast, which are indicated by the presence of knickpoints, have stagnated near Scotland's coastlines (Bishop et al., 2005; Castillo et al., 2013). Likewise, we also find the inferred denudation rates (0.175 - 1.356 mm/yr) do not correlate with any basin-wide topographic characteristics, such as the normalised channel steepness index. Our findings therefore align with studies which have suggested that without the renewal of relief through sustained tectonic activity or base-level lowering, post-glaciated landscapes in tectonically quiescent terrains may remain in a state of transient dynamics that last for millions of years (e.g. Ballantyne, 2002; Egholm et al., 2013; Whitbread et al., 2015). In the absence of sustained tectonic uplift, valleys are likely to maintain their glacially inherited "U" shaped topography, meaning hillslopes will remain largely decoupled from channels.

2.5.2 Variations in the spatial distribution of the inferred denudation rates

To explain the spatial distribution of our inferred denudation rates, we suggest catchments with paraglacial terraces, into which the rivers are actively eroding (inferred from flood modelling, geomorphic mapping and remote sensing observations), record apparently higher CRN denudation rates in comparison to catchments with little alluvial fill. The novel sediment mixing model presented can reproduce basin outlet ^{14}C concentrations that correlate to those observed in ^{14}C measurements, using terrace heights, lengths and realistic terrace migration distances. Thus, we interpret paraglacial terraces to be a primary source of sediment in the Feshie River which supports previous studies (Robertson-Rintoul, 1986; Young, 1976) and highlights the long-lasting impact of the glacial legacy.

Our interpretation of ^{14}C-derived denudation rates to not reflect basin-wide denudation in catchments with significant sediment storage aligns with theoretical and recent applied ^{14}C studies (e.g. Hippe, 2017; Slosson et al., 2022). For example, Slosson et al. (2022) attributed the relatively lower concentrations of ^{14}C in comparison to ^{10}Be concentrations in their study area in the Andes to the presence of complex sediment storage dynamics in hillslope deposits. Future studies should therefore carefully characterise upstream geomorphic processes when using ^{14}C to infer denudation rates, as ^{14}C concentrations appear highly sensitive to such processes due to the relatively short timescales over which ^{14}C accumulates and decays.

In our mixing model, we assume that the Garbhlach's denudation rate of 0.175 mm/yr represents the 'background' denudation rate because the Garbhlach is largely devoid of transient sediment stores. As mentioned previously, we believe this rate of 0.175 mm/yr is likely to be an upper bound as the Garbhlach is the steepest tributary catchment in the Feshie basin; the real background denudation rate in the Feshie may be lower. We find that lowering the 'background' denudation rate in our mixing model makes a minor difference to the terrace migration rates (see Figure A.S7 in Appendix A). A future research direction therefore includes sampling across a range of slope gradients where the upstream basins are devoid of sediment stores.

Studies have shown that CRN-derived erosion rates based on samples of a given grain size fraction (e.g., sand) may not give a complete picture of the denudation of the surrounding hillslopes, as sediment of different grain size fractions may experience different denudation histories: sand may originate from the abrasion of clasts during fluvial transport, whereas larger clasts may originate from processes such as deep-seated landslides (e.g. Belmont et al., 2007; Lupker et al., 2017). This may challenge the interpretation of the GAR sample (0.175 mm/yr) which is assumed to represent basin-wide denudation. However, field observations of hillslope material in the Garbhlach basin show abundant sand in soils within hillslope material and debris flows (see Figure A.S8 in Appendix A), due to the granite weathering by granular disintegration in this climate. This observation suggests that the sand sampled in the Garbhlach is representative of surrounding hillslope erosion from debris flows and plateau erosional processes. Extracting ^{14}C concentrations from the pebble fraction would shed further light on this theory.

2.5.3 Terrace migration and terrace ages in Scottish rivers

The modelled terrace migration distances presented in Section 2.4.3 are basin-averaged (and nested basin-averaged), that is, the model assumes that all terraces connected to the channel at high flow erode at the same rate. The migration rates we have calculated appear reasonable for such an active river, which is a characteristic feature of the Feshie (e.g. Ballantyne, 2019; Rumsby et al., 2008; Williams et al., 2020). We found that terraces migration rates between 0.08 and 0.5 meters per flood event are required to explain our measured ^{14}C concentrations. However, it is unlikely that terraces migrate at the same rate across the catchment: the values we derived may instead represent an average that reflects a mix between sections that erode slowly and terrace reaches that experience large amounts of geomorphic change locally. For example, through flood modelling, Fieman et al. (2020) did not observe widespread change in the channel planform along the 140 km long River Dee, Aberdeenshire, following Storm Frank ($>$200 year recurrence interval). Instead, they observed meter-scale change at the reach scale (1 km). Our results show that to obtain MILC's basin outlet concentration, the terrace migration distances must be higher between the MILC and ALEAN sampling locations, even when taking into account production rate uncertainties and terrace age variations. This supports the idea that significant geomorphic changes may occur locally, as exemplified by the 5-km reach downstream

of the confluence with the Fhearnasdail tributary. Satellite imagery observations show this reach to be exceptionally braided with tens of meters of bank migration observed between 2006 and 2019 (Figure 2.3). Repeat topographic surveys and bank inundation modelling would shed light on the spatial distribution, timing and frequency of terrace erosion (e.g. Williams et al., 2020,1).

The mixing model presented in equation (2.9) assumes that the total height of a terrace column collapses into the river during a flood event. It is likely, however, that not all terraces eroded through total column collapse during the flood event before sample collection. That is, some terraces may have eroded by undercutting alone, meaning that only their base was eroded, while others may have eroded from top collapse, due to destabilisation of the base from previous flood events. If we consider a scenario where all three mechanisms of terrace collapse occur throughout the Feshie basin, then the average concentration of ^{14}C coming from the terraces will be similar to a scenario where we only consider total column collapse. For example, if terraces in the Feshie formed 1000 years ago and have an average total height of 2.2 m, with one third eroding due to undercutting (e.g. depth from surface = 1.1 to 2.2 m, average terrace concentration = 4000 atoms/g), one third eroding from the terrace top collapsing (e.g. depth from surface = 0 to 1.1 m, average terrace concentration = 12000 atoms/g), and one third eroding based on total terrace thickness (e.g. average terrace concentration = 8000 atoms/g), then the average terrace concentration (8000 atoms/g) is the same as concentrations from the terrace erosion model based on the total terrace column thickness alone. In addition, a combination of terrace erosion mechanisms (i.e., undercutting, top collapse, and total column collapse) would also mean that the average terrace height in equation (2.9) would be lower than a scenario where we just consider the whole terrace column collapsing. The basin average terrace retreat rates would therefore be higher in a scenario where terraces erode by various mechanisms.

A future research direction includes constraining the concentrations of paraglacial terraces in the Feshie basin, which would shed light on their ages and burial history. Designing a sampling strategy to correlate preserved terraces by terrace height (relative to the channel) appears challenging, however. Field observations of bedrock reaches (e.g. bedrock knickzone marked on Figure 2.2, bedrock reach at the bridge downstream from sample ALEAN) between alluvial reaches suggests terraces could

be longitudinally disconnected. This means that inferring basin-wide terrace ages (from a small number of sampled terrace profiles) by terrace heights requires careful consideration of the aforementioned geographical, morphological and temporal complexities.

In the terrace column model, we assume there is no initial ^{14}C concentration, on the basis that the material was buried deep enough before the formation of the terrace such that all pre-existing ^{14}C had decayed. This latter assumption may not perfectly reflect reality: some of the sediment in the terraces may have come from upstream sediment sources (e.g., hillslopes, terraces) during episodes of floodplain aggradation in the Holocene. As a result, the sediment may not have been completely shielded until terrace formation, potentially leading to higher ^{14}C concentrations in the terraces than those modelled in this study (see Section 2.4.3). As discussed in the previous paragraph, we highlight the dating of terraces in the Feshie basin as a future research direction.

2.5.4 Choice of cosmogenic radionuclide to infer denudation rates in post-glacial landscapes

The average integration timescale of the denudation rate for the Garbhlach basin is approximately 3400 years (Lal, 1991). According to this integration timescale, it could be possible to constrain denudation rates with ^{10}Be in high-relief basins with complex Late Pleistocene glacial histories. However, it is important to consider that the erosion rates and integration timescales are catchment averaged, and that in reality, a basin will very rarely erode uniformly; some areas will undergo faster denudation, while others will erode more slowly. Regarding the Garbhlach basin, it is likely that its upper reaches, which drain the low-relief Cairngorm plateau (see Figure 2.1), erode at a lower rate than the catchment-averaged rate, and potentially integrate over the Late Pleistocene. For example, denudation rates lower than approximately 0.05 mm/yr would integrate over the Late Pleistocene, when the Feshie catchment may have been glaciated (Chandler et al., 2019; Sissons, 1974)). The long half-life of ^{10}Be (1.39 Myr) relative to ^{14}C (5700 years) means that ^{10}Be would contain larger amounts of uncertainty from prior exposure during interglacial and interstadial periods. The short half-life of ^{14}C means that inferred denudation rates from ^{14}C atoms in stream sediments will mainly reflect Holocene denudation rates and sediment storage dynamics.

^{14}C is therefore particularly useful for understanding landscape evolution in regions with complex Pleistocene glacial histories. Moreover, sediment grains in glacial and paraglacial deposits (e.g., till, paraglacial terraces), which we suggest contribute to the modern channel sediment flux, may have been transported across topographic divides with different glacial histories. Understanding the inherited component of ^{10}Be (due to its long half-life) in these sediment stores is challenging.

2.6 Conclusions

In this study, we calculate Scotland's first denudation rates over millennial scales from ^{14}C concentrations in stream sediments. We counter-intuitively find the inferred denudation rates (0.175 - 1.356 mm/yr) do not correlate with any basin-wide topographic characteristics (e.g. slope) and are, on average, lower than the glacial isostatic uplift rates predicted for the Feshie basin of $>$1 mm/yr.

We find that catchments with paraglacial terraces into which the rivers are actively eroding (inferred from field observations, flood modelling and geomorphic mapping) record apparently higher CRN denudation rates in comparison to catchments with little alluvial fill. Terraces are expected to deliver lower concentration material because terrace material has experienced CRN decay with depth and terraces were buried until the last phase of major Holocene incision (post-4000 years). The steepest tributary catchment of the Feshie River, the Garbhlach, which is largely devoid of terraces, records an apparent denudation rate of 0.175 mm/yr, providing an upper bound on the background erosion rate in the Feshie. We propose that the higher apparent denudation rates along the main stem of the Feshie River and the Lorgaidh tributary result from the mixing of 'background' sediment with low-CRN-concentration material derived from terrace erosion. These results suggest that ^{14}C-derived denudation rates in catchments with paraglacial terraces are not representative of true catchment-averaged denudation rates because the ^{14}C concentrations can be influenced by short-lived sediment routing and storage processes due to the isotope's short half-life (5700 years).

We present a sediment mixing model which combines the 'background' sediment from catchment-wide denudation with sediment derived from the incision of paraglacial terraces. We model terrace migration distances between major flood events and calculate the ^{14}C concentration at each sampling location using two terrace age scenarios (1000 and 4000-year old). We demonstrate that the samples from the upper and middle sections of the Feshie basin require similar catchment-averaged terrace migration distances of 0.08 m/flood event (1000-year old terraces) to produce the observed ^{14}C concentrations, when considering a flood event with a return period of around 5 years. We show that the lower area of the Feshie basin requires higher terrace migration distances (e.g. 0.5 m/flood event for the area between ALEAN and MILC for 1000 year scenario) to obtain the measured ^{14}C concentration at the downstream-most sampling site. These rates are compatible with terrace migration rates derived from satellite imagery between 2006 and 2019. These novel results highlight the long-lasting impacts of the glacial legacy on sediment dynamics and indicate that future studies should carefully characterise upstream geomorphic processes when using ^{14}C to infer denudation rates.

Chapter 3

Controls on fluvial grain sizes in post-glacial landscapes

Simon Mudd, Mikael Attal, Fiona Clubb and I conceptualised the study. I directed the project, processed and visualised the data and wrote the manuscript with input from all authors.

This chapter has been submitted as a manuscript to *Earth Surface Dynamics* and can be viewed as a preprint at https://doi.org/10.5194/egusphere-2024-3084.

Abstract

The grain sizes of sediments in channels have been linked to landscape characteristics, such as flow distance from headwaters, topographic relief, lithology and climate, in landscapes with little past or present glacial influence. Few studies have explored the controls on sediment characteristics in formerly glaciated landscapes. In this study, we document river surface grain sizes at 279 localities across Scotland. We collect photographs of gravel bars through a citizen science survey, Scotland's Big Sediment Survey. Grain sizes distributions are extracted from the photographs using both manual and automated techniques. We investigate whether grain sizes can be correlated and predicted from environmental variables (e.g., basin slope, flow distance from headwaters) through Spearman's correlation statistics and random forest regression modelling. In contrast to other studies that have primarily focused on non-glaciated landscapes, we find no apparent controls on surface grain sizes in channels across Scotland. Specifically, we find no significant Spearman's relationships between d84 and environmental variables; the strongest relationship was found between d84 and average basin aridity with a weak r^2 value of 0.29. We also find that the predictability of our random forest model is poor and only captures 22% of the variance of d84. We find no correlation between grain size and flow competence, which suggests that sediment is both transport-limited and supply-limited. We propose that Scotland's post-glacial legacy drives the lack of sedimentological trends documented in this study, and that changes in landscape morphology and sediment sources caused by glacial processes lead to a complete decoupling between fluvial sediment grain size and environmental variables. This interpretation aligns with other studies that have highlighted the ongoing role of the post-glacial legacy on landscape evolution in tectonically quiescent terrains, both in Scotland and globally. Our results suggest that fluvial sediment grain size cannot be predicted by a global model based on environmental variables in post-glacial landscapes.

3.1 Introduction

The delivery of sediments through river basins influences river morphology, hazards (e.g., flood risk), habitat value (e.g., spawning of salmonids) and landscape response to climatic and tectonic forcings. The characteristics of sediments delivered from hillslopes to fluvial systems influences the properties of sediments transported by

rivers which are eventually exported to terminal sedimentary sinks (e.g., lacustrine and coastal environments, Attal and Lavé, 2006; Parker, 1991; Sklar et al., 2006; Whittaker et al., 2010).

Bed grain sizes, the focus of this study, are a key characteristic for understanding fluvial environments. For example, bed grain sizes influence river transport conditions, provide information on sediment sources, control rates of bedrock incision (e.g., Sklar and Dietrich, 2004) and the width of channels (e.g. Baynes et al., 2020; Finnegan et al., 2005; Li et al., 2020a,2). Initial grain size distributions delivered to rivers are controlled by fragmentation, weathering and rock mass structure (e.g., Sklar, 2001; Sklar et al., 2017; Wells et al., 2008). Individual sediment particles then reduce in size, primarily by abrasion, during downstream fluvial transport (Sternberg, 1875). The distributions of fluvial grain sizes have therefore been correlated to the longitudinal flow distance along a channel (e.g., Gomez et al., 2001; Moussavi-Harami et al., 2004; Rice and Church, 1998; Sklar et al., 2006). Downstream fining trends can be offset by variations in the supply of sediment (e.g., sediment input from landslides) and the transport ability of a channel (e.g., Attal and Lavé, 2006; Attal et al., 2015; Sklar et al., 2006).

A handful of studies have further explored the effects of landscape characteristics, such as topography, lithology and climate, on the size distributions of channel sediments at the local scale. For example, hillslope gradient has been shown to be one of the most important topographic controls on grain sizes (Sklar et al., 2017), and several studies have shown fluvial grain sizes to increase with hillslope steepness (e.g., Attal et al., 2015; Purinton and Bookhagen, 2021; Whittaker et al., 2010). Attal et al. (2015) found hillslope grain sizes to increase with hillslope steepness and erosion rates in the Feather River basin, Northern California. They showed an increase in the channel sediment grain sizes to arise from an increase in the flow competence (i.e., ability of a river to transport sediment) and changes in hillslope sediment sources from soil-mantled to mass-wasting processes (e.g., landslides, debris flows). A similar trend was documented by Whittaker et al. (2010) in the Appenine Mountains of Italy, whereby coarser fluvial grain sizes were measured in landslide-dominated areas. Likewise, the importance of lithology in controlling bedload characteristics, including grain sizes, has been demonstrated by several studies (e.g., Mueller and Pitlick, 2013; Purinton and Bookhagen, 2021; Sklar et al., 2020). For example, Mueller and

Pitlick (2013) showed that more erodible rock types, such as sedimentary rocks, were associated with higher sediment yields in comparison to more resistance rocks, such as granitic rocks, in the Rocky Mountains, USA.

Studies have tested the predictability and controls of fluvial grain sizes and sediment substrate cover at large spatial scales by documenting sediment characteristics across multiple basins with gradients in topography, lithology, climate and hydrology (Abeshu et al., 2021; Haddadchi et al., 2018; Mugodo et al., 2006; Snelder et al., 2011). Given the large spatial extent of these studies, they have focused on applying data-driven machine learning techniques, such as a random forest regressor. These empirical models have used readily available environmental variables that broadly reflect the upstream network structure and sediment source characteristics of each locality, such as flow distance, basin slope, lithology and precipitation indices. Snelder et al. (2011) found that surface grain sizes could be reasonably well predicted from a random forest model for rivers across France which, outside high mountain environments, has largely not been glaciated. Their study found an r^2 value of 0.52 between the observed and predicted values, and identified channel slope, basin averaged slope and rock hardness to be the most important variables controlling the modelled grain sizes.

Research into controls on bedload grain sizes has largely focused on landscapes with no past or present glacial influence. Formerly glaciated landscapes are typically more complex than landscapes with no glacial influence. Key challenges associated with understanding geomorphic processes in post-glacial landscapes originate from the glacial modification of hillslopes and channels, such as decoupling of hillslopes from channels due to the over-deepening and widening of valleys by glaciers, or extensive glacial sediment drapes (e.g., till, moraines, paraglacial terraces) which influence sediment supply and transport capacity (Attal and Lavé, 2006; Ballantyne, 2019; Mason and Polvi, 2023; Reid et al., 2022; Whitbread et al., 2015). Such areas represent a significant fraction of global land (e.g., most of the UK, Scandinavia, North America) and their extent will inevitably grow as a result of glacial retreat driven by climate change. A key research avenue therefore includes exploring the applicability of global predictive grain size models, such as that proposed by Snelder et al. (2011) which was tested in a largely non-glaciated landscape, to post-glacial landscapes.

In this study, we adopt a similar approach to Snelder et al. (2011) and test whether grain sizes can be predicted in Scottish river basins. Scotland was deglaciated around 12 kyr ago following the disappearance of the British-Irish Ice Sheet (Ballantyne, 2019; Clark et al., 2018; Firth and Stewart, 2000; Shennan et al., 2009). Scotland has subsequently been in a phase of glacial isostatic uplift, with average present-day rates varying between 0.5 and 1.2 m/kyr (Bradley et al., 2023). Many Scottish river basins exhibit typical features of post-glacial landscapes, such as U-shaped valleys and paraglacial sediment stores, many of which contribute large quantities of material to modern rivers (e.g., Ballantyne, 2008). We consider the hypothesis that grain sizes can be reasonably well predicted from environmental variables similar to those outlined by Snelder et al. (2011) in Scottish river basins. That is, we question if 12000 years is a sufficient period to allow a formerly glaciated landscape to adjust its sediment characteristics to reflect local fluvial conditions. The corresponding null hypothesis is that grain sizes cannot be predicted.

To test our hypotheses, we develop a photograph-based methodology for gathering a spatially extensive dataset of grain size distributions. After a description of our photograph-based methodology, we describe the predictive variables and the random forest regressor model. Subsequently, we present our model predictions and discuss the complexities associated with documenting large-scale trends and controls on fluvial grain sizes in post-glacial landscapes.

3.2 Methods

3.2.1 Grain size data collection

Sediment characteristics, including grain sizes, are poorly documented in Scotland. In light of the limited grain size data available and the time-consuming nature of traditional field sediment surveys (Bunte and Abt, 2001; Wolman, 1954), we gathered surface sediment size data through a citizen science project, Scotland's Big Sediment Survey (SBSS). SBSS was designed through ESRI's Survey123 platform (https://survey123.arcgis.com/). Users were asked for two types of photographs: a context photograph of the sediment deposit, and a surface photograph of the sediment bar (see Figure 3.1 for examples). Users were requested to include an object for scale in the surface photograph (e.g., penknife, plastic card) and to take the photograph parallel to the bar from a known height (e.g., person's height, chest-height). Both of these measurements were then recorded by the user on the Survey123 form. Users provided the location of the sediment bar through either dropping a pin on a map (which was provided on the survey platform), uploading a geographic position or enabling the camera's location feature. Prior to sediment grain size extraction, all photographs and corresponding survey information were pre-screened for quality assurance (e.g. photos were removed with spurious locations). A total of 275 locations were obtained across Scotland from SBSS (Figure 3.1).

In addition to the locations collected through SBSS, we used Wolman Point Counts (Wolman, 1954) to survey the intermediate axis of 100 clasts at four locations (see Figure 3.1 for locations). At these sites, a tape measure was positioned on the sediment bar parallel to the river's flow direction, and sediment grains were measured every 50 cm.

3.2.2 Grain size extraction methods: PebbleCounts and manual counting

We examine trends in sediment sizes through photo-based measurements of the intermediate axis (b-axis) which we extract through automated and manual techniques. Automated and semi-automated techniques have received significant attention in recent years because they are typically less time-consuming and can be used to obtain

a larger sample size (Harvey et al., 2022; Purinton and Bookhagen, 2019). Automated algorithms include both image segmentation (e.g., Detert and Weitbrecht, 2013; Purinton and Bookhagen, 2019) and texture-based approaches (e.g., Brasington et al., 2012; Westoby et al., 2015).

In this study, we apply PebbleCountsAuto which is an automated grain segmentation algorithm (Purinton and Bookhagen, 2019). PebbleCountsAuto initiates the segmentation process from both the grain colour and interstices. The algorithm then fits an ellipse to the segmented area from which the pebbles axes values are extracted. Purinton and Bookhagen (2019) compared PebbleCountsAuto to a manually measured control dataset at 12 sites in North-West Argentina and reported an average mean error of 0.15 ψ across several percentiles, where ψ represents the negation of the ϕ unit typically used to describe grain size data ($\psi = -\phi$ = log2(mm)). In this study, we also compare PebbleCountsAuto results to a manually measured control dataset, the procedures of which are described below.

Images are scaled in PebbleCountsAuto from the camera resolution, R, which is calculated from the camera's sensor height or width, S, focal length, f, image height or width, I, and the camera height, h, the latter of which is recorded in the survey data. The camera resolution is given by:

$$R = \frac{Sh}{fI} \tag{3.1}$$

In this study, the average and maximum resolution of images processed through PebbleCountsAuto were 0.54 mm/pixel and 1.05 mm/pixel respectively. The lower detection limit of a pebble's b-axis length in PebbleCountsAuto is 20 pixels which equates to a minimum b-axis length of 21 mm with our maximum camera resolution of 1.05 mm/pixel. We conservatively truncate the grain size distributions at 25 mm for all photographs.

A potential user-derived uncertainty associated with the camera resolution of the photographs and the final grain size measurements originates from the height at which the photographs were taken. We perform a sensitivity analysis to test the influence of camera height on camera resolution with a standard consumer-grade camera (e.g., sensor height = 4.55 mm, focal length = 4.3 mm, image height = 3024

pixels). For example, an increase in height of 15 cm increases the camera resolution by 0.05 mm/pixel. Thus, for our average camera resolution of 0.54 mm/pixel, an increase in camera height by 15 cm increases the final grain size measurements by ≈ 10 % (see Table B.S2 in Appendix B for full sensitivity analysis). We further discuss the overall influence of camera height-derived uncertainties in the sample comparison (Section 3.2.2).

Photos that could not be processed through PebbleCountsAuto due to issues with calculating camera resolutions (e.g., missing metadata) or significant segmentation faults were manually processed by overlaying a regular square grid with 100 line intersections (Kellerhals and Bray, 1971). Clasts were scaled according to the object placed in the image and the object's corresponding dimensions which were recorded on the survey platform. Ideally, the size of the grid applied to the photographs should be chosen so that no more than one grid intersection falls on one pebble. However, such a requirement is nearly impossible to fulfil where large grains span multiple intersections. Clasts that cover grid intersections *n* times were therefore counted *n* times following the voidless cube model presented by Kellerhals and Bray (1971). Overall, 37 % of the images obtained through SBSS were processed through PebbleCountsAuto and 63 % were processed manually.

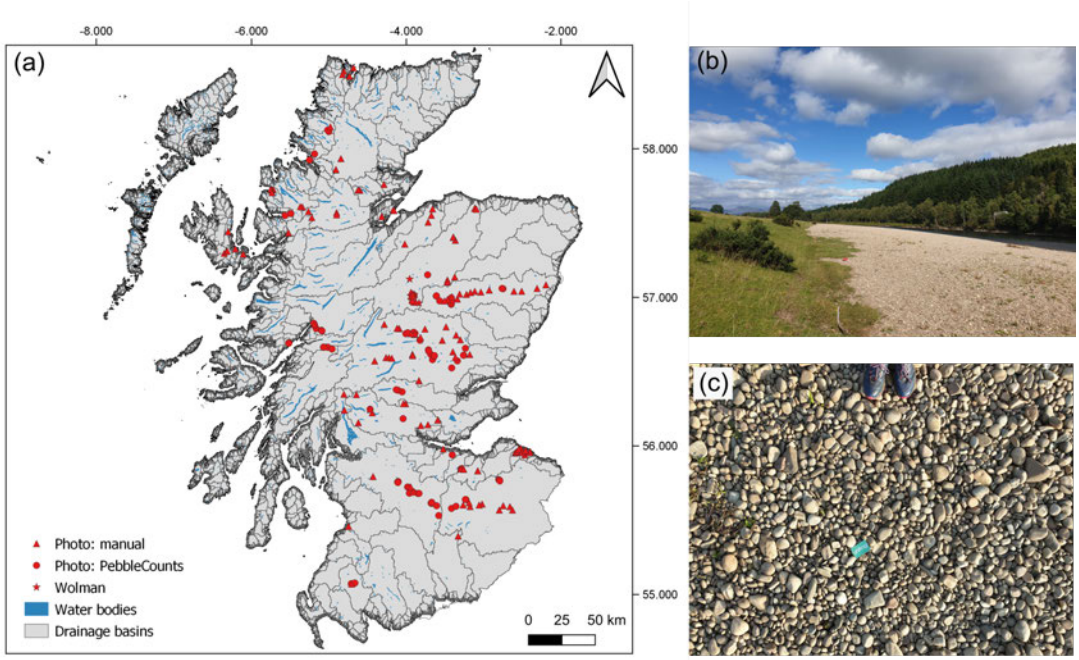

Figure 3.1: (a) Map of Scotland (focused on the mainland) showing 279 surveyed locations. Circles represent samples processed with PebbleCountsAuto, triangles show manually clicked sites, and stars represent samples measured using Wolman Point Counts. Water bodies are shown in dark blue and drainage basin outlines (15 arc-second resolution) in black (sourced from the HydroLAKES and HydroBASINS databases, (Lehner and Grill, 2013; Messager et al., 2016)). **(b)** Context photograph of gravel bar. **(c)** Top-down, surface photograph of sediment with a card that is 8.5 cm in length for scale.

Comparison between grain sizing tools

To test the performance of PebbleCountsAuto, we compare the apparent 50^{th} (d50) and 84^{th} (d84) percentiles at 9 sites in the Tay basin to a manually measured control dataset. These sites represent a range of pebble sizes and lithologies, spanning from the Tay's source in the Highlands to upstream of its estuary (see Table B.S1 in Appendix B for sample locations). All 9 sites have an image resolution of 0.47 mm/pixel. We exclude grains with a b-axis below 25 mm which is consistent with the minimum truncation value that we apply to our Scotland-wide dataset (see Section 3.2.2). We compare the 50^{th} and 84^{th} percentiles in mm by the mean error (*me*), normalised root mean squared error (*nrmse*) and r-squared linear regression coefficient (r^2). We also compare the 50^{th} and 84^{th} percentiles derived from PebbleCounts and the manually measured dataset using t-tests.

Error bars are plotted on both the manual and PebbleCounts measurements in Figure 3.2. With regards to our manually measured samples, we assess the impact of the largest clast covering multiple grid nodes using the method presented by Attal et al. (2015). Firstly, the largest clast was removed from the grain size distribution to estimate d50 and d84 percentiles; secondly, a large clast of the same size as our largest clast was added, covering the same number of grid nodes. Error bars on manually measured grain size figures represent the range of values between these scenarios. For PebbleCountsAuto measurements, we plot error values of +/- 10% to account for potential uncertainties associated with the height of the photograph. An uncertainty of $\approx$ 10% represents a change in camera height by 15 cm for a camera resolution of 0.47 mm/pixel (see Section 3.2.2).

We find that PebbleCountsAuto generally underestimates the grain sizes compared to manual measurements of photos, especially at the localities with larger grain sizes (sample sites 6-9, Figure 3.2). The PebbleCounts d84 measurements are statistically similar (p-value from t-test $>$ 0.05, r^2 = 0.94) to the manual measurements whereas the d50 percentiles are different (p-value $<$ 0.05, r^2 = 0.73). Likewise, the d84 comparison has a lower *nrmse* (0.28) than the d50 comparison (*nrmse* = 0.44, Figure 3.2).

Our PebbleCounts comparison aligns with results from other studies that have compared PebbleCounts to manually measured datasets (e.g., Chardon et al., 2022; Miazza et al., 2024). In line with our findings, these studies have shown that PebbleCounts generally underestimates grain sizes. These studies attributed these trends to over-segmentation issues which arise from inter-granular textures (e.g., veins, fractures), and irregular shadowing (Figure 3.2c). Visual observations of our PebbleCounts output images suggest that larger grains have more inter-granular textures (e.g., veins, fractures), which may explain the apparent over-segmentation at locations with larger grain size distributions (sample sites 6-9, Figure 3.2). Given the lower errors associated with the d84 percentile, we focus our analysis on this percentile.

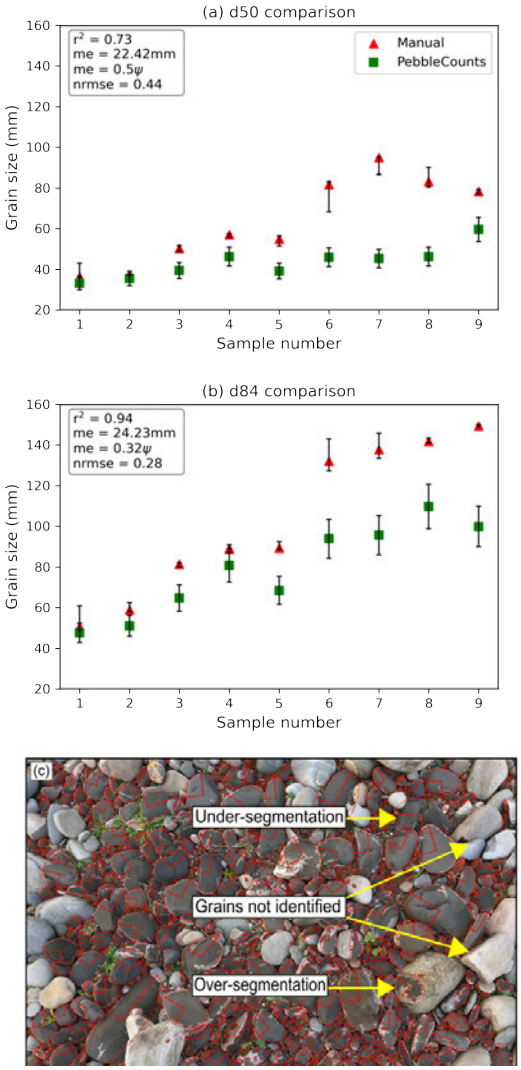

Figure 3.2: Figures **(a)** and **(b)** show comparisons between PebbleCounts and the manually measured control dataset at 9 sites in the Tay basin (see Table B.S1 in Appendix B for sample locations). Error bars are plotted according to the procedure outlined in Section 3.2.2. The mean error (*me*), normalised root mean squared error (*nrmse*) and r-squared linear regression coefficient (r^2) are shown on figures **(a)** and **(b)**. Figure **(c)** shows an example of an output image from PebbleCounts. Common errors such as under-segmentation, over-segmentation and undetected grains are highlighted.

3.2.3 Selection of environmental variables

We test the applicability of global empirical grain size models (e.g., Abeshu et al., 2021; Snelder et al., 2011) to Scottish river basins by using similar environmental variables and Machine Learning techniques. For each sample, we determine channel slope, elevation and flow distance in LSDTopoTools (Mudd et al., 2023) from a 5 m Digital Terrain Model (DTM) sourced from the Ordnance Survey (Ordnance Survey, 2021). Channel slope was averaged over 100 m. We delineate the upstream contributing basin area, and then calculate basin-averaged topographic metrics including basin area, slope and drainage density. We record basin-averaged aridity for each sample from a global aridity map by Zomer et al. (2022). For each of the sampled sites, we measure bankfull channel width from Bing Satellite Imagery. We define bankfull width as the distance orthogonal to the flow direction between either bedrock banks or the limit of vegetated bars on the edge of channels (e.g., Baynes et al., 2020).

Like other global empirical grain size studies, we calculate average bedrock erodibility of each sample's upstream basin. We attribute an erodibility value to every lithological unit present on a geological map of Scotland sourced from the British Geological Survey (BGS, 2021). We estimate each lithology's erodibility using an index developed by Campforts et al. (2020) and Clubb et al. (2023). The lithological erodibility index, L_E, incorporates approximations of rock strength, L_L, and the degree of metamorphism, L_M, on the assumption that stronger and highly metamorphosed rocks are less erodible (Clubb et al., 2023). L_E assumes that the erodibility of a unit is based on L_L and L_M for non-igneous rocks, and L_L alone for igneous rocks. L_L ranges from 2 (e.g., granite, gneiss) to 12 (e.g., unconsolidated deposits). Similarly, L_M varies from 2 (highly metamorphosed) to 12 (unmetamorphosed); sedimentary rocks are classified as unmetamorphosed. The lithological erodibility, L_E, is calculated as:

$$L_E = \frac{2}{7} L' \tag{3.2}$$

$$L' = \begin{cases} \dfrac{(L_M + L_L)}{3}, & \text{non-igneous rocks} \\ \dfrac{L_L}{2}, & \text{igneous rocks} \end{cases} \tag{3.3}$$

We refer the reader to Figure B.S2 in Appendix B for the lithological erodibility map of Scotland.

Finally, we document the percentages of peat, alluvium, glacial till and glaciofluvial material in each sample's upstream basin (Haddadchi et al., 2018; Snelder et al., 2011). Superficial maps were downloaded from the British Geological Survey (BGS, 2021). A list of the environmental variables is provided in Table 3.1.

Variable Name	Description	Data source
Aridity index	Mean basin ratio of annual mean potential evaporation to annual mean precipitation	Zomer et al. (2022)
Drainage density	Total stream length divided by drainage area	5 m DTM from Ordnance Survey (2021)
Drainage area	Upstream contributing basin area	
Basin slope	Mean basin slope	
Channel slope	Channel slope of sample averaged over 100 m upstream	
Channel elevation	Elevation of sample	
Flow distance	Longitudinal flow distance from a channel's most upstream source. A contributing area of 0.125 km^2 was used to define the beginning of a channel.	
Bankfull channel width	Distance orthogonal to the flow direction measured between banks	Bing Satellite imagery
Basin bedrock erodibility	Mean basin bedrock erodibility	BGS (2021), bedrock layer
Percentage of Till in catchment	Material deposited underneath a glacier without subsequent fluvial reworking	BGS (2021), superficial layer
Percentage of Alluvium in catchment	Material deposited by rivers	
Percentage of Glaciofluvial in catchment	Material deposited by glacial meltwater streams	
Percentage of Peat in catchment	Partially decomposed mass of vegetation	

Table 3.1: Description of environmental variables and their data sources.

3.2.4 Random forest regressor model

To assess the relative importance of the environmental variables in controlling grain sizes, we apply the same methodology as Snelder et al. (2011) and use a random forest regression (RFR). RFR is a form of supervised Machine Learning which uses an ensemble of decision trees to predict a target variable (Breiman, 2001). Predictions are made by formulating unforeseen, multi-dimensional relationships between the input features. The model performance and apparent feature importance can then be evaluated by assessing the correlation between the observed and predicted grain sizes. In this study, we perform a leave-one-out-cross-validation (LOOCV) which trains the model on all but one sample and then evaluates the performance of the model on the excluded data point. This process is then repeated for each data point.

3.2.5 Flow Competence and sediment entrainment

In a scenario where all grain sizes are available for transport, the grain size of the sediment mobilized by a river is expected to increase with flow competence (Bathurst, 2013; Ferguson and Ashworth, 1991; Whitaker and Potts, 2007). In this case, the grain size can be considered 'transport-limited', that is, limited by the ability of the river to transport a given grain size. In some situations, rivers are only provided with fine grained sediment; in such systems where there is a lack of coarse grains available for transport, the grain size mobilized by the river will be 'supply-limited' (Attal et al., 2015). Thus, the relationship between flow competence and grain size can provide information on sediment supply-limited and transport-limited conditions. Both scenarios may arise in our study area due to post-glacial processes affecting the distribution of sediment stores and the transport ability of channels. We therefore analyse this relationship to assess whether trends can be observed, that may reflect the dominance of one or the other of these conditions.

Flow competence is typically expressed as a function of shear stress (e.g., Buffington and Montgomery, 1997; Mueller and Pitlick, 2014), which is calculated from the hydraulic radius of a channel and other parameters (Shields, 1936). However, the hydraulic radius can be challenging to measure due to access to sampling locations, identification of reference conditions (e.g., reference discharge) for comparison

across all sites, and unmanageable sample sizes. An alternative approach consists of using the relationship between unit discharge and grain size that has been explored by researchers based on experimental work and field data (Attal et al., 2015; Bathurst, 2013; Whitaker and Potts, 2007). In its simplest form, the equation is:

$$q_{ci} = aD_i^b \tag{3.4}$$

where q_{ci} is the critical unit discharge required for the entrainment of sediment of grain size D_i, a is a coefficient and b an exponent that should take the value of 1.5 for sediment of uniform grain size (Bathurst, 2013; Whitaker and Potts, 2007). The b exponent was found to vary between 0.15 and 1.3 based on a compilation of field data by Bathurst (2013) and Whitaker and Potts (2007), with the values being self-consistent within given datasets, and seemingly dependent on the flow regime (rainfall versus snowmelt-dominated; Bathurst (2013)), sampling method, and the definition of the grain size of interest D_i (taken as D_{max} in the study by (Whitaker and Potts, 2007)). Importantly, both studies showed a strong dependency of the relationship to the channel slope S. Considering that our dataset includes channel slopes spanning orders of magnitude, we believe that using a relationship that includes S as a controlling variable is essential.

Bathurst et al. (1987) proposed the following equation based on flume experiments using sediment of uniform grain size in the range 3-44 mm and slopes ranging between 0.0025 and 0.2 m/m:

$$q_c = 0.15 g^{0.5} D^{1.5} S^{-M} \tag{3.5}$$

where q_c is the critical unit discharge required for the entrainment of sediment of grain size D, g is the acceleration due to gravity and M is an exponent found to vary in a narrow range: Bathurst et al. (1987) found a value of 1.12 in their experiments, while Bathurst (2013) found a value of 1.15 based on a compilation of flume data, close to the value of 1.17 'derived by Schoklitsch (1962) from the Shields equation and Manning-Strickler flow resistance equation'.

Equation 3.5 can be rearranged as:

$$D = [0.15 g^{0.5} Q S^M / W]^{2/3} \tag{3.6}$$

where W is channel width and Q the discharge. If sediment grain size is transport-limited, i.e., controlled by flow competence, a power relationship can therefore be expected between the grain size D and the quantity ω_m (Attal et al., 2015), where

$$\omega_m = Q S^M / W. \tag{3.7}$$

For the purpose of this Scotland-wide analysis, we assume that drainage area A can be used as a proxy for discharge and use the variable ω'_m that substitutes Q for A:

$$\omega'_m = A S^M / W \tag{3.8}$$

Attal et al. (2015) had found a significant power relationship between the grain size of surface sediment and ω'_m in tributaries of the Feather River, Sierra Nevada, California. The exponent derived from their dataset was 0.61, 0.53 and 0.4 for d50, d84 and d100, respectively, with an exponent closest to the expected 2/3 value for the median grain size d50.

Here, we use a value of 1.15 for the exponent M (Attal et al., 2015). We use the measured bankfull width (described in Section 3.2.3) to calculate ω'_m and make the assumption that the modelled percentiles (d50 and d84) are transported during the bankfull width's corresponding flow conditions, which is, by definition, the bankfull flow.

3.3 Results

In this section, we present the following results: (1) national-scale map of grain sizes, (2) correlations between grain sizes and environmental variables outlined in Table 3.1, (3) RFR predictions and associated variable importances, and (4) flow competence analysis. We convert our grain size percentiles to the typical ψ scale for correlation statistics and RFR analysis. This allows direct comparison of statistical results with Snelder et al. (2011).

The d84 percentiles documented in this study range from 4.91 ψ to 8.64 ψ and follow a positively skewed distribution where the majority of the values fall between 5.7 ψ and 7 ψ (Figure 3.3). A map of the d50 percentiles is shown in Figure B.S1 in Appendix B. There is generally no discernible spatial patterns of grain size. Rivers along which multiple samples were taken show no obvious fining trends. The coarsest sediment (d84 in excess of 175 mm) is found both in the headwaters (e.g., Spey), in the middle reaches (e.g., Dee) or near outlets (e.g., Findhorn) of river catchments. Likewise, the finest sediment is found in diverse regions of the various river systems.

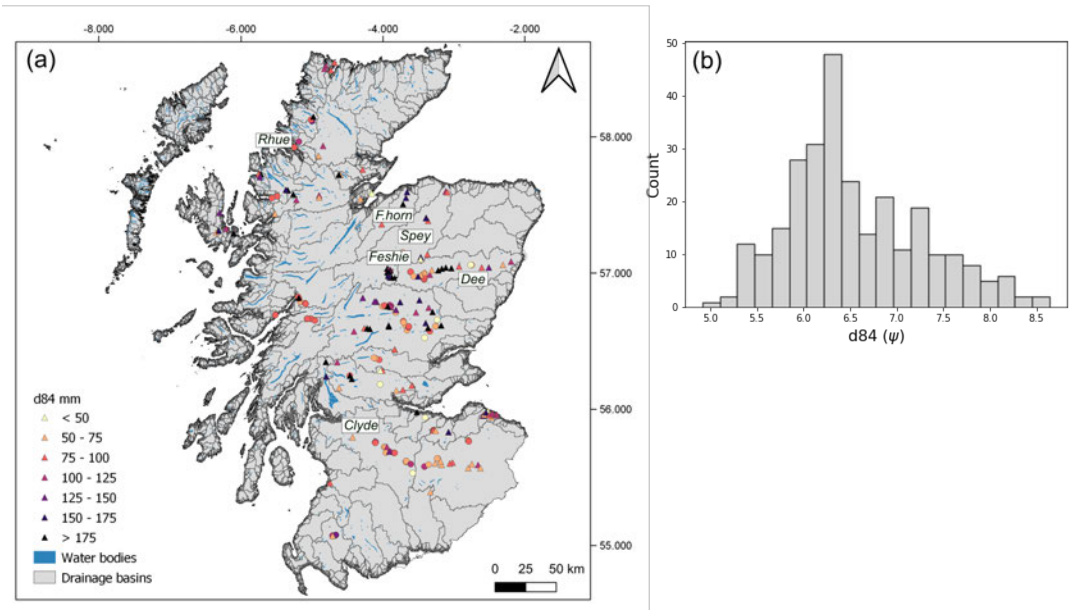

Figure 3.3: (a) Map of Scotland (focused on the mainland) showing 279 surveyed locations coloured according to d84 (mm). Circles represent samples processed with PebbleCountsAuto, triangles show manually clicked sites, and stars represent samples measured using Wolman Point Counts. Water bodies ($<$10 hectares) are shown in dark blue and drainage basin outlines (15 arc-second resolution) in black (sourced from the HydroLAKES and HydroBASINS databases, (Lehner and Grill, 2013; Messager et al., 2016)). Drainage basins that are referred to in the main text are labelled. **(b)** Histogram of d84 grain sizes converted to the ψ scale.

Overall, grain size does not show any significant Spearman's correlations with the independent variables (Figure 3.4). The strongest correlations observed for the d84 are with the average basin aridity (0.29) and average basin bedrock erodibility (-0.26). The percentages of alluvium, peat and glaciofluvial material also display similar correlation values of ≈ 0.2.

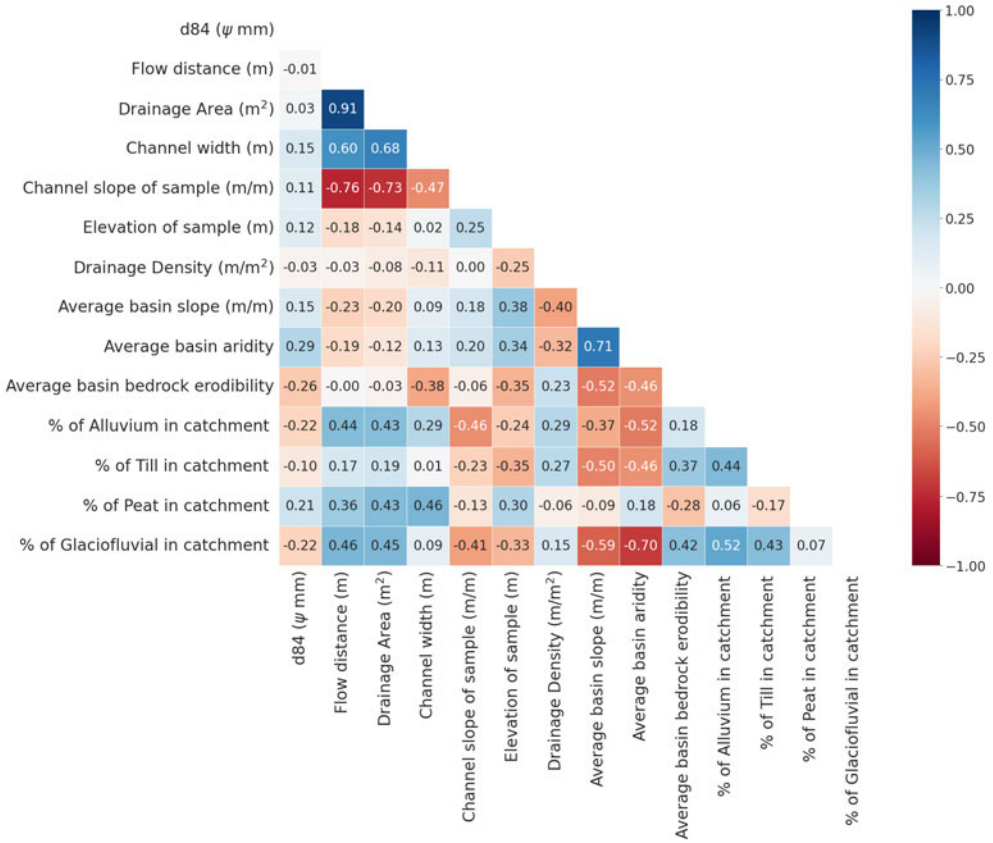

Figure 3.4: Spearman's correlations between measured grain size (d84) and various hydrological, climatic and topographic variables.

Results from the Random Forest Regressor model show the normalised importance of each environmental variable using the impurity reduction method, and the model's predictive ability (Figure 3.5). The most important variables modelled for the d84 are the average basin bedrock erodibility and channel slope of the sample, which have normalised importance values of 0.16 and 0.12, respectively. These variables present some of the strongest Pearsons correlations with grain size (Figure 3.4). However, the predictive ability of the RFR model is poor, which raises caution to the interpretation

of variable importance. When validated against the unseen testing data through the LOOCV method with all features included, the RFR presents a $nrmse$ of 0.10 ψ and r^2 of 0.22. Similar results are also observed for the d50 (see Figure B.S3 in Appendix B).

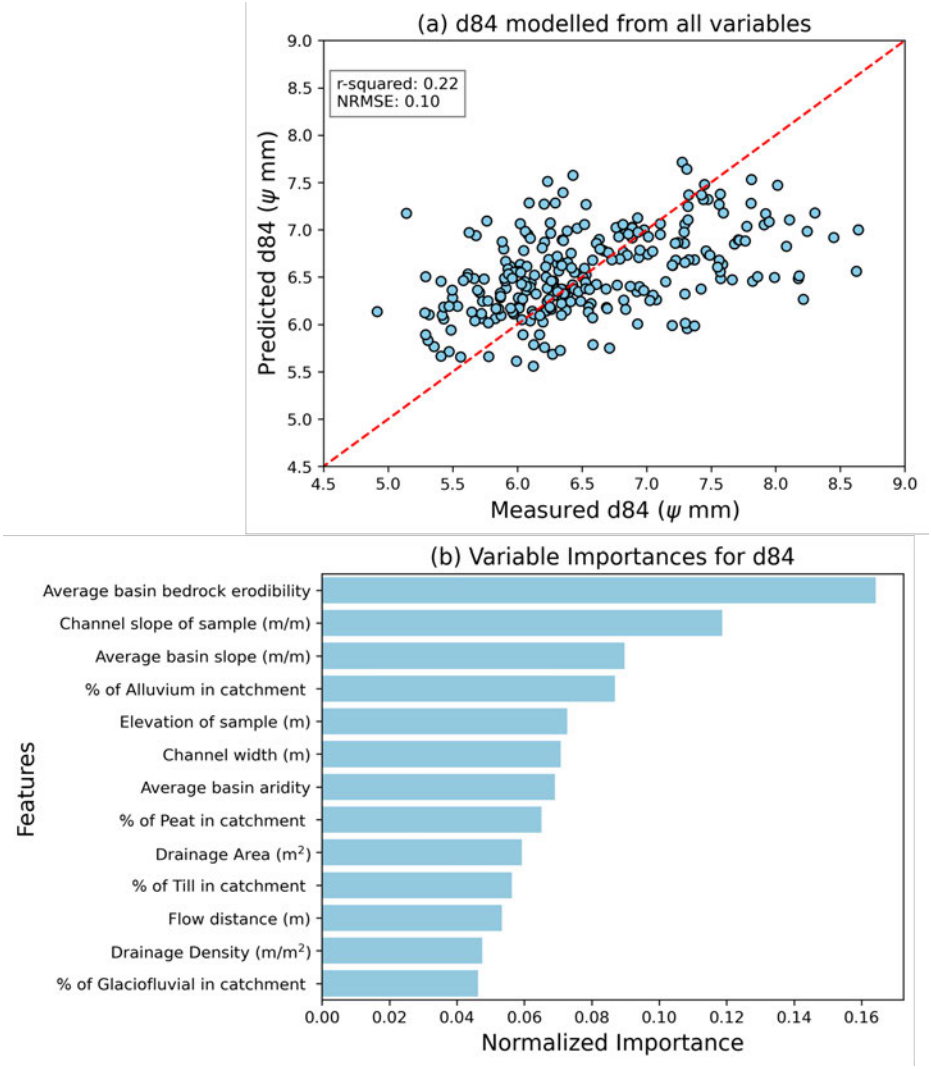

Figure 3.5: Results from the random forest regressor analysis. **(a)** shows the model's predictive ability, which is extremely poor. The dashed red line represents the 1:1 relationship. **(b)** shows the normalised variables' importance for predicting the d84 percentile. Normalisation is performed by dividing each importance score by the sum of all importance scores.

As discussed in Section 3.2.5, the relationship between ω'_m, which we use a proxy for flow competence, and grain size can provide information on supply-limited and transport-limited grain size conditions. In supply-limited systems, there would be an apparent grain size threshold that would not be exceeded, even at high flow compet-

ence. A power relationship between grain size and ω'_m would be expected to reflect transport-limited grain size conditions. Neither of these is obvious in our Scotland-wide d84 dataset (Figure 3.6a): a wide range of grain sizes is observed across a wide range of flow competences. Similar results are also observed for the d50 and samples that have been measured manually (see Figure B.S4 in Appendix B). We note however that $\approx$ 50 % of the d84 data at high flow competence ($\omega'_m > 50000$ m) sits in the lower two quartiles of the entire d84 distribution, potentially reflecting supply-limited grain size conditions (i.e., the river has the potential to transport coarser sediment but coarse sediment is not available for transport). We acknowledge that actual trends may be obscured in the noise due to the dataset amalgamating data from a very wide range of geological and geomorphological settings across Scotland. We therefore isolate the Feshie River basin which is very dynamic, with evidence of frequent bedload transport (Matthews et al., 2024) and for which we have 18 data points (Figure 3.6b). Similarly, we observe no apparent correlation between ω'_m and d84, although we note again that three of the four data points with the highest flow competence sit at values close to the median of the entire Feshie dataset.

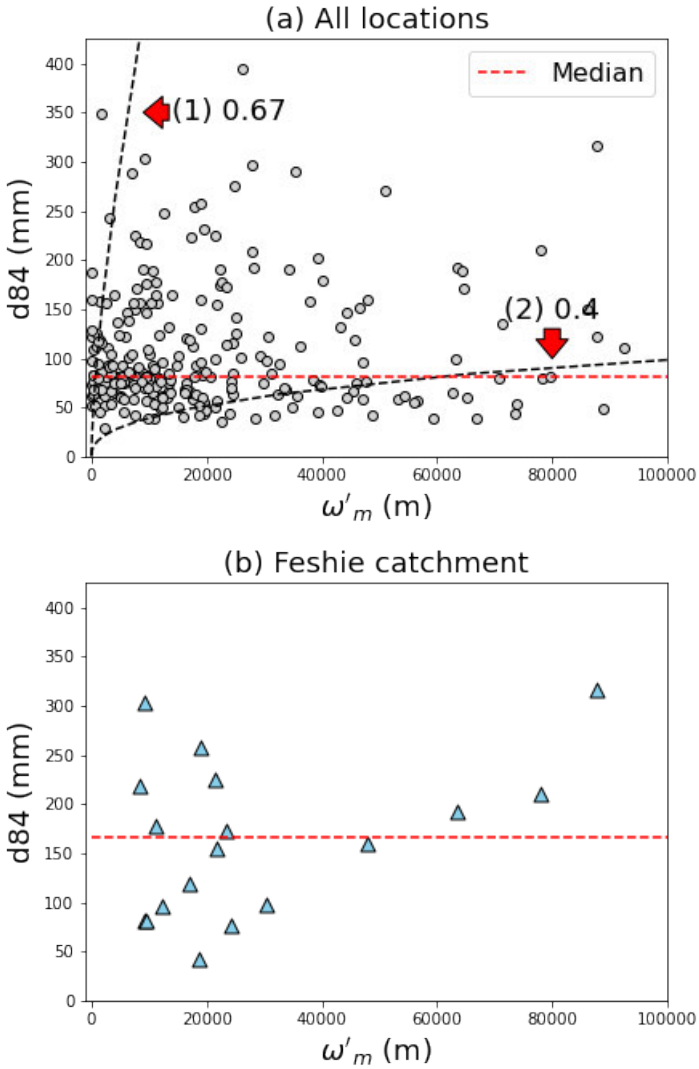

Figure 3.6: d84 as a function of variable ω'_m which is a proxy for flow competence (Equation 3.8). **(a)** shows the results for our Scotland-wide dataset. The median of the entire d84 distribution is shown by the red dashed line. Black dashed lines represent power law relationships between d84 and ω'_m with exponents of 2/3 and 0.4 (curves (1) and (2), respectively). These curves bracket the range of exponents found by Attal et al. (2015) in the Feather River basin, Sierra Nevada, California: they found exponents of 0.4, 0.53 and 0.61 best fit their data for the d100, d84 and d50 of their measured surface sediment, respectively. Median grain size d50 was fit with the exponent closest to the expected 2/3 value from experimental work and compilation of field studies (Bathurst, 2013; Whitaker and Potts, 2007). In a scenario where sediment grain size is controlled by flow competence ('transport-limited'), a power relationship between grain size and ω'_m would be expected. **(b)** shows the relationship between ω'_m and d84 for the Feshie basin which is a mountain river in the Spey catchment where 18 data points are available (see Figure 3.3 for the Feshie's location). The median of the Feshie's d84 distribution is shown by the red dashed line.

3.4 Discussion

In this study, we do not find any apparent control on surface grain sizes in channels across Scotland. Our results contrast with those of Snelder et al. (2011) and Mugodo et al. (2006) who found that grain sizes and/or substrate cover could be reasonably well predicted for rivers at large spatial scales. Snelder et al. (2011) found that grain sizes could be reasonably well predicted for rivers across France using a random forest model: in their study, the random forest predictor captured 52 percent of the variance in the measured grain sizes (sample size > 500), whereas in Scotland we find the random forest predictor only captures 22 percent of the variance of d84. Mugodo et al. (2006) found that 65 percent of the variance in fluvial substrate cover could be predicted for rivers across eastern Australia (sample size $<$ 100). We also find no correlation between flow competence and grain size: d84 values ranging from 40-350 mm are observed across several orders of magnitude of the parameter ω'_m (Figure 3.6).

Scotland's post-glacial legacy may drive our inability to predict grain size based on a number of landscape properties that have been shown to control grain size elsewhere, such as gradient, underlying lithology and downstream flow distance (e.g., Attal and Lavé, 2006; Sklar et al., 2017; Snelder et al., 2011). As discussed so far in this thesis, past glaciations have modified the spatial locations and grain size distributions of sediment stores, and the drivers of flow competence (i.e., channel slope and width) (Attal and Lavé, 2006; Ballantyne, 2019; Johnson et al., 2022; Mason and Polvi, 2023; Reid et al., 2022; Whitbread et al., 2015). In many Scottish river basins, channel erosion has exposed paraglacial sediment stores that contribute large quantities of sediment to modern rivers (e.g., Ballantyne (2019), Chapter 2). The longitudinal profiles of rivers also shows a strong glacial control that can influence sediment transport; many profiles are highly irregular, with long stretches of low gradient reaches that are interspersed by shorter, steeper reaches (Jansen et al., 2010; Whitbread et al., 2015). The empirical modelling approach applied in this study uses, in some cases, catchment-averaged variables that do not reflect spatial variations in sediment supply and transport capacity along river profiles. Studies have shown that spatial variations in the grain size of sediment supplied to rivers can significantly impact the grain size of sediments in rivers locally and further downstream (e.g., Attal and Lavé, 2006; Attal

et al., 2015; Sklar et al., 2006; Whittaker, 2012). We therefore suggest that Scotland's post-glacial legacy contributes to the absence of correlation between grain size and landscape properties.

Snelder et al. (2011) found average basin slope to be the most important control on fluvial grain sizes for rivers across France. In contrast, we did not find a significant relationship between grain size and basin slope at our sampled locations. In addition to the supply of material from glacial and paraglacial sediment stores and irregularities in channel profiles, we suggest that the general decoupling between hillslopes and channels in post-glacial landscapes also contributes to such observations. Many Scottish river valleys exhibit 'U' shaped valleys with wide valley floors meaning that significant stretches of the channel network are disconnected from hillslope sediment sources (Ballantyne, 2008; Whitbread et al., 2015). Studies have suggested that in the absence of sustained tectonic uplift or base level lowering, valleys are likely to maintain their glacially inherited 'U' shaped topography and remain in a state of transient dynamics that last for millions of years (Ballantyne, 2002; Egholm et al., 2013; Prasicek et al., 2015; Whitbread et al., 2015).

While we observe no apparent relationship between flow competence and grain size in Figure 3.6, we find fine grain sizes across a wide range of flow competences, including high flow competences. This observation may indicate that sediment grain size is supply-limited in some rivers, that is, river stretches with high competence transport fine sediment because no coarse sediment is available for transport. Likewise, coarse grain sizes are found in rivers with relatively low flow competence. We propose that the heterogeneous nature of post-glacial sediment supply and post-glacial channel morphology contributes significantly to the supply-limited and transport-limited grain size conditions observed in the flow competence analysis. Steep, powerful rivers may source sediment from fine-grained glacial and paraglacial deposits. Likewise, rivers with a low flow competence, such as those that drain plateaus and low gradient valleys, may be locally supplied with sediment from coarse-grained glacial and paraglacial sediment sources (Figure 3.7). For example, the Garry River (Spey basin) has a low apparent flow competence, but exhibits some of the coarsest sediment on our Scotland-wide map (d84 = 188 mm). A potential explanation for this could be that sediments are largely sourced from the abundant upstream paraglacial and glacial

deposits. These coarse deposits are only likely to become mobile during the largest of flood events. Diagrams and photographs in Figure 3.7 illustrate the post-glacial geomorphic processes discussed in this paragraph.

In this study, we used citizen science to gather grain size data on a national scale in a relatively data-sparse country. This extensive spatial coverage enabled us to explore controls on grain sizes across a range of landscapes, allowing us to document large distributions in channel slopes, widths and other environmental variables. Documenting grain sizes at such a large spatial scale would not have been feasible using current remote sensing techniques, as these methods are labour-intensive, costly, and of limited spatial coverage. The survey was cost-effective and quick, and contributes to the growing body of research using citizen science to monitor river characteristics (e.g., Riverfly Monitoring Initiative; https://www.riverflies.org/). Importantly, the survey fostered significant public engagement due to the importance of sediment on applied matters such as flood risk and habitat value.

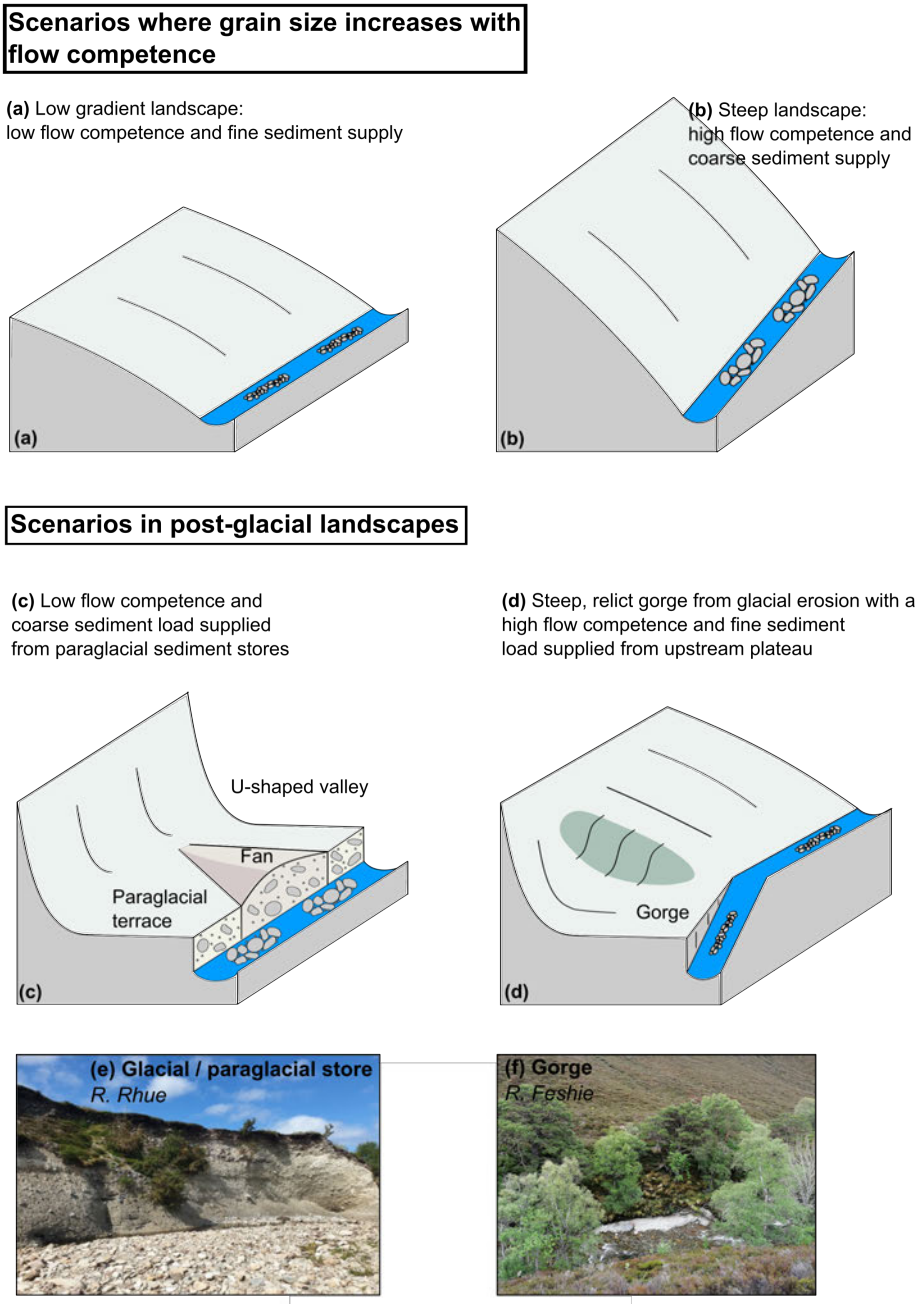

Figure 3.7: Caption on next page.

Diagrams and photographs illustrating the contrast in sediment dynamics between non-glaciated landscapes and post-glacial landscapes. **(a-b)** In non-glaciated landscapes, feedbacks are expected between erosion rates, hillslope steepness, channel steepness, and the grain size of the sediment supplied to rivers (Attal et al., 2015). In slowly eroding, low relief landscapes, low competence rivers (low gradient) are supplied with and transport fine sediment **(a)**. As relief increases, rivers become more powerful (steeper gradient, higher competence) and are supplied with a wider range of grain sizes **(b)**. In a scenario where all grain sizes are available for transport, the grain size of the sediment mobilized by a river is expected to increase with flow competence. In this case, the grain size can be considered 'transport-limited'. **(c-f)** In post-glacial landscapes, these feedbacks do not operate anymore. **(c)** shows a channel with low flow competence (low gradient) but a coarse sediment load, which is supplied from glacial and paraglacial sediment stores. **(d)** shows a steep relict gorge from glacial erosion (e.g., gorge connecting a hanging valley) with a high flow competence (steep gradient) but a fine sediment load as no coarse sediment is available on the upstream plateau. These situations are illustrated by photographs **(e)** and **(f)**, respectively. **(e)** shows a glacial/paraglacial sediment store feeding large quantities of coarse sediment to the River Rhue (scarp is approximately 10 m high). **(f)** shows a relatively fine-grained, well-sorted gravel bar along a steep bedrock reach of the River Feshie which is a tributary of the upper Spey basin (channel is approximately 5 m wide).

3.5 Conclusion

In this study, we document river surface grain sizes across Scotland using photographs of gravel bars. Grain sizes are extracted from the photographs through a combination of manual and automated techniques. We investigate whether grain sizes can be correlated with, and predicted from, a series of environmental variables (such as upstream basin slope) that have been suggested to control grain sizes in previous studies. In contrast to other studies that have primarily focused on non-glaciated landscapes, we find no apparent controls on grain sizes. We find weak Spearman's rank correlations between grain size and environmental variables. We also find that grain sizes cannot be predicted from a random forest model, in contrast to Snelder et al. (2011) who found that grain sizes could be reasonably well predicted for rivers across France. We find no correlation between flow competence and grain size.

We propose that Scotland's post-glacial legacy drives the lack of sedimentological trends documented in this study. This interpretation aligns with our findings from Chapter 2 and other studies that have highlighted the ongoing role of the post-glacial legacy on landscape evolution in tectonically quiescent terrains, both in Scotland and globally. Key geomorphic processes in post-glacial landscapes that contribute to a decoupling between channel, catchment morphology and fluvial sediment grain size include the disconnection between hillslopes and channels in "U"-shaped valleys, presence of steep reaches at various locations along river long-profiles (and not just in the headwaters), presence of high-elevation low-relief plateaus and hanging valleys, and paraglacial and glacial sediment stores (e.g., till, fluvio-glacial terraces and fans) acting as sediment sources at many locations along rivers. Thus, steep reaches (high competence) may transport only fine sediment due to the absence of coarse sediment available for transport upstream (grain size is 'supply-limited'). Meanwhile, low gradient (low competence) reaches may source sediment from coarse-grained glacial and paraglacial deposits, leading to anomalously coarse fluvial deposits that are mobilized only during the most extreme events. As a result, surface fluvial sediment grain size cannot be predicted by a global model based on environmental variables in post-glacial landscapes. Our results suggest that studies aiming to assess the controls and importance of sediment on hazards (e.g., flood risk), habitats, and river morphology in post-glacial landscapes need to rely on the careful characterisation of upstream grain size distributions and geomorphic processes.

Chapter 4

Investigating the response of rivers to coastal erosion and base-level rise in Southern England

Mikael Attal, Simon Mudd and I conceptualised the study. I directed the project, processed and visualised the data and wrote the manuscript with input from all authors.

This chapter will be submitted to a journal upon revision.

Abstract

This study investigates how rivers in Southern England responded to coastal erosion and sea-level rise over the Holocene. Emerging research has shown that coastal erosion can initiate the formation of migrating knickpoints. We test a model based on well-established fluvial geomorphometry relationships with a coastal erosion component. If the model is valid, we expect the percentage of incising channel outlets to decrease with drainage area for a given lithology and coastal erosion rate. Lithology and coastal erosion rates should also control the outlet type. That is, we expect incising outlets to form in larger drainage basins in regions with higher coastal erosion rates, if all other factors are equal. For more resistant lithologies, we expect a greater proportion of channel outlets to incise compared to less resistant lithologies, because rivers incising more resistant lithologies are expected to be relatively steeper. By examining over 400 river profiles through topographic analysis, we find some evidence that our observations of channels in Southern England align with the model, but also evidence to the contrary. We find that channels underlain by more resistant rocks have steeper gradients and a higher percentages of these channels incise for a given drainage area ($< 25\text{km}^2$), compared to channels underlain by less resistant rocks. This finding supports the model. However, we observe a mix of incising and non-incising outlets across all drainage areas within each region, suggesting that the model does not fully explain the outlet type of rivers in Southern England. Additionally, we do not observe a clear influence of coastal erosion on the threshold drainage area between incising and not incising channels. To explain the apparent discrepancies between the model and our observations, we suggest that channels may not have exhibited the classic power-law relationship between slope and drainage area before coastal erosion. We also question the assumption that long stretches of the coast experienced comparable rates of erosion, the simplified grouping of lithologies, and the impact of past Quaternary sea-level stands on sea-cliff formation.

4.1 Introduction

The upstream propagation of knickpoints is an important mechanism for channel incision and the communication of changes in external drivers such as climate, sea level and tectonics throughout a landscape. Migrating knickpoints are commonly associated with base-level fall, with knickpoints typically forming in response to an increase

in the rate of rock uplift or base-level fall (e.g., Castillo et al., 2013; Crosby and Whipple, 2006; Jansen et al., 2011; Whipple and Tucker, 1999; Whittaker, 2012). For example, studies have shown that glacio-isostatic rebound during the Holocene has driven the formation of retreating bedrock knickpoints in Scotland (Castillo et al., 2013; Jansen et al., 2011). Knickpoints can also form due to changes in lithology, such as a channel cutting across a lithological contact from less to more resistant rock (Forte et al., 2016; Haviv et al., 2010; Stock and Montgomery, 1999).

Coastal erosion, which is more prevalent in regions where relative base-levels are rising (Shadrick et al., 2022), can also initiate the formation of migrating knickpoints (e.g., Hackney et al., 2015; Leyland and Darby, 2009; Limber and Barnard, 2018; Mackey et al., 2014; Snyder et al., 2002). These knickpoints, or knickzones when the steepening is sustained over a reach rather than at one specific location along a river profile, have received comparatively little study, however. Waves that cut into the channel bed at the river mouth can lead to the initiation of a hanging waterfall that discharges directly into the ocean (Emery and Kuhn, 1982; Mackey et al., 2014; Snyder et al., 2002; Wolinsky and Murray, 2009). Coastal erosion leads to the horizontal translation of a river's base-level, in contrast to channel incision that operates vertically. Horizontal migration of knickpoints as a result of river incision occurs due to differences in erosion rates, with erosion being maximized immediately downstream of the knickpoint, leading to a wave-like propagation of the knickpoint upstream. Sea-cliff erosion has been suggested to explain the formation of channels that steepen and incise near the coast on the Isle of Wight (Southern England) and Hawaii (USA) (Leyland and Darby, 2009; Mackey et al., 2014).

To further explore the formation of these knickpoints, Limber and Barnard (2018) developed a numerical model based on simple fluvial geomorphometry relationships with a coastal erosion component, as described below. The nearshore channel slope is a fundamental control on knickpoint formation; when the land is steep, wave erosion can create cliffs (Limber and Barnard, 2018; Snyder et al., 2002). It has long been established that rivers tend to evolve towards an equilibrium, characterised in locations with uniform lithology by a channel gradient that decreases with increasing drainage area following a power law (Flint, 1974; Gilbert, 1877):

$$S = k_s A^{-\theta} \tag{4.1}$$

where S is the river gradient ($S = \frac{dz}{dx}$ where z is the elevation and x is the distance along the channel); k_s is the steepness index, A is the drainage area; and θ the concavity index dictating the rate at which channel gradient declines downstream. Limber and Barnard (2018) demonstrated that the likelihood of coastal erosion generating knickpoints is inversely proportional to drainage basin area. Assuming a steady-state landscape, uniform and sufficient coastal erosion, and all other factors being equal (e.g., lithology), they demonstrated that wave erosion forms cliffs in small basins because they have higher slopes at their outlets. In comparison, large basins have lower slopes at their outlets meaning that wave erosion does not form cliffs (Figure 4.1). The implication of this is that the higher the coastal erosion rate, the greater the drainage area at which knickpoints are expected to form at the coast due to coastal erosion. Identifying this threshold drainage area along stretches of the coast that are expected to experience comparable rates of coastal erosion could therefore, in theory, help bring constraints on the rate of coastal erosion (the greater the area, the greater the coastal erosion rate).

Limber and Barnard (2018) also demonstrated in their model that coastal knickpoints were more likely to develop in more resistant lithologies based on the sole fact that more resistant lithologies have steeper channel profiles (e.g., Forte et al., 2016; Gilbert, 1877; Hack, 1960). Model results were broadly shown to match observations of channel outlets in basins along the Californian coastline, USA (Limber and Barnard, 2018). Drainage area was found to be a first-order control on the outlet type. They also found some evidence linking knickpoint formation in larger drainage basins to higher coastal erosion rates, which were about 20 cm/yr greater in these regions.

The aim of this study is to test and build upon the ideas developed primarily by Limber and Barnard (2018) and Snyder et al. (2002). These studies suggested that the outlet type of river systems in regions experiencing active coastal erosion is a function of both coastal erosion rates and nearshore channel slope. If the model is valid, we expect the percentage of incising channel outlets to decrease with drainage area for a given lithology and coastal erosion rate. Similarly, we expect incising outlets to form in larger drainage basins in regions with higher coastal erosion rates, if all other factors are equal. For more resistant lithologies, we expect a greater proportion of channel

outlets to incise compared to less resistant lithologies, because rivers incising more resistant lithologies are expected to be relatively steeper (e.g., Forte et al., 2016; Gilbert, 1877; Hack, 1960).

We test if the model is applicable regionally to Southern England, which is an ideal place for testing because of different, well mapped lithologies and high-resolution topographic data (BGS, 2021; Ordnance Survey, 2021). Southern England experienced considerable variations in rates of sea-level rise, which have been largely driven by the Glacial Isostatic Adjustment of the British Isles following the last glacial period, and coastal erosion (Bradley et al., 2023; Hurst et al., 2016; Shadrick et al., 2022; Shennan et al., 2009). Southern England has a well constrained wave climate, at least over the last few decades (Scott et al., 2021; Tolman, 2009) and stretches of coastlines with relatively uniform orientation with respect to the dominant wave direction, along which we may therefore consider coastal erosion rates to be relatively uniform, one of the central assumption in this work which will be discussed in light of our results. Showing that the model is valid at the regional scale, along a series of coastline stretches with different lithologies and/or exposure to erosional elements, would demonstrate that river profiles can be used as tools to constrain coastal erosion rates. The research presented in this Chapter continues the theme of fluvial base-level change driven by GIA, which was a key geomorphic process discussed in Chapter 2.

4.2 Study area

Southern England is geomorphologically highly diverse. The south-west is characterised by more resistant rock types of Palaeozoic age, the exceptions being the areas of Precambrian igneous and metamorphic rocks (Figure 4.1, BGS (2021)). Compared to the rest of Southern England, the topgraphic relief in the south-west is greater, with elevations exceeding 600 m. The Hampshire basin and Wealdon district are lower-relief regions located in the south-central and south-east of England, respectively. These areas largely consist of more erodible sedimentary rocks of Jurassic, Cretaceous and Tertiary age (BGS, 2021). The highest elevation in the Hampshire basin and Wealdon district are 300 m and 200 m, respectively.

Southern England is tectonically quiescent. The Glacial Isostatic Adjustment of the British Isles following the last glacial period has resulted in considerable spatial and temporal variations in the rates of relative sea-level (RSL) change throughout the Holocene (Bradley et al., 2023; Shennan et al., 2009). RSLs are rising in Southern England, which was largely ice-free during the Pleistocene. Rates of RSL rise generally peaked after deglaciation and subsequently declined throughout the Holocene (Bradley et al., 2011). Present-day rates of RSL change are between approximately 0.4 and 0.7 mm/yr along the south coast of England, with the highest rates in the south west (Bradley et al. (2023), Figure 4.2).

A large proportion of Southern England's coastline is experiencing coastal erosion (Masselink et al., 2020). Coastal erosion is a complex process determined by site-specific factors. Foremost, coastal erosion is largely controlled by the type and structure of rock present at the coast (Buchanan et al., 2020; Prémaillon et al., 2018; Rosser et al., 2013; Sunamura, 2015). For example, modern rates of coastal erosion in Southern England are 0.01 - 0.1 m/yr and 0.1 - 1 m/yr for hard and soft rock coastlines, respectively (Masselink et al., 2020). SLR, tides and tidal currents, wave energy and the state and variability of air and water temperature also influence coastal erosion (Kennedy et al., 2014). Specifically, studies have linked higher rates of RSL rise to increased rates of coastal cliff retreat (e.g., Limber and Barnard, 2018; Shadrick et al., 2022). This is because SLR results in wave energy reaching further inland, which can attack coastal cliffs and trigger increased rates of cliff retreat. Southern England experiences large storm events and powerful wave energy from the Atlantic Ocean (Masselink et al., 2020). Mean wave heights and wave periods are generally greater in the south west (i.e., Devon and Cornwall) than the south east (Scott et al., 2021; Tolman, 2009). Moreover, in Devon and Cornwall, mean wave heights and wave periods are generally greater along west-facing coastlines compared to south-facing coastlines (Scott et al., 2021). Overall, long-term records of coastal erosion in Southern England are sparse.

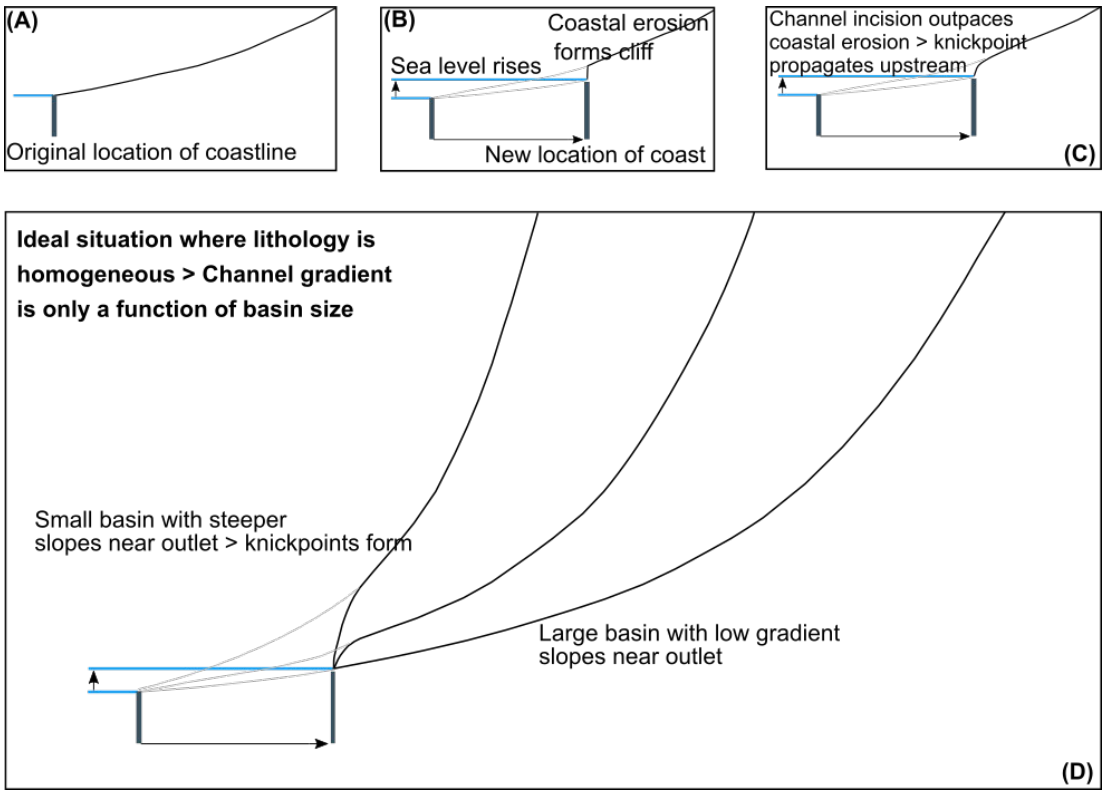

Figure 4.1: Cartoon diagrams illustrating the effects of sea-level rise and coastal erosion on river outlet morphology. These figures summarise the concepts and models presented by Limber and Barnard (2018) and Snyder et al. (2002). (A) Channel profile (marked by black line) in steady-state that drains to sea-level (marked by blue line). (B) Sea-levels rise and waves erode the land in the horizontal direction, creating coastal cliffs, especially when the landscape is steep. (C) Channel incision translates the knickpoint upstream. (D) Diagram showing the long profile of channels as a function of basin size. Small basins have steeper slopes at their outlets, which results in coastal erosion forming cliffs. In contrast, large basins have lower slopes meaning that coastal erosion does not form cliffs.

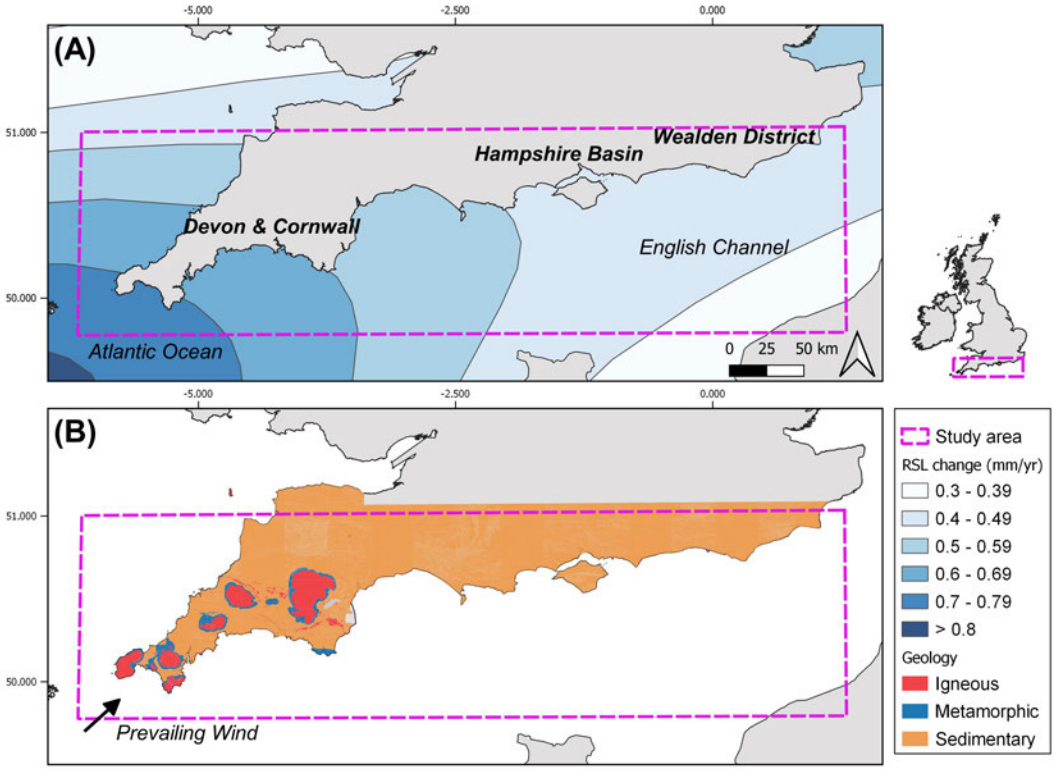

Figure 4.2: Maps of Southern England showing present-day rates of relative sea level change (A) and geology (B). RSL reconstructions are taken directly from Bradley et al. (2023) and geological shapefiles are sourced from BGS (2021). Area of interest for this study is indicated by the pink dashed box. Inset map shows a map of the UK with the study area marked. Key geographical regions are shown. These include Devon and Cornwall, the Hampshire Basin and the Wealden District.

4.3 Methods

The aim of this study is to test and build upon the ideas developed primarily by Limber and Barnard (2018) and Snyder et al. (2002). These studies suggested that the outlet type (i.e., 'incising' or 'not incising') of river systems in regions experiencing active coastal erosion is a function of both coastal erosion rates and nearshore channel slope. Therefore, we need to extract river channels and their properties (i.e., drainage area, channel steepness, presence or absence of knickpoints) and classify channel outlets as either 'incising' or 'not incising'. The hypotheses we are testing are sensitive to coastal erosion rates, so we ideally need to compare data over stretches that are likely to experience comparable coastal erosion rates. The methods for obtaining these metrics are described below.

4.3.1 Extracting river profiles and lithology

We use the LSDTopoTools software to extract river channels and quantitatively characterise the topography from the 5 m Digital Terrain Model (DTM) sourced from the Ordnance Survey (Mudd et al., 2023; Ordnance Survey, 2021). We calculate the normalised channel steepness index, k_{sn}, which is the channel slope normalised to drainage area and typically reflects the erosive ability of a channel (Flint, 1974; Wobus et al., 2006). We use the algorithms from Mudd et al. (2014) to calculate k_{sn}, using a concavity index of 0.45 (Mudd et al., 2014). We also extract the χ coordinate for each channel node, which normalises streamwise distance by the channel's drainage area (Perron and Royden, 2013).

$$\chi = \int_{x_b}^{x} \left(\frac{A_0}{A(x)} \right)^{\theta} dx. \tag{4.2}$$

where x_b is the flow distance of the outlet and A_0 is a reference drainage area, used to non-dimensionalise the term in the integral. This integral has the property that, at any point in the channel, the gradient in χ–elevation space can be related to the channel steepness index:

$$z(x) = z(x_b) + \left(\frac{k_s}{{A_0}^{\theta}} \right) \chi. \tag{4.3}$$

We set A_0 to 1 m^2 so the gradient in χ–elevation space is equivalent to k_{sn}. This gradient is thought to be linearly proportional to the local erosion rate (Perron and Royden, 2013).

We extract the channel network using a contributing area of 0.1 km^2 to define the beginning of a channel. All basins with outlet nodes (i.e., the node with the largest drainage area within each basin) larger than 3 km^2 are analysed. In total, over 400 basins are analysed.

A geological map of Southern England was sourced from the British Geological Survey (BGS, 2021). The underlying surface geology (i.e., igneous, metamorphic and sedimentary) of every channel node was extracted.

As discussed in the Introduction, the concepts and models presented by Limber and Barnard (2018) rely on the assumption that channels exhibit the classic power relationship between slope and drainage area before coastal erosion (Flint, 1974). Such a relationship will appear in the form of a linear relationships between χ and elevation in χ space, which we test. We also investigate if more resistant rocks have steeper slopes by comparing the distribution of k_{sn} values and the gradients of χ plots for each lithological group (igneous, metamorphic and sedimentary). When calculating k_{sn} and χ statistics for each lithological group, we exclude reaches downstream of any identified outlet knickzones (see Section 4.3.3 for knickzone extraction), as these reaches are assumed to be transient and do not reflect the pre-perturbation 'background' topography.

4.3.2 Coastal erosion

Rates of coastal erosion influence knickzone characteristics (Limber and Barnard, 2018). To our knowledge, no spatially continuous datasets of coastal erosion rates are available for Southern England, however. As described in Section 4.2, lithology is a primary control on coastal erosion, while wave energy, SLR, tides, and other factors also affect erosion rates (Buchanan et al., 2020; Kennedy et al., 2014; Prémaillon et al., 2018; Rosser et al., 2013; Sunamura, 2015). To test the model and understand how coastal erosion influences channel outlet characteristics in Southern England,

we compare channels with similar drainage areas and lithologies across regions with differences in wave energy and SLR rates. We use wave climate data published in Scott et al. (2021), based on the WAVEWATCH III third-generation spectral wave model (version 3.14; Tolman (2009)). We divide Southern England into four regions, representing a general decrease in mean wave height and wave period: Western Devon and Cornwall, Southern Devon and Cornwall, the Hampshire Basin, and the Wealden District. Rates of SLR in England are also higher in the south-west than in the south-east.

4.3.3 Classifying channel outlets: incising versus not-incising

All channels that drain to the coast across Southern England are classified as either 'incising' or 'not incising' according to their outlet morphology (Figure 4.3). Firstly, we identify knickpoints, which represent a change in k_{sn}, using a threshold of +/- 5 (e.g., Gailleton et al., 2019). Then, we identify the downstream most knickpoint for each basin if knickpoints are present. If this knickpoint represents a decrease in k_{sn} (i.e., the channel segment nearest the coast has a higher k_{sn} than the upstream reach), the basin outlet is classified as 'incising'. If the downstream most knickpoint represents an increase in k_{sn} (i.e., the channel segment nearest the coast has a lower k_{sn} than the upstream reach), the basin is classified as 'not incising'. Moreover, if knickpoints are not present along the entire channel profile, then the basin is classified as 'not incising'.

We further filter the incising versus non-incising dataset by removing channels with outlet knickpoints that flow over lithological contacts. Broadly, this enables us to exclude knickpoints associated with changing lithologies and isolate knickpoints potentially generated by coastal erosion. Based on this criteria, a total of 8 out of over 400 channels were removed.

Following the classification of channel outlets, we test whether the percentage of 'incising' channels decreases with drainage area, as indicated by Limber and Barnard (2018)'s model. We explore relationships between drainage area and outlet type for each lithological category (i.e., igneous, metamorphic and sedimentary rocks). According to Limber and Barnard (2018)'s model, we expect a higher percentage of channels in more resistant lithological groups to incise in comparison to less resistant

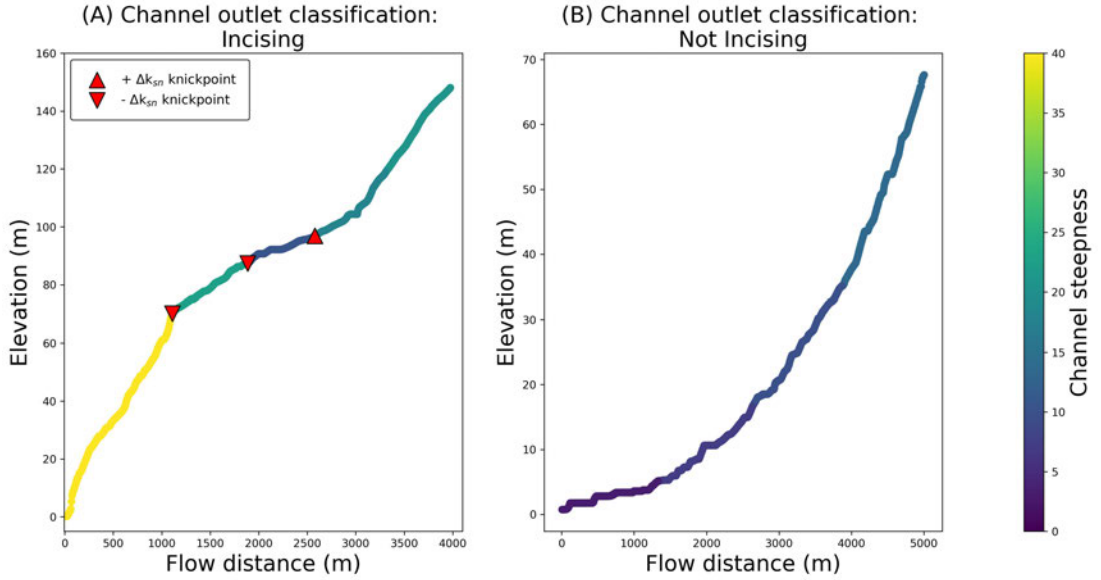

Figure 4.3: Channel profiles coloured according to the normalised channel steepness index, which was extracted in LSDTopoTools using a concavity index of 0.45 (Mudd et al., 2023). Knickpoints are marked on the channel profile by red triangles. Downwards-pointing and upwards-pointing triangles (negative and positive Δk_{sn}) represent an decrease and increase in k_{sn} relative to the nearest downstream segment, respectively. The channel outlet in panel (A) is classified as 'incising' because the channel segment nearest the coast is steeper than the upstream segment. The channel outlet in panel (B) is classified as 'not incising' because the segment nearest the coast does not incise relative to the upstream segment.

lithologies. This is because more resistant lithologies have inherently steeper channel slopes at their outlets according to basic fluvial incision theory (see Section 4.1). We also explore the role of coastal erosion: in regions with higher coastal erosion rates, we expect incising outlets to form in larger drainage basis if all other factors are equal.

4.4 Results

This section presents k_{sn} distributions and χ plots for each lithological group within each region (Western Devon and Cornwall, Southern Devon and Cornwall, the Hampshire basin and the Wealden District). We find that in Southern England, channel profiles are generally composed of linear segments in χ space except from a few groups (e.g., metamorphic rocks in Western in Devon and Cornwall, see Figure 4.4). Igneous and metamorphic rocks generally have higher median normalised channel steepness values and steeper χ profiles than sedimentary rocks (Figure 4.4), confirming our initial hypothesis that igneous and metamorphic rocks are broadly more resistant to fluvial erosion than sedimentary rocks, and that rocks that are more resistant to erosion form steeper slopes (Gilbert, 1877; Hack, 1960). In regions where multiple rock groups exist (i.e. Devon and Cornwall), all rock groups are statistically different from each other, with p-values less than 0.05. We also observe differences between regions. Igneous rocks have a higher median k_{sn} value and steeper χ profiles in Southern Devon and Cornwall (median k_{sn} = 19) than Western Devon and Cornwall (median k_{sn} = 12). Sedimentary rocks in Devon and Cornwall have higher median k_{sn} values (median k_{sn}=11) and steeper χ profiles than the Hampshire Basin (median k_{sn} = 6) and Wealden District (median k_{sn} = 4). These findings support regional rock and topographic descriptions by the BGS (2021).

Here, we present observations of channel outlet types (i.e., incising versus non-incising) expressed as a function of drainage area for lithological categories in Southern England. This tests our hypothesis that within a given region with comparable exposure to the elements that control coastal erosion, smaller catchments within a lithological group should exhibit incising outlets, with a threshold drainage area over which catchments will display non-incising outlets (Figure 4.1). Results conforming to our hypothesis would manifest in all small catchments displaying incising outlets, all large catchments displaying non-incising outlets, and a mix at the transition around the threshold drainage area. We observe this in none of the regions (Figure 4.5). We find a range of channel outlet types across a range of drainage areas. We note, however, that within each region, a handful of small sedimentary basins (< 20 km^2) incise. Larger catchments display mixed results, with the percentage of incising outlets varying between 0 and 100%.

Igneous and metamorphic rocks are present in Devon and Cornwall, which enables the generic exploration of the role of lithology on outlet type. According to Limber and Barnard (2018)'s model, we expect a higher percentage of channels in more resistant lithological groups to incise in comparison to less resistant lithologies, all else equal. The maximum drainage within the igneous and metamorphic category is less than 25 km^2, limiting the scope of the analysis. In Western Devon and Cornwall, between 90 and 100% of igneous and metamorphic channels incise, which is significantly higher than the sedimentary channels (Figure 4.5). This may be the only data that conforms to our initial hypothesis, whereby nearly all small catchments have an incising outlet; the threshold area at which the transition to non-incising outlet occurs may be greater than 25 km^2 in this area for these lithologies. The picture is different in Southern and Eastern Devon and Cornwall, with a mix of incising and non-incising outlets for catchments with sizes up to 15 km^2, and the smallest catchments (less than 5 km^2) having non-incising outlets. Nevertheless, we note that the percentage of incising outlets is generally higher for igneous and metamorphic channels compared to sedimentary channels for catchments smaller than 15 km^2 in this region.

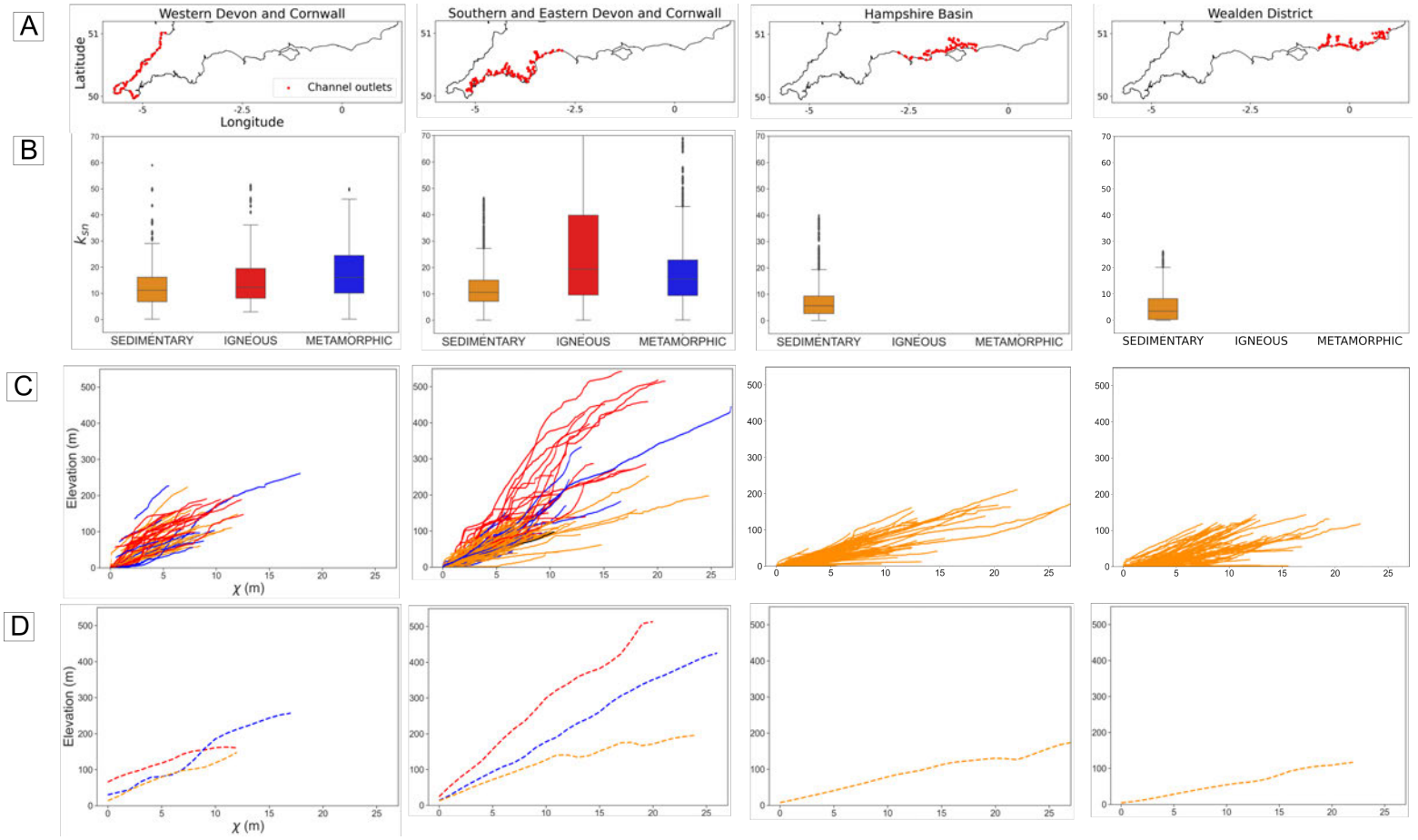

Figure 4.4: k_{sn} distributions and χ profiles of rivers in Southern England. Panels in row **A** show channel outlets (marked by red dots) within each of the four study regions (Western Devon and Cornwall, Southern and Eastern Devon and Cornwall, the Hampshire Basin and the Wealden District). Plots in row **B** show k_{sn} distributions for each lithological group (sedimentary = orange, igneous = red, metamorphic = blue) within each region. Plots in row **C** show χ profiles coloured according to lithology. Plots in row **D** shows the average elevation for each χ value for each lithological group. When calculating k_{sn} and χ statistics for each lithological group, we exclude reaches downstream of any identified outlet knickzones (see Section 4.3.3 for knickzone extraction), as these reaches are assumed to be transient and not reflect the pre-perturbation 'background' topography.

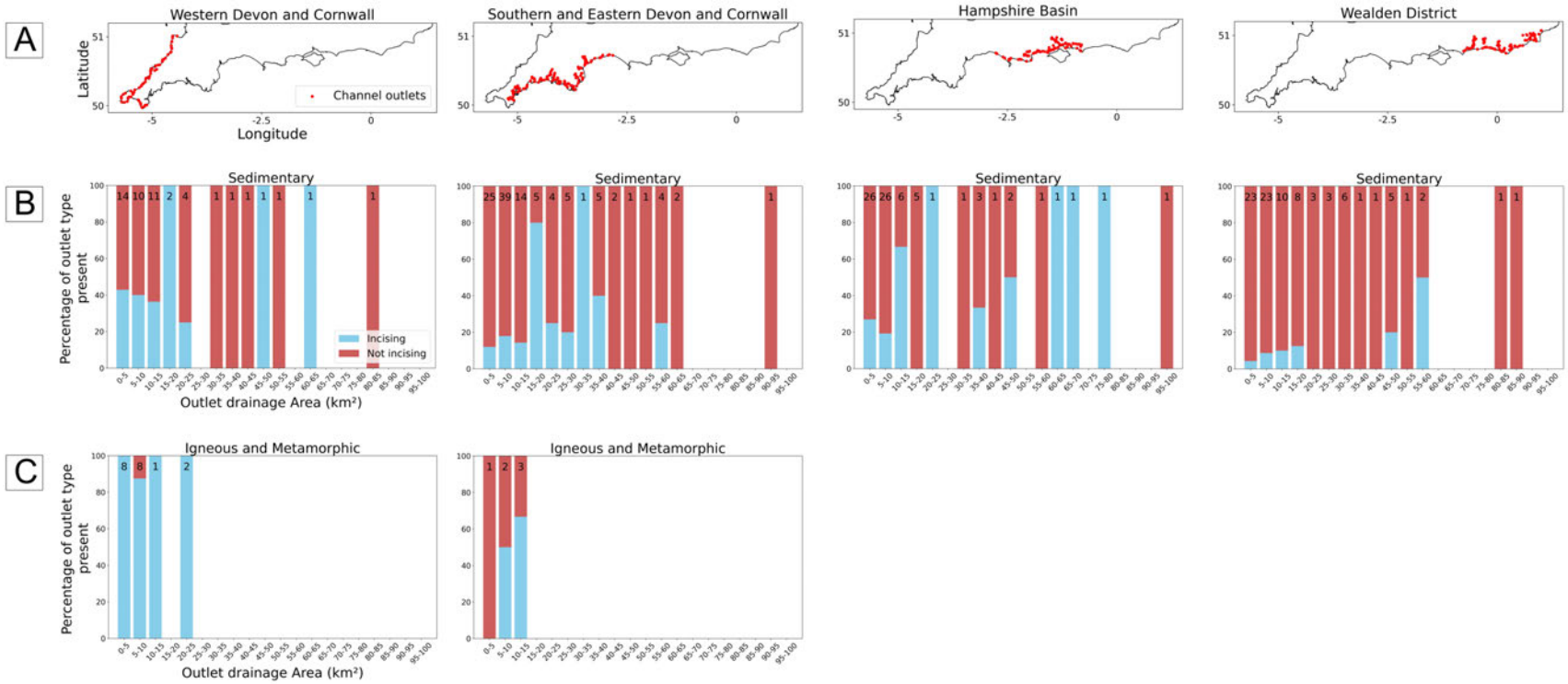

Figure 4.5: Panels in row **A** show channel outlets (marked by red dots) within each study region in Southern England. The relationship between outlet drainage area and percentage of outlet type (i.e, incising or not incising) is shown in rows **B** and **C**. Row **B** represents sedimentary outlet lithologies and row **C** represents igneous and metamorphic lithologies. 'Incising' outlets are shown in blue and 'not incising' outlets are shown in red. There is a general decrease in mean wave height and wave period across the four regions from left to right. The total number of samples within each drainage area bin is shown at the top of the corresponding bin.

4.5 Discussion

4.5.1 Can the presence/absence of coastal knickpoints be explained by the model?

By analysing over 400 river profiles along 700 km of coastline in Southern England, we demonstrate that some channels steepen as they flow towards the coast. We explore if coastal erosion can explain the presence of these knickzones, and test a simple model which primarily depends on coastal erosion rates and nearshore channel slope. We find some evidence that our observations of channels align with the model, but also evidence that they do not. In the following section, we discuss observations that match the model and those that do not.

Firstly, according to Limber and Barnard (2018)'s model, we expect a higher percentage of channels in more resistant lithological groups to incise in comparison to less resistant lithologies for a given drainage area. This is based on the assumption that harder lithologies have steeper gradients, which facilitates sea-cliff formation through wave erosion. Broadly, we find that our observations generally match this aspect of the model in all regions where there are contrasts in rock resistance to erosion. That is, in Devon and Cornwall, channels underlain by more resistant rocks have steeper gradients and a higher percentage of these channels incise for a given drainage area, in comparison to less resistant rocks (i.e., sedimentary rocks, see Figure 4.5).

Secondly, according to the idealized model, for a given lithology and coastal erosion rate, we expect small catchments to display incising outlets, large catchments to display non-incising outlets, and a mix of both types of outlets around the threshold drainage area at which the transition from one behaviour to the other occurs. A wide range of drainage areas (between 3 and >60 km^2) is observed in the sedimentary category within each region, making this category ideal for testing the drainage area hypothesis. We find a mix of incising and non-incising outlets across all drainage areas suggesting that the model is not valid.

Rates of coastal erosion influence the formation of knickpoints. For a given lithology, we expect incising outlets at larger drainage areas where coastal erosion rates are higher (Limber and Barnard, 2018). By using wave energy and rates of sea-level rise as regional proxies for coastal erosion, we do not observe a clear influence of coastal erosion on knickpoint presence, although we note that the area with the lowest wave energy and inferred coastal erosion rates (Wealdon District) exhibits the lowest overall percentage of incising outlets, which is consistent with the model (Figure 4.5).

4.5.2 Can the model assumptions explain the discrepancies between expected outcomes and observations?

The model assumes that channels exhibit concave-up longitudinal profiles with a power relationship between slope and drainage area (Flint (1974)), modulated by a coefficient that accounts for difference in bedrock erodibility, before they are modified by coastal erosion. By analysing channels upstream of knickzones, we find that not all profiles in Southern England perfectly obey this relationship, as shown by the irregularities in the χ profiles. Moreover, as with many studies that span large geospatial scales (Harel et al., 2016), a limitation of our methodology is the simplified grouping of lithologies (igneous, metamorphic and sedimentary), as well as the assumption that long stretches of the coast are experiencing comparable coastal erosion rates.

Figure 4.4 shows that channel steepness varies within the defined lithological groups. Variations in bedrock erodibility within a lithological group, along with general irregularities in channel profiles, may explain some of the noise in our results. Accounting for detailed lithological subgroups would be challenging due to the large lithological diversity of the study area, which encompasses 100 subgroups (and not all subgroups span a range of drainage areas and coastal erosion rates). A potential approach to address this limitation would be a systematic survey of each of these lithologies, including measurements of rock strength using a Schmidt hammer and of joint density (e.g., fractures, bedding), in order to group lithologies in categories of relative rock resistance to erosion rather than type of rock.

The lithology hypotheses tested here assumes that harder lithologies form incised outlets because they have steeper nearshore channel slopes for a given drainage area. However, the model does not account for the fact that harder lithologies may also be more resistant to coastal erosion (Buchanan et al., 2020; Masselink et al., 2020; Prémaillon et al., 2018; Rosser et al., 2013; Sunamura, 2015), which could counterbalance the effect of greater channel steepness when estimating the susceptibility of a channel to the formation of knickzones by coastal erosion. Our observations do however, show that harder lithologies such as igneous and metamorphic rocks, characterized by steeper channels than sedimentary rocks, are more likely to form incised outlets. This could be due to the fact that the properties that make a rock type more resistant to fluvial incision may not be the same as those that make a rock more resistant to coastal erosion (e.g., the existence of fractures with a spacing in excess of 1 m may have a limited impact on fluvial erosion in a small stream (Whipple et al., 2000) but could enhance the susceptibility to coastal erosion by wave action).

We highlight the limitations of our simplified approach for estimating coastal erosion, which is based on regional exposure to wave energy and rates of sea-level rise. Studies have highlighted the challenges associated with estimating regional-scale rates of coastal erosion because of the multitude of controls (e.g., rock structure, tides and tidal currents, air and water temperature, sediment accretion Dickson et al. (2023); Masselink et al. (2020)). Crucially, these studies emphasise that coastal erosion is a 'local process'. Future research therefore requires better constraints on coastal erosion rates, which could be achieved through remote sensing at the yearly to decadal scale (Gómez-Pazo et al., 2022), and through CRN dating and numerical modelling of rocky coastal platforms at the millennial scale (Hurst et al., 2016; Shadrick et al., 2022). Comparing channel outlet morphologies in areas with well constrained coastal erosion rates would offer a better opportunity to test and calibrate the proposed model, with implications for constraining coastal erosion rates using the shape of river profiles in lithologically complex areas (Mackey et al., 2014).

Finally, the model assumes that waves cut into steep channels, forming coastal cliffs with waterfalls (Limber and Barnard, 2018). However, coastal cliffs and migrating knickpoints may have existed at channel mouths since the beginning of the Holocene (e.g., due to past base-level fall, Jansen et al. (2011)). Rising sea-levels throughout the Holocene may have also reactivated relic cliffs associated with earlier sea-levels.

For example, incising coastal gullies on the Isle of Wight, Southern England, are thought to have formed due to rising sea-levels reoccupying former cliffs in the mid to late Holocene (Leyland and Darby, 2009). Overall, we highlight the legacy and complexity of Quaternary sea-level change on coastal-fluvial interactions.

4.6 Conclusions

We demonstrate that some channels steepen as they flow towards the coast in Southern England. We explore whether coastal erosion can explain the presence of these knickzones, and test a simple model that primarily depends on coastal erosion rates and nearshore channel slope. We find some evidence that our observations of channels align with the model, but also evidence to the contrary. Specifically, we find that a higher percentage of channels underlain by more resistant rocks incise for a given drainage area compared to channels underlain by less resistant rocks, thus supporting the model. However, we observe a mix of incising and non-incising outlets across all drainage areas within each region, suggesting that the model is not valid. Additionally, we do not observe a clear influence of coastal erosion on the threshold drainage area between incising and not incising channels.

We suggest that the discrepancies between the expected model outcomes and our observations arise from the fact that channels did not always exhibit the classic power relationship between slope and drainage area before coastal erosion, as demonstrated by irregularities in the χ profiles upstream of knickzones. We also highlight the simplified grouping of lithologies in our analysis, the assumption that long stretches of the coast experienced comparable coastal erosion rates, and the legacy of past Quaternary sea-level stands on sea-cliff formation. Overall, this study highlights that migrating knickpoints exist at channel outlets where base-levels are rising.

Chapter 5

General discussion and conclusions

The previous three chapters of this thesis have contributed to the understanding of Holocene fluvial processes of the British. In particular, this thesis has answered the following questions:

1. What controls post-glacial denudation rates and CRN concentrations in the Scottish mountain ranges?
2. What controls the grain size of modern river sediments in Scotland?
3. How do rivers respond to coastal erosion and sea-level rise in Southern England?

In the rest of this chapter I will summarise the key findings from each of the previous three chapters, and place them in context of the wider body of research of geomorphology. I will also discuss the uncertainties, limitations and areas for further research.

5.1 What controls post-glacial denudation rates in the Scottish mountain ranges?

5.1.1 Post-glacial fluvial bedrock incision

In Chapter 2 I infer basin-wide denudation rates from the concentration of *in situ* ^{14}C in stream sediments. I interpret the Garbhlach's denudation rate of 0.175 mm/yr to be the only sample that is representative of true catchment-wide denudation. Unlike the remainder of our sampled basins, the Garbhlach is largely devoid of transient sediment stores and the hillslopes in the Garbhlach basin appear to be connected to the channel, as shown by the "V" shaped valley. The Garbhlach's denudation rate is near the upper bound of previously reported Late Holocene bedrock incision rates in

rivers in Scotland. Jansen et al. (2011) and Kim (2004) inferred present-day vertical incision rates of 0.07 - 0.24 mm/yr by measuring ^{10}Be concentrations of bedrock surfaces along knickpoint reaches that are assumed to be caused by base-level fall. The Garbhlach is also the steepest catchment in the Feshie basin which supports the idea that 0.175 mm/yr is likely to be an upper bound and that the real background denudation rate in the Feshie may be lower. Nonetheless, the Garbhlach's denudation rate is an order of magnitude lower than the glacial isostatic uplift rates predicted for the Feshie basin of $>$1 mm/yr (Shennan et al., 2009). I also find that erosion rates calculated from sediment fluxes, which represent the sum of the 'background' and terrace erosion rates and vary between 0.2 - 0.6 mm/yr, are lower than the isostatic uplift rate. These results support studies which have proposed that base-level signals propagating inland from the coast, which are indicated by the presence of knickpoints, have stagnated near Scotland's coastlines (Bishop et al., 2005; Castillo et al., 2013). Our findings therefore align with studies which have suggested that without the renewal of relief through sustained tectonic activity or base-level change, post-glaciated landscapes in tectonically quiescent terrains may remain in a state of transient dynamics that last for millions of years (e.g. Ballantyne, 2002; Egholm et al., 2013; Whitbread et al., 2015). In the absence of sustained tectonic uplift, valleys are likely to maintain their glacially inherited "U" shaped topography, meaning hillslopes will remain largely decoupled from channels.

A limitation of the above interpretation is that, although it aligns with other studies (e.g., Jansen et al., 2011; Whitbread et al., 2015), it is based on one basin-wide denudation rate. A future research direction therefore includes inferring true basin-wide erosion rates from ^{14}C in Scotland (e.g., across a range of slope gradients). I emphasise the importance of sampling in basins that are largely devoid of transient sediment stores.

A future research topic involves investigating the role of sediment flux on post-glacial bedrock incision rates. By dating strath terraces downstream of knickpoints, which were presumed to be triggered by base-level fall, Jansen et al. (2011) found an overall decline in Holocene bedrock incision rates. They attributed this trend to a general reduction in sediment supply. Future research involves constraining Holocene incision rates from strath terraces across a range of sediment supply regimes. For example, rates derived downstream of lochs could be considered a supply-limited end-member

scenario based on the assumption that lochs trap sediment. Likewise, rates derived from rivers that appear connected throughout the Holocene to a coarse sediment supply (e.g., paraglacial and glacial deposits) could be considered a sediment-rich end-member.

Future research involves the large-scale mapping of knickpoints presumed to be caused by base-level fall in Scotland. To date, studies on base-level fall knickpoints have focused on the local scale, such as the Isle of Jura (Castillo et al., 2013; Jansen et al., 2011). Large-scale mapping of base-level fall signals would enable the investigation of isostatic, lithologic, climatic and sedimentological controls on landscape transience in post-glacial landscapes. A key uncertainty will be the assumption that knickpoints upstream of river mouths are caused by base-level fall rather than direct glacial modification to channel profiles.

Future research involves investigating drainage reorganisation in post-glacial landscapes. Research from the 20th century suggested that large-scale drainage capture occurred throughout Scotland during past glaciations (Linton, 1949). However, relatively little is known about the extent of drainage reorganisation and the post-glacial channel response. Do captured basins exhibit anomalous fluvial geomorphometry scalings (e.g., the Upper River Tilt, which was once part of the River Dee) compared to basins that have not been captured (e.g., the Lower Tilt)? How are current drainage divides responding?

5.1.2 Tracking the paraglacial sediment load

In Chapter 2, I find that catchments with paraglacial terraces into which the rivers are actively eroding (inferred from field observations, flood modelling and geomorphic mapping) record apparently higher CRN denudation rates in comparison to catchments with little alluvial fill. I propose that the higher apparent denudation rates in these catchments results from the mixing of 'background' sediment with low-CRN-concentration material derived from terrace erosion. Terraces are expected to deliver lower concentration material because terrace material has experienced CRN decay with depth and terraces were buried until the last phase of major Holocene incision (post-4000 years). These results suggest that ^{14}C-derived denudation rates in catchments with paraglacial terraces are not representative of true catchment-averaged

denudation rates because the ^{14}C concentrations can be influenced by short-lived sediment routing and storage processes due to the isotope's short half-life (5700 years).

I present a sediment mixing model which combines the 'background' sediment from catchment-wide denudation with sediment derived from the incision of paraglacial terraces. Our mixing model indicates that the observed distribution of ^{14}C concentrations can be explained if terrace escarpments have basin-averaged migration distances of 8 to 30 cm during large flood events. This interpretation is consistent with remotely sensed images of channel activity and terrace bank retreat within the catchment. Our results show that paraglacial sediment stores contribute to sediment fluxes in the late Holocene and highlight the on-going glacial legacy on landscape evolution.

A future research direction involves understanding the contribution of paraglacial and glacial deposits to sediment fluxes in other post-glacial regions, both in Scotland and globally. For example, glaciofluvial deposits appear to be contributing large quantities of material to modern rivers in British Columbia, Canada (Reid et al., 2022). It is likely that CRN concentrations in these settings may not reflect true basin-wide denudation rates. In the following paragraphs, I summarise the limitations of the CRN sediment mixing model used in Chapter 2 and suggest methods for improvement.

In this study, I use an average terrace concentration in the sediment mixing model because both terrace production rates and heights are largely similar throughout the Feshie basin. I therefore do not directly account for variations in terrace concentrations. Future studies spanning significant variations in terrace CRN production rates and terrace heights must directly take into account of varying terrace concentrations in the sediment mixing model. For example, a more complex model could assign each terrace 'node' a CRN concentration based on the terrace height and production rate. Moreover, the sediment mixing model presented in Chapter 2 focuses purely on mixing 'background' sediments with paraglacial terrace sediments, and does not account for the contribution of other types of paraglacial and glacial deposits (e.g., drumlins, till, alluvial fans). The CRN concentrations and connectivity of these landforms must therefore be considered in future studies.

Finally, the timescales of sediment delivery from sediment stores must be considered. In this study, I assume that terraces input sediment to the modern river channel during large flood events. The time since the last flood event is thus considered in our mixing model. Future study therefore should involve repeat CRN sampling of stream sediments following flood events to confirm sediment supply and transport timescales. Such an investigation would also benefit from repeat high-resolution remotely sensed imagery. Moreover, future study involves exploring the response of post-glacial landscapes to extreme flow events driven by anthropogenic climate change (e.g., are there locations where rivers could reconnect with glacial/paraglacial sediment stores during high flow events?).

5.2 What controls the grain size of modern river sediments in Scotland?

In Chapter 3, I document river surface grain sizes across Scotland using photographs of gravel bars. Grain sizes are extracted from the photographs through a combination of manual and automated techniques. I investigate whether grain sizes can be correlated with and predicted from a series of environmental variables (such as upstream basin slope) that have been suggested to control grain sizes in previous studies. In contrast to other studies that have primarily focused on non-glaciated landscapes, I find no apparent controls on grain sizes. I find weak Spearman's rank correlations between grain size and environmental variables. I also find that grain sizes cannot be predicted from a random forest model, in contrast to Snelder et al. (2011) who found that grain sizes could be reasonably well predicted for rivers across France. I find no correlation between flow competence and grain size.

I propose that Scotland's post-glacial legacy drives the lack of sedimentological trends documented in this study. This interpretation aligns with Chapter 2 and other studies that have highlighted the ongoing role of the post-glacial legacy on landscape evolution in tectonically quiescent terrains, both in Scotland and globally (e.g., Ballantyne, 2002; Johnson et al., 2022; Whitbread et al., 2015). Key geomorphic processes in post-glacial landscapes that contribute to a decoupling between channel, catchment morphology and fluvial sediment grain size include the disconnection between hillslopes and channels in "U"-shaped valleys, presence of steep reaches at various

locations along river long-profiles (and not just in the headwaters), presence of high-elevation low-relief plateaus and hanging valleys, and paraglacial and glacial sediment stores (e.g., till, fluvio-glacial terraces and fans) acting as sediment sources at many locations along rivers. Thus, steep reaches (high competence) may transport only fine sediment due to the absence of coarse sediment available for transport upstream (grain size is 'supply-limited'). Meanwhile, low gradient (low competence) reaches may source sediment from coarse-grained glacial and paraglacial deposits, leading to anomalously coarse fluvial deposits that are mobilized only during the most extreme events. As a result, surface fluvial sediment grain size cannot be predicted by a global model based on environmental variables in post-glacial landscapes. Results from both Chapter 2 and Chapter 3 suggest that studies aiming to assess the controls and importance of sediment on hazards (e.g., flood risk), habitats, and river morphology in post-glacial landscapes need to rely on the careful characterisation of upstream sediment sources, grain size distributions and geomorphic processes.

5.3 How do rivers respond to coastal erosion and sea-level rise in Southern England?

In Chapter 4, I investigate how rivers in Southern England responded to coastal erosion and sea-level rise over the Holocene. Emerging research has shown that coastal erosion can initiate the formation of migrating knickpoints. Waves that cut into the channel bed at the river mouth can lead to the initiation of a hanging waterfall that discharges directly into the ocean (Emery and Kuhn, 1982; Mackey et al., 2014; Snyder et al., 2002; Wolinsky and Murray, 2009). Channel incision erodes a landscape vertically and can translate the waterfall upstream as a migrating knickpoint. The nearshore channel slope is a fundamental control on knickpoint formation, and can be expressed by well-established fluvial geomorphometry laws (Flint, 1974; Limber and Barnard, 2018; Snyder et al., 2002).

I test a model developed by Limber and Barnard (2018) based on well-established fluvial geomorphometry relationships with a coastal erosion component. If the model is valid, I expect the percentage of incising channel outlets to decrease with drainage area for a given lithology and coastal erosion rate. Similarly, I expect incising outlets

to form in larger drainage basins in regions with higher coastal erosion rates, if all other factors are equal. For more resistant lithologies, I expect a greater proportion of channel outlets to incise compared to less resistant lithologies, because rivers incising more resistant lithologies are expected to be relatively steeper. By examining over 400 river profiles through topographic analysis, I find some evidence that channels in Southern England align with the model, suggesting that coastal erosion drives migrating knickpoints, but also evidence to the contrary. I find that channels underlain by more resistant rocks have steeper gradients and a higher percentages of these channels incise for a given drainage area ($< 25\text{km}^2$), compared to channels underlain by less resistant rocks. This finding supports the model. However, I observe a mix of incising and non-incising outlets across all drainage areas within each region, suggesting that the model is not valid. Additionally, I do not observe a clear influence of coastal erosion on the threshold drainage area between incising and not incising channels. To explain the apparent discrepancies between the model and our observations, I suggest that channels may not have exhibited the classic power-law relationship between slope and drainage area before coastal erosion. I also question the assumption that long stretches of the coast experienced comparable rates of erosion, the simplified grouping of lithologies, and the impact of past Quaternary sea-level stands on sea-cliff formation.

For the first time since deglaciation, rates of eustatic sea-level rise are expected to outpace rates of isostatic rebound in regions such as Scotland (Hansom et al., 2017; Masselink et al., 2020). It has been suggested that this shift may be starting to occur along Scotland's coastlines (Rennie and Hansom, 2011), although some studies have challenged this finding (Dawson et al., 2013). Sea-level rise has been linked to increased rates of coastal erosion (Shadrick et al., 2022), meaning that channels in Scotland could therefore develop migrating knickpoints from coastal erosion. A future research direction thus involves predicting the response of channels to base-level flipping in these settings.

Future research involves testing the model in geographically simpler areas with known long-term coastal erosion rates. In regions where the model works, it should be theoretically possible to constrain rates of coastal erosion from river profiles by reconstructing river profiles before subsidence.

5.3.1 Wider Implications

The key research gap that largely motivated this thesis was the lack of quantification of geomorphic processes in post-glacial landscapes. Following the recent development of quantitative geomorphic tools (e.g., CRN erosion rates, DEMs), this thesis has quantitatively characterised sediment sources, sediment transport and landscape evolution in landscapes affected by Quaternary glaciations. A key finding of this thesis is that post-glacial rivers in low-relief, post-orogenic settings source sediment from paraglacial and glacial sediment stores more than 10 ka after deglaciation (see Chapters 2 and 3). Studies aiming to understand the role of sediments on hazards (e.g. flood risk) in post-glacial landscapes should therefore consider the contribution of paraglacial and glacial deposits to rivers. I emphasise that this finding is particularly relevant to other post-glacial landscapes such as North America and Scandanavia which were glaciated during the Quaternary.

This thesis also explored the impacts of base-level change, specifically the role of GIA and coastal erosion, on fluvial systems. A wider implication from Chapters 2 and 4 is the impact of potential 'base-level flipping' on fluvial systems. For the first time since deglaciation, rates of eustatic sea-level rise are expected to outpace rates of isostatic rebound in regions such as Scotland (Hansom et al., 2017; Masselink et al., 2020). Sea-level rise has been linked to increased rates of coastal erosion (Shadrick et al., 2022), meaning that channels in Scotland could therefore develop migrating knickpoints from coastal erosion.

Novel methods have been used in this thesis to understand geomorphic processes, specifically in-situ cosmogenic ^{14}C and citizen science. Cosmogenic ^{14}C has been used to infer catchment-wide erosion rates and track sediment routing pathways. A key reason behind the use of ^{14}C, as opposed to the more commonly used ^{10}Be, was to avoid problems associated with inheritance in post-glacial landscapes (see Chapter 2 for further discussion). Applying cosmogenic ^{14}C to infer catchment-averaged erosion rates remains limited, however, because of challenges associated with constraining ^{14}C production rates and analytical methods, such as sample extraction (see Hippe (2017) for a review). Following recent advancements in the extraction techniques and scaling of ^{14}C production rates (e.g. Lifton et al., 2014,2; Lupker et al., 2015), studies have used ^{14}C alongside ^{10}Be to identify complex erosional histories (Hippe et al., 2021; Kober et al., 2019; Slosson et al., 2022). This thesis thus

contributes to the growing body of research using cosmogenic ^{14}C to understand denudation. A wider implication of Chapter 2 is that studies should carefully select the most appropriate isotope when investigating sediment routing pathways in post-glacial landscapes.

Another novel method used in this study involves citizen science to gather sediment data (Chapter 3). SBSS enabled us to collect data at a national scale, which would have otherwise been impossible with current remote sensing methods or manual surveys. Key challenges associated with the application of citizen science include the clustering of samples, meaning that samples are not necessarily evenly distributed. Challenges also exist in processing the data. For example, I had to carefully assess whether photographs could be processed through the automatic pebble counting tool, PebbleCounts, or if they needed to be manually measured, which was time-consuming. To evaluate whether the output from PebbleCounts was suitable for the project, I visually assessed how well PebbleCounts fitted ellipses to the pebbles and examined the number of pebbles that had been counted (i.e., meaning that the PebbleCounts output is representative of a distribution 'by area').

5.4 Thesis Conclusions

This thesis aimed to explore geomorphic processes in tectonically quiescent landscapes influenced by past glaciations. Much geomorphological research has focused on unglaciated landscapes and glaciated landscapes in tectonically active regions. This thesis explored the controls on sediment sources and transport in Scotland. It also investigated how fluvial systems in Britain responded to base-level change, largely driven by glacial isostatic adjustment during the Holocene. The main conclusions of this thesis are as follows:

1. *Glacial isostatic adjustment does not control denudation in Scotland's central mountain ranges*

   Denudation rates in Scotland's central mountain ranges are an order of magnitude lower than the glacial isostatic uplift rates. This result supports studies which have proposed that base-level signals propagating inland from the coast have stagnated near Scotland's coastlines.

2. *The glacial legacy influences sediment supply and transport conditions in post-glacial landscapes more than 10 ka after deglaciation*

   I suggest that CRN-derived denudation rates inferred from river sands in catchments with abundant paraglacial sediment stores, into which the rivers are actively eroding, are not representative of true catchment-wide denudation rates. I suggest that these apparent denudation rates represent a mixture of sand sourced from both 'background' hillslopes and paraglacial terraces.

   I also show that, unlike landscapes with little past or present glacial influence, grain sizes cannot be predicted in post-glacial landscapes. Key geomorphic processes in post-glacial landscapes that contribute to a decoupling between channel, catchment morphology and fluvial sediment grain size include the disconnection between hillslopes and channels in "U"-shaped valleys, presence of steep reaches at various locations along river long-profiles (and not just in the headwaters), presence of high-elevation low-relief plateaus and hanging valleys, and paraglacial and glacial sediment stores (e.g., till, fluvio-glacial terraces and fans) acting as sediment sources at many locations along rivers.

Thus, steep reaches (high competence) may transport only fine sediment due to the absence of coarse sediment available for transport upstream (grain size is 'supply-limited'). Meanwhile, low gradient (low competence) reaches may source sediment from coarse-grained glacial and paraglacial deposits, leading to anomalously coarse fluvial deposits that are mobilized only during the most extreme events.

3. *Rivers steepen as the flow towards the coast in Southern England which, in some cases, can be explained by coastal erosion and Holocene sea-level change*

   Migrating knickpoints are commonly associated with base-level fall. However, I show that rivers steepen as the flow towards the coast in settings where relative base-levels are rising. I suggest that coastal erosion and sea-level rise can, in some cases, explain the presence of these knickpoints. These findings highlight the role of coastal processes in driving channel incision and landscape evolution.

Appendix A

This Appendix refers to Chapter 2 and includes figures and tables presenting information on mathematical symbols, topographic analysis, hydrology of Feshie River and flood modelling calibration, hillslope morphology and sedimentology, terrace characteristics and mixing model results for the study sites not presented in the main text.

Symbol	Description
C_j	Concentration of nuclide j (atoms g^{-1})
P_j	Nuclide production rate (atoms g^{-1} yr^{-1})
λ_j	Nuclide decay coefficient (1/yr)
$P_{j,SLHL}$	Total surface production rate (atoms g^{-1} yr^{-1})
$F_{i,j}$	Scaling that relates the relative production of neutron spallation and muon production (dimensionless)
$S_{i,j}$	Scaling that combines the effects of production scaling and shielding of cosmic rays (dimensionless)
Λ_j	Attenuation length for reaction type j (g cm^{-2})
d	Shielding depth (g cm^{-2})
ζ	Elevation of the surface (cm)
η	Depth in the subsurface of the sample (cm)
z	Elevation in a fixed reference frame (cm)
ρ	Material density (g cm^{-3})
ε	Denudation rate (g cm^{-2} yr^{-1})
S_{tot}	Surface production scaling
Λ_v	Virtual attenuation length (g cm^{-2})

Table A.S1: Description of symbols that are used to calculate denudation rates (see Section 2.3.1 of Chapter 2).

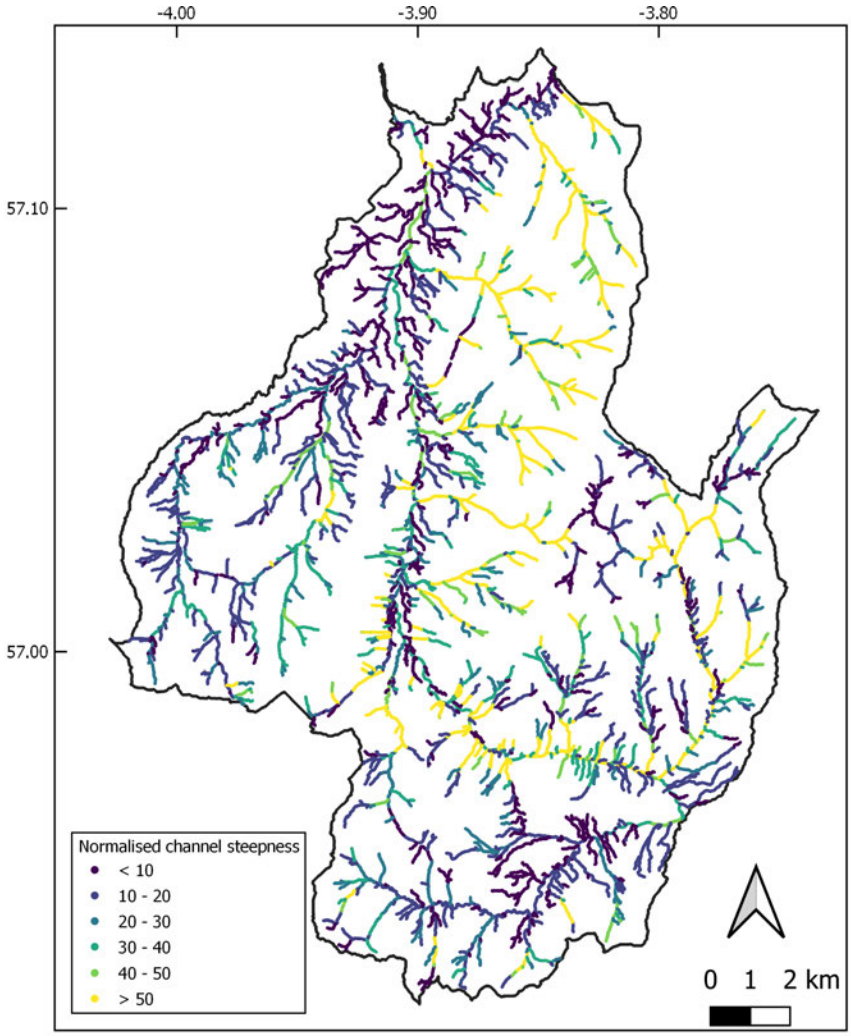

Figure A.S1: Distribution of the normalised channel steepness index (k_{sn}) in the Feshie catchment using the algorithms from Mudd et al. (2014). A concavity index value of 0.45 was used.

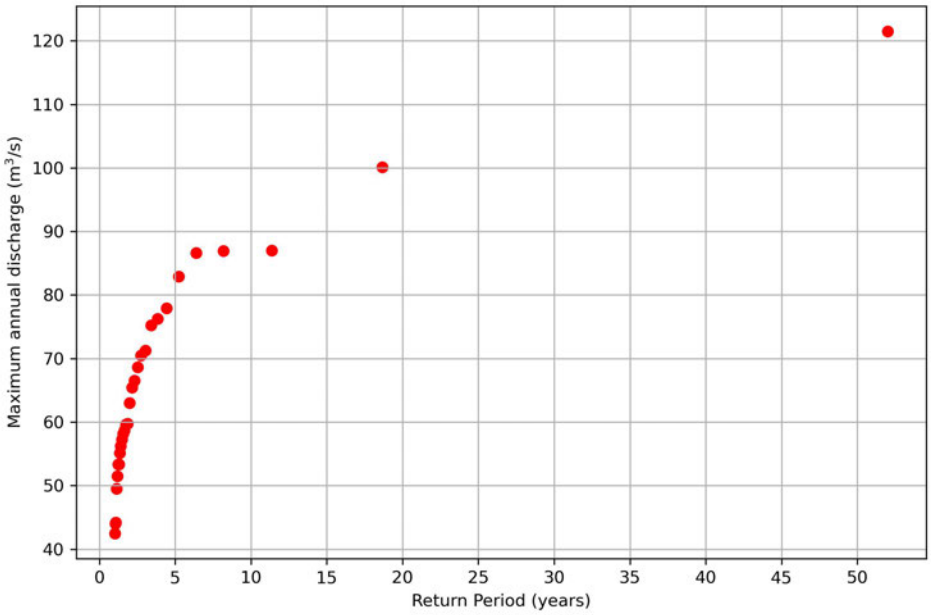

Figure A.S2: Flood return periods of the maximum annual discharges recorded at the Feshiebridge gauging station between 1992-2021. Return periods were calculated according to the Gumbel's Distribution Method.

Terrace age (yr)	Terrace elevation (m)		
	220	420	620
1000	7000 atoms g^{-1}, 13 %	8000 atoms g^{-1}	9000 atoms g^{-1}, 15 %
10000	23000 atoms g^{-1}, 13 %	27000 atoms g^{-1}	31000 atoms g^{-1}, 15 %

Table A.S2: Sensitivity of (depth-averaged) terrace concentrations to variations in the terrace elevation. An average terrace height of 2.2 m was used. Analysis was carried out using terrace ages of 1000 and 4000 years, and terrace elevations 200 m below and above the mean following the terrace elevation distribution presented in the main text. Percentage following the concentrations for terrace elevations of 220 and 620 m represents the difference with the concentration calculated for the corresponding 420 m terrace. A percentage uncertainty of 10 % is plotted on Figure 2.10 in Chapter 2.

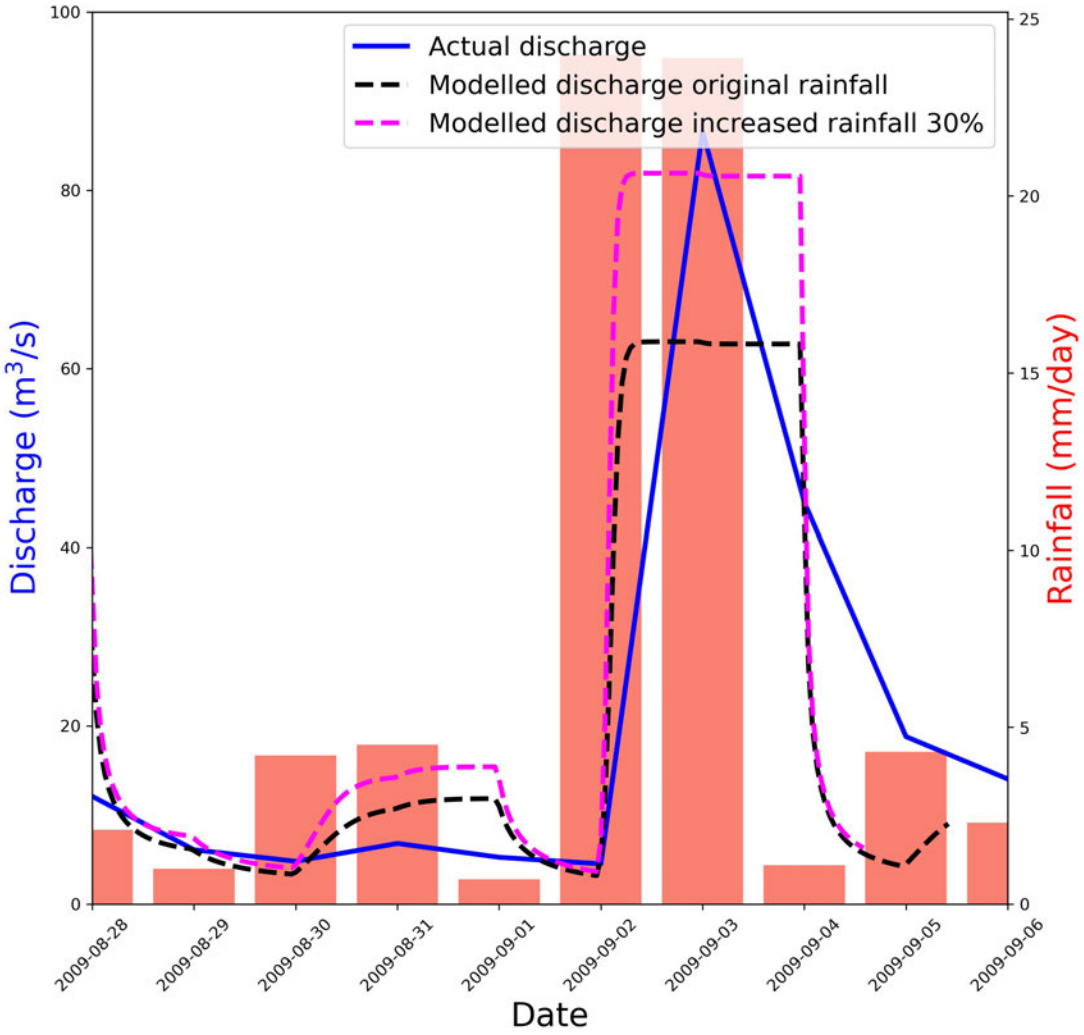

Figure A.S3: Hydrograph of the measured and modelled 2009 flood event at the Feshiebridge gauging station. Blue line represents the mean daily discharge (downloaded from UKCEH). Dashed lines represent hourly discharges simulated in HAIL-CAESAR using a Manning's n value of 0.04 and topmodel m value of 0.001. Black line represents discharges simulated using the original rainfall (sourced from UKCEH) whereas dark pink line represents simulation associated with an overall 30 $\%$ increase in the rainfall. Histogram presents rainfall data.

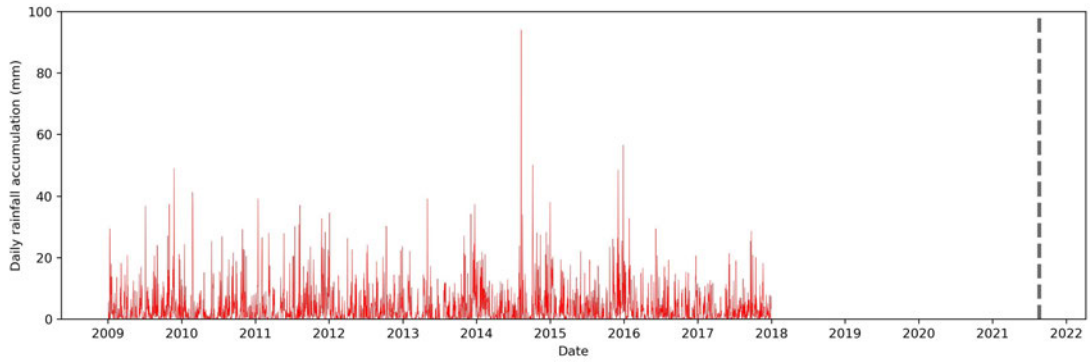

Figure A.S4: Available rainfall data at the Feshiebridge gauging station between 01/01/2009 and 20/08/2021. Rainfall and discharge data was downloaded from UK-CEH (https://nrfa.ceh.ac.uk/data/station/peakflow/8013). Grey dashed line marks date of CRN sample collection.

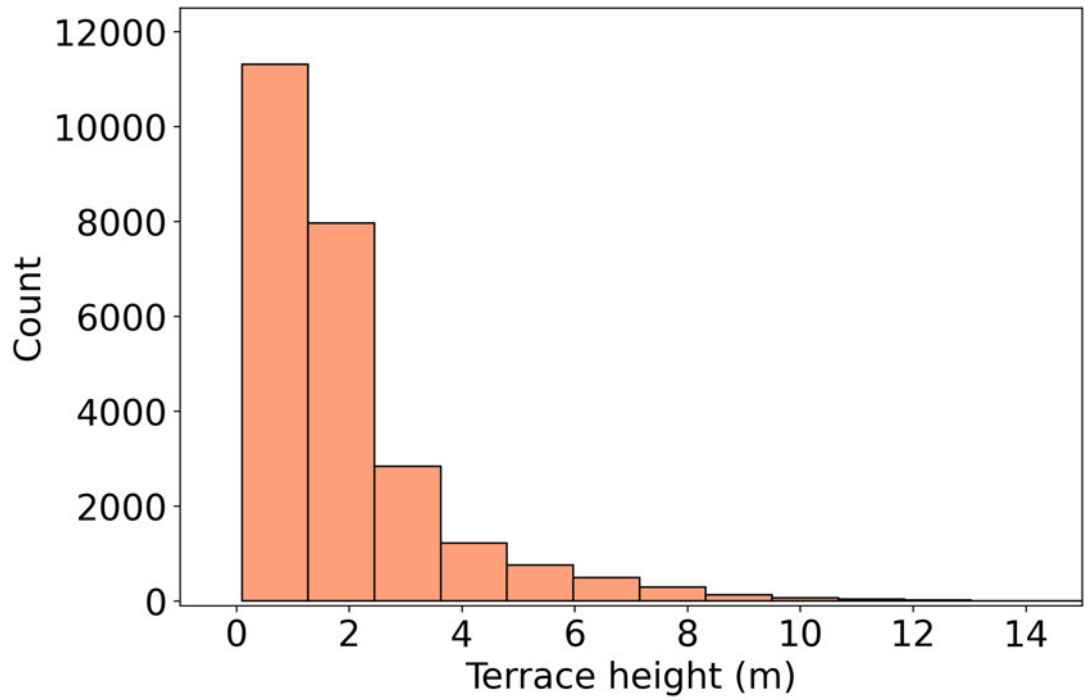

Figure A.S5: Histogram of the terrace heights above 0.1 m in the Feshie basin derived using the 10 m buffer zone approach (see Section 2.3.3 in Chapter 2 for details).

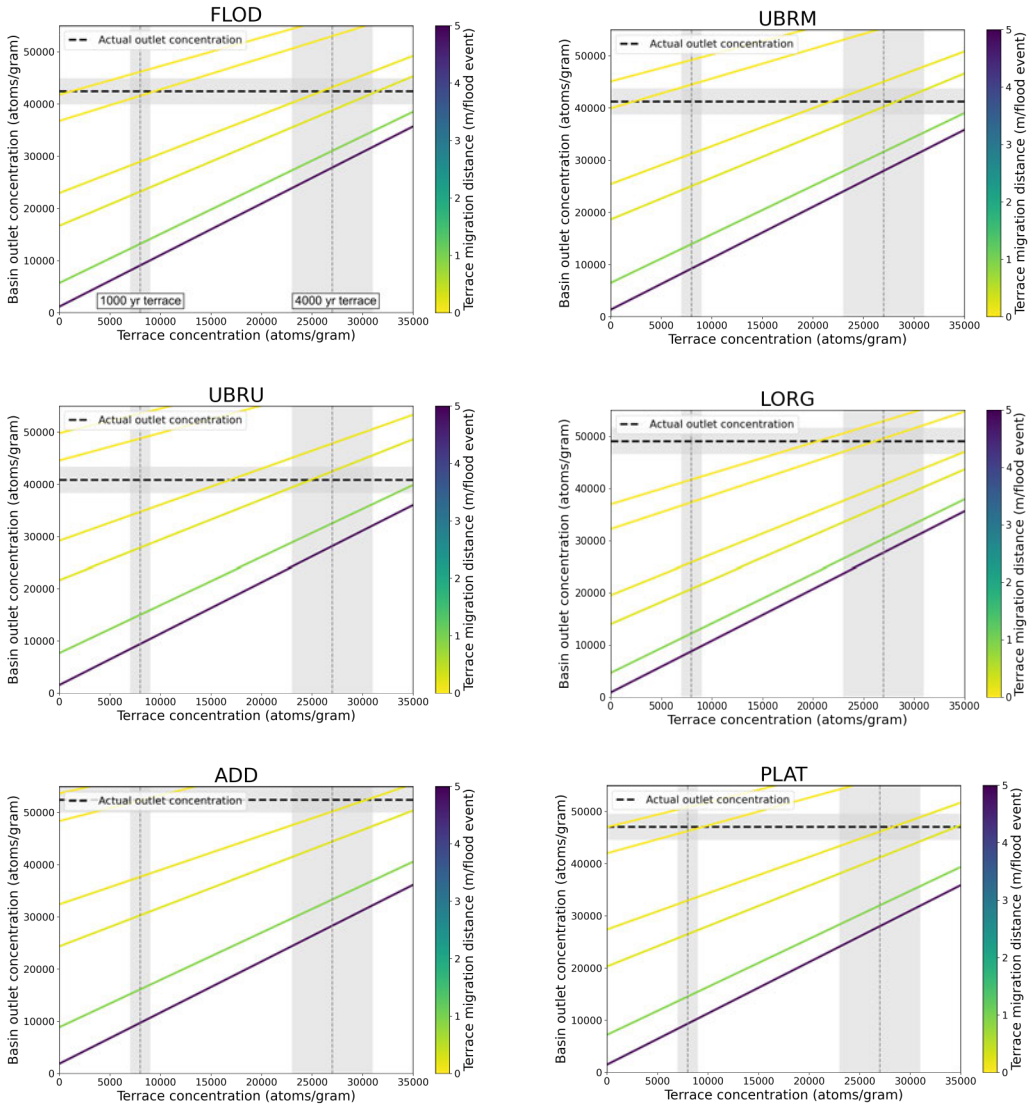

Figure A.S6: Results of the mixing model for samples not presented in the main text. The measured ^{14}C concentration at these sites ('actual outlet concentration') is shown by the black horizontal dashed line. Blank-correct analytical uncertainties are shown by the grey shaded error bars on the 'actual outlet concentration'. The influence of various terrace migration distances per flood event (0.08, 0.1, 0.2, 0.3, 1, 5 m) on the predicted ^{14}C concentration at these sites is shown by the coloured lines. Grey vertical lines represent concentrations for terrace with ages of 1000 (8000 atoms/g) and 4000 years (27000 atoms/g), with shaded 10 % error bars. These error bars represent uncertainty from terrace elevation-derived ^{14}C production rates.

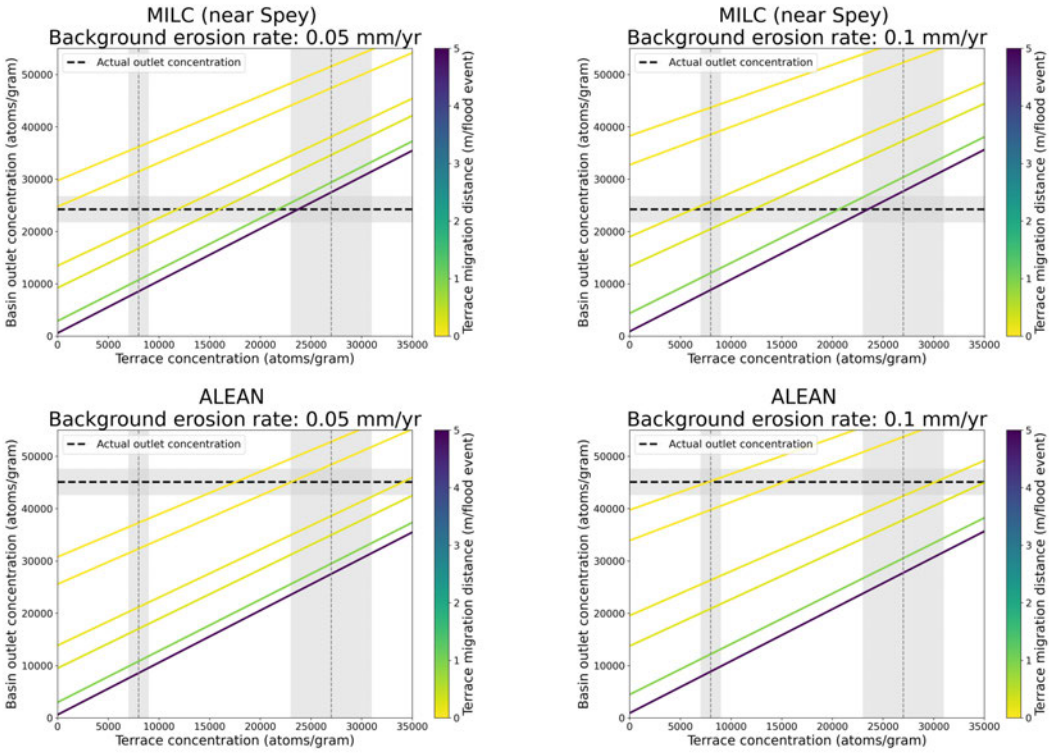

Figure A.S7: Results of the mixing model using different 'background' erosion rates and background concentrations. The mixing model results presented in the main text and Figure S6 use the Garbhlach's denudation rate of 0.175 mm/yr. The plots above show terrace migration rates associated with lower 'background' denudation rates (0.05, 0.1 mm/yr) for samples MILC and ALEAN. The measured ^{14}C concentration at these sites ('actual outlet concentration') is shown by the black horizontal dashed line. Blank-correct analytical uncertainties are shown by the grey shaded error bars on the 'actual outlet concentration'. The influence of various terrace migration distances per flood event (0.08, 0.1, 0.2, 0.3, 1, 5 m) on the predicted ^{14}C concentration at these sites is shown by the coloured lines. Grey vertical lines represent concentrations for terrace with ages of 1000 (8000 atoms/g) and 4000 years (27000 atoms/g), with shaded 10 $\%$ error bars. These error bars represent uncertainty from terrace elevation-derived ^{14}C production rates.

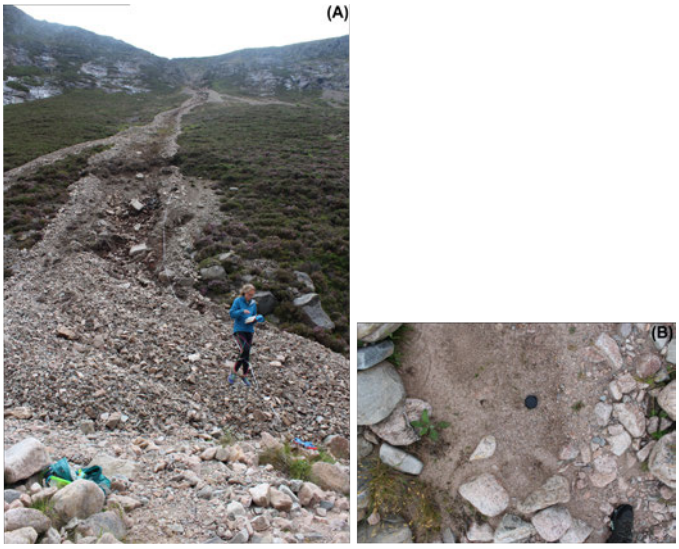

Figure A.S8: (A) Debris flow observed in Garbhlach catchment at GR 57.029744, -3.856973. (B) Photograph shows sand in debris flow with 5.8 cm camera lens cap for scale.

Appendix B

This Appendix refers to Chapter 3 and includes figures and tables presenting information on d50 grain sizes, manually measured grain sizes, bedrock erodibility, and the PebbleCounts algorithm.

Sample number	Sample name	Latitude	Longitude
1	Mei	56.53787	-3.38905
2	Dalguise	56.59245	-3.62323
3	Garryfalls	56.76528	-3.95298
4	Tummel_lower	56.65848	-3.67399
5	Garry_Bridge	56.7221	-3.7792
6	DallCottage_Trib	56.79954	-4.03774
7	Drum	56.82606	-4.21938
8	SoldiersLeep	56.74118	-3.77322
9	Trib_Soldiers_Leep	56.741178	-3.77314

Table B.S1: Details of samples used to compare PebbleCountsAuto to the manually measured control dataset. Sample numbers correspond to the sample numbers in Figure 3.2 in the main text.

Change in height (cm)	Camera resolution (mm/pixel)	Pebble size (mm)	Pebble size % difference relative to original resolution
0	0.54	108.47	
5	0.56	111.97	3
10	0.58	115.47	6
15	0.60	119.28	10

Table B.S2: Sensitivity of PebbleCounts-derived grain size measurements to variations in camera height. The camera resolution and final pebble size (mm) were calculated using a standard consumer-grade mobile phone camera (e.g., sensor height = 4.55 mm, sensor width = 6.17 mm, focal length = 4.3 mm, image height = 3024 pixels, image width = 4032 pixels) and a pebble pixel size of 200 pixels. The percentage differences represent the differences in the pebble size relative to that calculated from a resolution of 0.54 mm/pixel (ie., 108.47 mm for a 200 pixel pebble), which is the average camera resolution used in this study.

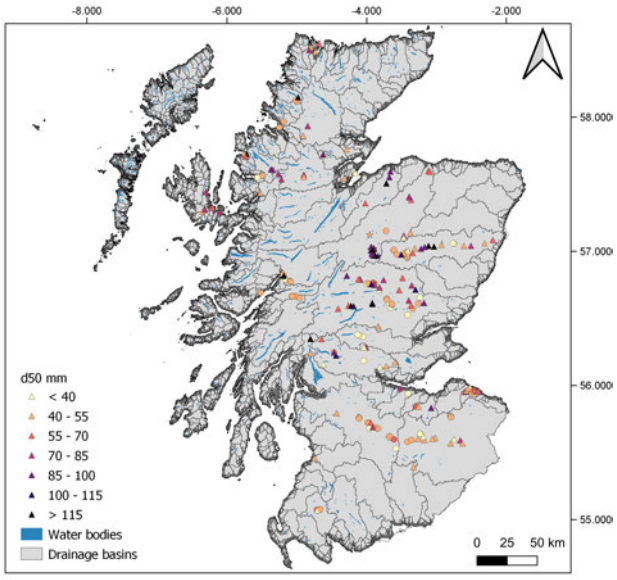

Figure B.S1: Map of Scotland (focused on the mainland) showing 279 locations coloured according to d50 (mm). Circles represent samples processed with PebbleCountsAuto, triangles show manually clicked sites, and stars represent samples measured using Wolman Point Counts. Water bodies ($<$10 hectares) are shown in dark blue and drainage basin outlines (15 arc-second resolution) in black (sourced from the HydroLAKES and HydroBASINS databases, (Lehner and Grill, 2013; Messager et al., 2016))

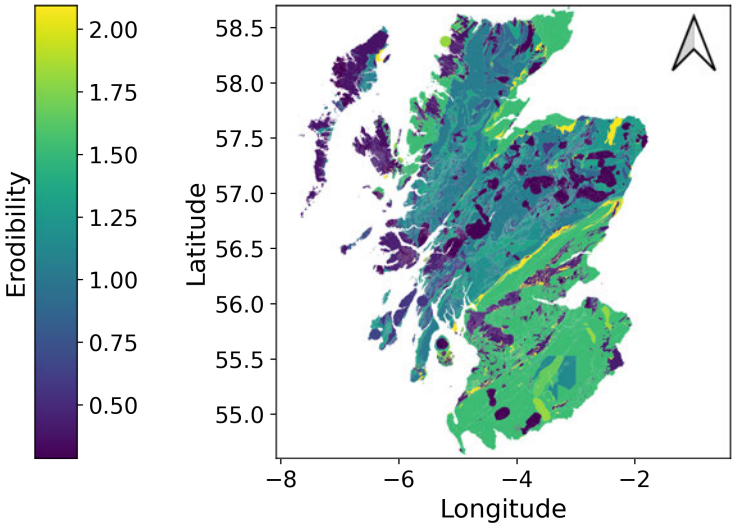

Figure B.S2: Map of Scotland (focused on the mainland) showing bedrock erodibility which was calculated using the method outlined by Clubb et al. (2023).

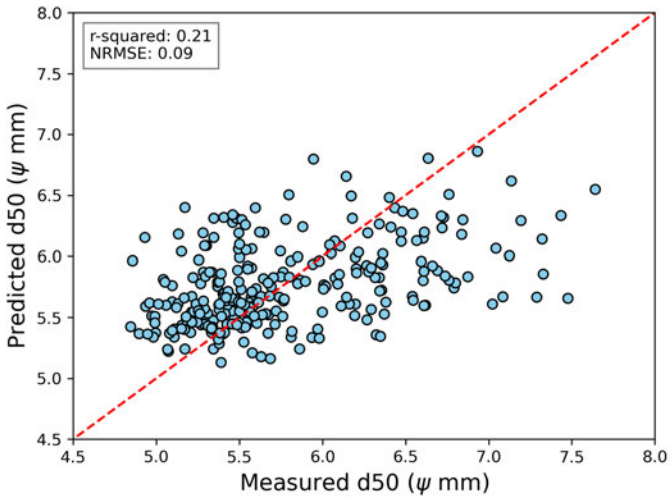

Figure B.S3: Results from the Random Forest Regressor analysis for the d50. Figure shows the model's predictive ability which is poor. The dashed red line represents the 1:1 relationship.

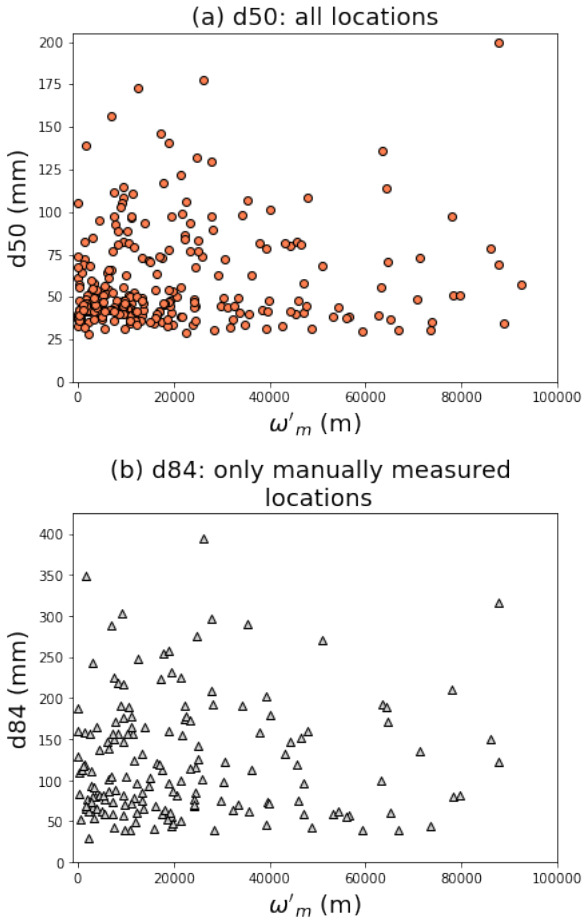

Figure B.S4: (a) d50 as a function of ω'_m, for all surveyed locations. (b) d84 as a function of ω'_m for only the sites that have been manually measured (i.e., photos that have been manually clicked and sites that were surveyed using Wolman Point Counts). Both plots display null correlations.

Bibliography

Abeshu, G. W., Li, H.-Y., Zhu, Z., Tan, Z., and Leung, L. R. (2021). Median bed-material sediment particle size across rivers in the contiguous U.S. *Earth System Science Data Discussions*, pages 1–22.

Adams, B. A. and Ehlers, T. A. (2018). Tectonic controls of Holocene erosion in a glaciated orogen. *Earth Surface Dynamics*, 6(3):595–610.

Attal, M. and Lavé, J. (2006). Changes of bedload characteristics along the Marsyandi River (central Nepal): Implications for understanding hillslope sediment supply, sediment load evolution along fluvial networks, and denudation in active orogenic belts. *Special Paper of the Geological Society of America*, 398(January):143–171.

Attal, M., Mudd, S. M., Hurst, M. D., Weinman, B., Yoo, K., and Naylor, M. (2015). Impact of change in erosion rate and landscape steepness on hillslope and fluvial sediments grain size in the Feather River basin (Sierra Nevada, California). *Earth Surface Dynamics*, 3(1):201–222.

Bailey FE and Koleske JV (1990). *Alkylene oxides and their polymers.* Dekker, New York, 1 edition.

Balco, G., Stone, J. O., Lifton, N. A., and Dunai, T. J. (2008). A complete and easily accessible means of calculating surface exposure ages or erosion rates from 10Be and 26Al measurements. *Quaternary Geochronology*, 3(3):174–195.

Ballantyne, C. K. (2002). A general model of paraglacial landscape response. *Holocene*, 12(3):371–376.

Ballantyne, C. K. (2008). *After the ice: Holocene geomorphic activity in the Scottish Highlands*, volume 124.

Ballantyne, C. K. (2019). After the ice: Lateglacial and holocene landforms and landscape evolution in Scotland. *Earth and Environmental Science Transactions of the Royal Society of Edinburgh*, 110(1-2):133–171.

Ballantyne, C. K., Hall, A. M., and Dawson, A. G. (2021). The Quaternary in Scotland. In *World Geomorphological Landscapes*, pages 53–96. Springer Science and Business Media B.V.

Bathurst, J. C. (2013). Critical conditions for particle motion in coarse bed materials of nonuniform size distribution. *Geomorphology*, 197:170–184.

Bathurst, J. C., Graf, W. H., and Cao, H. H. (1987). Sediment Transport in Gravel-bed Rivers Edited by CR Thorne, JC Bathurst and RD Hey C 1987 John Wiley & Sons Ltd. *Sediment Transport in Gravel-Bed Rivers*, page 453.

Baynes, E. R., Lague, D., Steer, P., Bonnet, S., and Illien, L. (2020). Sediment flux-driven channel geometry adjustment of bedrock and mixed gravel–bedrock rivers. *Earth Surface Processes and Landforms*, 45(14):3714–3731.

Belmont, P., Pazzaglia, F. J., and Gosse, J. C. (2007). Cosmogenic 10Be as a tracer for hillslope and channel sediment dynamics in the Clearwater River, western Washington State. *Earth and Planetary Science Letters*, 264(1):123–135.

Benn, D. and Evans, D. J. (2014). *Glaciers and glaciation*. Routledge.

Beven, K. (1997). TOPMODEL: a critique. *Hydrological Processes*, 11(9):1069–1085.

BGS (2021). British Geological Survey: Bedrock and Superficial Maps. Available at: https://digimap.edina.ac.uk/ [Accessed June 2015].

Bierman, P. R. (1994). Using in situ produced cosmogenic isotopes to estimate rates of landscape evolution: a review from the geomorphic perspective. *Journal of Geophysical Research*, 99(B7).

Bing Maps (2023). Bing Maps. Available at: https://www.bing.com/maps/ [Accessed July 2023].

Bishop, P., Hoey, T. B., Jansen, J. D., and Lexartza Artza, I. (2005). Knickpoint recession rate and catchment area: The case of uplifted rivers in Eastern Scotland. *Earth Surface Processes and Landforms*, 30(6):767–778.

Bookhagen, B. and Strecker, M. R. (2012). Spatiotemporal trends in erosion rates across a pronounced rainfall gradient: Examples from the southern Central Andes. *Earth and Planetary Science Letters*, 327-328:97–110.

Borchers, B., Marrero, S., Balco, G., Caffee, M., Goehring, B., Lifton, N., Nishiizumi, K., Phillips, F., Schaefer, J., and Stone, J. (2016). Geological calibration of spallation production rates in the CRONUS-Earth project. *Quaternary Geochronology*, 31:188–198.

Bradley, S. A., Ely, J. E., Clark, C. H., Edwards, R. O., and Shennan, I. (2023). Reconstruction of the palaeo-sea level of Britain and Ireland arising from empirical constraints of ice extent: implications for regional sea level forecasts and North American ice sheet volume. *Journal of Quaternary Science*, 38(6):791–805.

Bradley, S. L., Milne, G. A., Shennan, I., and Edwards, R. (2011). An improved glacial isostatic adjustment model for the British Isles. *Journal of Quaternary Science*, 26(5):541–552.

Brasington, J., Vericat, D., and Rychkov, I. (2012). Modeling river bed morphology, roughness, and surface sedimentology using high resolution terrestrial laser scanning. *Water Resources Research*, 48(11):1–18.

Braucher, R., Del Castillo, P., Siame, L., Hidy, A. J., and Bourlés, D. L. (2009). Determination of both exposure time and denudation rate from an in situ-produced 10Be depth profile: A mathematical proof of uniqueness. Model sensitivity and applications to natural cases. *Quaternary Geochronology*, 4(1):56–67.

Breiman, L. (2001). Random Forests. Technical report.

Brown, E. T., Stallard, R. F., Larsen, M. C., Raisbeck, G. M., and Yiou, F. (1995). Denudation rates determined from the accumulation of in situ-produced 10Be in the luquillo experimental forest, Puerto Rico. *Earth and Planetary Science Letters*, 129(1-4):193–202.

Buchanan, D. H., Naylor, L. A., Hurst, M. D., and Stephenson, W. J. (2020). Erosion of rocky shore platforms by block detachment from layered stratigraphy. *Earth Surface Processes and Landforms*, 45(4):1028–1037.

Buffington, J. M. and Montgomery, D. R. (1997). A systematic analysis of eight decades of incipient motion studies, with special reference to gravel-bedded rivers. *Water Resources Research*, 33(8):1993–2029.

Bunte, K. and Abt, S. R. (2001). Sampling surface and subsurface particle-size distributions in wadable gravel-and cobble-bed streams for analyses in sediment transport, hydraulics, and streambed monitoring. *Gen. Tech. Rep. RMRS-GTR-74, US Department of Agriculture, Forest Service.*, page 428.

Campforts, B., Vanacker, V., Herman, F. d., Vanmaercke, M., Schwanghart, W., Tenorio, G. E., Willems, P., and Govers, G. (2020). Parameterization of river incision models requires accounting for environmental heterogeneity: Insights from the tropical Andes. *Earth Surface Dynamics*, 8(2):447–470.

Castillo, M., Bishop, P., and Jansen, J. D. (2013). Knickpoint retreat and transient bedrock channel morphology triggered by base-level fall in small bedrock river catchments: The case of the Isle of Jura, Scotland. *Geomorphology*, 180-181:1–9.

Chandler, B. M., Boston, C. M., and Lukas, S. (2019). A spatially-restricted Younger Dryas plateau icefield in the Gaick, Scotland: Reconstruction and palaeoclimatic implications. *Quaternary Science Reviews*, 211:107–135.

Chappell, J., Omura, A., Esat, T., McCulloch, M., Pandolfi, J., Ota, Y., and Pillans, B. (1996). Reconciliaion of late Quaternary sea levels derived from coral terraces at Huon Peninsula with deep sea oxygen isotope records. *Earth and Planetary Science Letters*, 141(1):227–236.

Chardon, V., Piasny, G., and Schmitt, L. (2022). Comparison of software accuracy to estimate the bed grain size distribution from digital images: A test performed along the Rhine River. *River Research and Applications*, 38(2):358–367.

Charreau, J., Blard, P.-H., Zumaque, J., Martin, L. C., Delobel, T., and Szafran, L. (2019). Basinga: A cell-by-cell GIS toolbox for computing basin average scaling factors, cosmogenic production rates and denudation rates. *Earth Surface Processes and Landforms*, 44(12):2349–2365.

Chmeleff, J., von Blanckenburg, F., Kossert, K., and Jakob, D. (2010). Determination of the 10Be half-life by multicollector ICP-MS and liquid scintillation counting. *Nuclear Instruments and Methods in Physics Research, Section B: Beam Interactions with Materials and Atoms*, 268(2):192–199.

Chow, V. (1959). Open channel hydraulics. *McGraw-Hill Book Co., New York*.

Church, M. and Ryder, J. M. (1972). Paraglacial sedimentation: A consideration of fluvial processes conditioned by glaciation. *Bulletin of the Geological Society of America*, 83(10):3059–3072.

Church, M. and Zimmermann, A. (2007). Form and stability of step-pool channels: Research progress. *Water Resources Research*, 43(3).

Clark, C. D., Ely, J. C., Greenwood, S. L., Hughes, A. L., Meehan, R., Barr, I. D., Bateman, M. D., Bradwell, T., Doole, J., Evans, D. J., Jordan, C. J., Monteys, X., Pellicer, X. M., and Sheehy, M. (2018). BRITICE Glacial Map, version 2: a map and GIS database of glacial landforms of the last British–Irish Ice Sheet. *Boreas*, 47(1):11–e8.

Clubb, F. J., Mudd, S. M., Milodowski, D. T., Valters, D. A., Slater, L. J., Hurst, M. D., and Limaye, A. B. (2017). Geomorphometric delineation of floodplains and terraces from objectively defined topographic thresholds. *Earth Surface Dynamics*, 5(3):369–385.

Clubb, F. J., Mudd, S. M., Schildgen, T. F., van der Beek, P. A., Devrani, R., and Sinclair, H. D. (2023). Himalayan valley-floor widths controlled by tectonically driven exhumation. *Nature Geoscience*, 16(8):739–746.

Codilean, A. T., Munack, H., Saktura, W. M., Cohen, T. J., Jacobs, Z., Ulm, S., Hesse, P. P., Heyman, J., Peters, K. J., Williams, A. N., Saktura, R. B. K., Rui, X., Chishiro-Dennelly, K., and Panta, A. (2022). OCTOPUS database (v.2). *Earth System Science Data*, 14(8):3695–3713.

Cook, K. L., Turowski, J. M., and Hovius, N. (2013). A demonstration of the importance of bedload transport for fluvial bedrock erosion and knickpoint propagation. *Earth Surface Processes and Landforms*, 38(7):683–695.

Coulthard, T. J., Neal, J. C., Bates, P. D., Ramirez, J., de Almeida, G. A., and Hancock, G. R. (2013). Integrating the LISFLOOD-FP 2D hydrodynamic model with the CAESAR model: Implications for modelling landscape evolution. *Earth Surface Processes and Landforms*, 38(15):1897–1906.

Crosby, B. T. and Whipple, K. X. (2006). Knickpoint initiation and distribution within fluvial networks: 236 waterfalls in the Waipaoa River, North Island, New Zealand. *Geomorphology*, 82(1):16–38.

Cyr, A. J., Granger, D. E., Olivetti, V., and Molin, P. (2010). Quantifying rock uplift rates using channel steepness and cosmogenic nuclide-determined erosion rates: Examples from northern and southern Italy. *Lithosphere*, 2(3):188–198.

Dawson, S., Powell, V. A., Duck, R. W., and McGlashan, D. J. (2013). Discussion of Rennie, A.F. and Hansom, J.D. 2011. Sea level trend reversal: Land uplift outpaced by sea level rise on Scotland's coast. Geomorphology, 125 (1), 193–202. *Geomorphology*, 197:185–186.

Delunel, R., Schlunegger, F., Valla, P. G., Dixon, J., Glotzbach, C., Hippe, K., Kober, F., Molliex, S., Norton, K. P., Salcher, B., Wittmann, H., Akçar, N., and Christl, M. (2020). Late-Pleistocene catchment-wide denudation patterns across the European Alps. *Earth-Science Reviews*, 211.

Delunel, R., van der Beek, P. A., Carcaillet, J., Bourlès, D. L., and Valla, P. G. (2010). Frost-cracking control on catchment denudation rates: Insights from in situ produced 10Be concentrations in stream sediments (Ecrins-Pelvoux massif, French Western Alps). *Earth and Planetary Science Letters*, 293(1-2):72–83.

Detert, M. and Weitbrecht, V. (2013). User guide to gravelometric image analysis by BASEGRAIN. *Advances in Science and Research*, (January):1789–1796.

DiBiase, R. A. (2018). Short communication: Increasing vertical attenuation length of cosmogenic nuclide production on steep slopes negates topographic shielding corrections for catchment erosion rates. *Earth Surface Dynamics*, 6(4):923–931.

Dickson, M.E, M., H, S., W.J, S., Z.M, T., C.F, Y., and A.P (2023). Sea-level rise may not uniformly accelerate cliff erosion rates. *Nat Commun*.

Egholm, D. L., Knudsen, M. F., and Sandiford, M. (2013). Lifespan of mountain ranges scaled by feedbacks between landsliding and erosion by rivers. *Nature*, 498(7455):475–478.

Ehlers, J., Gibbard, P. L., and Hughes, P. D. (2018). Chapter 4 - Quaternary Glaciations and Chronology. In Menzies, J. and van der Meer, J. J. M., editors, *Past Glacial Environments (Second Edition)*, pages 77–101. Elsevier, second edition edition.

Emery, K. O. and Kuhn, G. G. (1982). Sea cliffs: Their processes, profiles, and classification. *GSA Bulletin*, 93(7):644–654.

Ferguson, R. and Ashworth, P. (1991). Slope-induced changes in channel character along a gravel-bed stream: the allt dubhaig, scotland. *Earth surface processes and landforms*, 16(1):65–82.

Fieman, D. M., Attal, M., and Addy, S. (2020). Geomorphic response of a mountain gravel-bed river to an extreme flood in Aberdeenshire, Scotland. *Scottish Journal of Geology*, 56:2019–005.

Finnegan, N. J., Klier, R. A., Johnstone, S., Pfeiffer, A. M., and Johnson, K. (2017). Field evidence for the control of grain size and sediment supply on steady-state bedrock river channel slopes in a tectonically active setting. *Earth Surface Processes and Landforms*, 42(14):2338–2349.

Finnegan, N. J., Roe, G., Montgomery, D. R., and Hallet, B. (2005). Controls on the channel width of rivers: Implications for modeling fluvial incision of bedrock. *Geology*, 33(3):229–232.

Firth, C. R. and Stewart, I. S. (2000). Postglacial tectonics of the Scottish glacio-isostatic uplift centre. *Quaternary Science Reviews*, 19(14-15):1469–1493.

Flint, J. J. (1974). Stream gradient as a function of order, magnitude, and discharge. *Water Resources Research*, 10(5):969–973.

Forte, A. M., Yanites, B. J., and Whipple, K. X. (2016). Complexities of landscape evolution during incision through layered stratigraphy with contrasts in rock strength. *Earth Surface Processes and Landforms*, 41(12):1736–1757.

Fülöp, R. H., Wacker, L., and Dunai, T. J. (2015). Progress report on a novel in situ 14C extraction scheme at the University of Cologne. *Nuclear Instruments and Methods in Physics Research, Section B: Beam Interactions with Materials and Atoms*, 361:20–24.

Gailleton, B., Mudd, S. M., Clubb, F. J., Peifer, D., and Hurst, M. D. (2019). A segmentation approach for the reproducible extraction and quantification of knickpoints from river long profiles. *Earth Surface Dynamics*, 7(1):211–230.

Gilbert, G. (1877). Geology of the henry mountains. *(Technical Report). Government Printing Office.*

Godard, V., Bourlès, D. L., Spinabella, F., Burbank, D. W., Bookhagen, B., Fisher, G. B., Moulin, A., and Léanni, L. (2014). Dominance of tectonics over climate in himalayan denudation. *Geology*, 42(3):243–246.

Gomez, B., Rosser, B. J., Peacock, D. H., Hicks, D. M., and Palmer, J. A. (2001). Downstream fining in a rapidly aggrading gravel bed river. *Water Resources Research*, 37(6):1813–1823.

Gómez-Pazo, A., Payo, A., Paz-Delgado, M. V., and Delgadillo-Calzadilla, M. A. (2022). Open digital shoreline analysis system: Odsas v1. 0. *Journal of Marine Science and Engineering*, 10(1):26.

Google Maps (2023). Google Maps. Available at: Google Earth Pro [Accessed July 2023].

Gosse, J. C. and Phillips, F. M. (2001). Terrestrial in situ cosmogenic nuclides: theory and application. *Quaternary Science Reviews*, 20(14):1475–1560.

Granger, D. E., Kirchner, J. W., and Finkel, R. (1996). Spatially averaged long-term erosion rates measured from in situ-produced cosmogenic nuclides in alluvial sediment. *Journal of Geology*, 104(3):249–257.

Granger, D. E. and Smith, A. L. (2000). Dating buried sediments using radioactive decay and muogenic production of 26Al and 10Be. *Nuclear Instruments and Methods in Physics Research, Section B: Beam Interactions with Materials and Atoms*, 172(1-4):822–826.

Hack, J. (1960). Interpretation of erosional topography in humid temperate regions. *American Journal of Science*.

Hack, J. T., Seaton, F. A., and Nolan, T. B. (1957). Studies of Longitudinal Stream Profiles in Virginia and Maryland UNITED STATES DEPARTMENT OF THE INTERIOR. *Report*.

Hackney, C., Darby, S. E., and Leyland, J. (2015). Landscapes on the edge: Examining the role of climatic interactions in shaping coastal watersheds using a coastal-terrestrial landscape evolution model. *Earth Surface Processes and Landforms*, 40(3):313–325.

Haddadchi, A., Booker, D. J., and Measures, R. J. (2018). Predicting river bed substrate cover proportions across New Zealand. *Catena*, 163(January 2017):130–146.

Hallet, B. (1979). A theoretical model of glacial abrasion. *Journal of Glaciology*, 23(89):39–50.

Hallet, B., Hunter, L., and Bogen, J. (1996). Rates of erosion and sediment evacuation by glaciers: A review of field data and their implications. *Global and Planetary Change*, 12(1-4):213–235.

Hansom, J., Fitton, J., and Rennie, A. (2017). *Dynamic Coast - National Coastal Change Assessment: National Overview*.

Harel, M. A., Mudd, S. M., and Attal, M. (2016). Global analysis of the stream power law parameters based on worldwide 10Be denudation rates. *Geomorphology*, 268:184–196.

Harvey, E. L., Hales, T. C., Hobley, D. E., Liu, J., and Fan, X. (2022). Measuring the grain-size distributions of mass movement deposits. *Earth Surface Processes and Landforms*, 47(6):1599–1614.

Haviv, I., Enzel, Y., Whipple, K. X., Zilberman, E., Matmon, A., Stone, J., and Fifield, K. L. (2010). Evolution of vertical knickpoints (waterfalls) with resistant caprock: Insights from numerical modeling. *Journal of Geophysical Research: Earth Surface*, 115(F3).

Herman, F., De Doncker, F., Delaney, I., Prasicek, G., and Koppes, M. (2021). The impact of glaciers on mountain erosion. *Nature Reviews Earth & Environment*, 2(6):422–435.

Hippe, K. (2017). Constraining processes of landscape change with combined in situ cosmogenic 14C-10Be analysis. *Quaternary Science Reviews*, 173:1–19.

Hippe, K., Jansen, J. D., Skov, D. S., Lupker, M., Ivy-Ochs, S., Kober, F., Zeilinger, G., Capriles, J. M., Christl, M., Maden, C., Vockenhuber, C., and Egholm, D. L. (2021). Cosmogenic in situ 14C-10Be reveals abrupt Late Holocene soil loss in the Andean Altiplano. *Nature Communications*, 12(1).

Howard, A. D. and Kerby, G. (1983). Channel changes in badlands. *Geological Society of America Bulletin*, 94(6):739–752.

Hurst, M. D., Rood, D. H., Ellis, M. A., Anderson, R. S., and Dornbusch, U. (2016). Recent acceleration in coastal cliff retreat rates on the south coast of Great Britain. *Proceedings of the National Academy of Sciences of the United States of America*, 113(47):13336–13341.

International Atomic Energy Agency (2024). IAEA - Nuclear Data Section. Available at: https://www-nds.iaea.org/ [Accessed Feb 2024] .

Jansen, J. D., Codilean, A. T., Bishop, P., and Hoey, T. B. (2010). Scale dependence of lithological control on topography: Bedrock channel geometry and catchment morphometry in western Scotland. *Journal of Geology*, 118(3):223–246.

Jansen, J. D., Fabel, D., Bishop, P., Xu, S., Schnabel, C., and Codilean, A. T. (2011). Does decreasing paraglacial sediment supply slow knickpoint retreat? *Geology*, 39(6):543–546.

Johnson, S. E., Swallom, M. L., Thigpen, R., McGlue, M., Dortch, J. M., Gallen, S., Woolery, E., and Yeager, K. M. (2022). The influence of glacial topography on fluvial efficiency in the Teton Range, Wyoming (USA). *Earth and Planetary Science Letters*, 592.

Kellerhals, R. and Bray, D. I. (1971). Sampling Procedures for Coarse Fluvial Sediments. *Journal of the Hydraulics Division*, 97(8):1165–1180.

Kennedy, D. M., Stephenson, W. J., and Naylor, L. A. (2014). Chapter 1 Introduction to the rock coasts of the world. *Geological Society, London, Memoirs*, 40(1):1–5.

Kim, J. Y. (2004). *Controls over bedrock channel incision [PhD thesis]*. University of Glasgow.

Kirby, E. and Whipple, K. X. (2012). Expression of active tectonics in erosional landscapes. *Journal of Structural Geology*, 44:54–75.

Knopf, E. B. (1924). Correlation of residual erosion surfaces in the eastern appalachian highlands. *Bulletin of the Geological Society of America*, 35(3):633–668.

Kober, F., Hippe, K., Salcher, B., Grischott, R., Zurfluh, R., Hajdas, I., Wacker, L., Christl, M., and Ivy-Ochs, S. (2019). Postglacial to Holocene landscape evolution and process rates in steep alpine catchments. *Earth Surface Processes and Landforms*, 44(1):242–258.

Kohl, C. P. and Nishiizumi, K. (1992). Chemical isolation of quartz for measurement of in-situ-produced cosmogenic nuclides. *Geochimica et Cosmochimica Acta*, 56:3583–3587.

Lal, D. (1991). Cosmic ray labeling of erosion surfaces: in situ nuclide production rates and erosion models: Earth and Planetary Science Letters. *Earth and Planetary Science Letters*, 104(2-4):424–439.

Lea, D. W., Martin, P. A., Pak, D. K., and Spero, H. J. (2002). Reconstructing a 350ky history of sea level using planktonic Mg/Ca and oxygen isotope records from a Cocos Ridge core. *Quaternary Science Reviews*, 21(1):283–293.

Lehner, B. and Grill, G. (2013). Global river hydrography and network routing: Baseline data and new approaches to study the world's large river systems. *Hydrological Processes*, 27(15):2171–2186.

Leyland, J. and Darby, S. E. (2009). Effects of Holocene climate and sea-level changes on coastal gully evolution: Insights from numerical modelling. *Earth Surface Processes and Landforms*, 34(14):1878–1893.

Li, T., Fuller, T. K., Sklar, L. S., Gran, K. B., and Venditti, J. G. (2020a). A Mechanistic Model for Lateral Erosion of Bedrock Channel Banks by Bedload Particle Impacts. *Journal of Geophysical Research: Earth Surface*, 125(6).

Li, T., Fuller, T. K., Sklar, L. S., Gran, K. B., and Venditti, J. G. (2020b). A Mechanistic Model for Lateral Erosion of Bedrock Channel Banks by Bedload Particle Impacts. *Journal of Geophysical Research: Earth Surface*, 125(6).

Lifton, N., Sato, T., and Dunai, T. J. (2014). Scaling in situ cosmogenic nuclide production rates using analytical approximations to atmospheric cosmic-ray fluxes. *Earth and Planetary Science Letters*, 386:149–160.

Lifton, N., Wilson, J., and Koester, A. (2023). Technical note: Studying lithium metaborate fluxes and extraction protocols with
}a new, fully automated in situ cosmogenic ˆ14C processing system at PRIME Lab. *Geochronology*, 5(2):361–375.

Limber, P. W. and Barnard, P. L. (2018). Coastal knickpoints and the competition between fluvial and wave-driven erosion on rocky coastlines. *Geomorphology*, 306:1–12.

Linton, D. L. (1949). Some scottish river captures re-examined. *Scottish Geographical Magazine*, 65(3):123–132.

Lisiecki, L. E. and Raymo, M. E. (2005). A Pliocene-Pleistocene stack of 57 globally distributed benthic δ 18O records. *Paleoceanography*, 20(1):1–17.

Lupker, M., Hippe, K., Wacker, L., Kober, F., Maden, C., Braucher, R., Bourlès, D., Romani, J. R., and Wieler, R. (2015). Depth-dependence of the production rate of in situ14C in quartz from the Leymon High core, Spain. *Quaternary Geochronology*, 28:80–87.

Lupker, M., Hippe, K., Wacker, L., Steinemann, O., Tikhomirov, D., Maden, C., Haghipour, N., and Synal, H.-A. (2019). In-situ cosmogenic 14C analysis at ETH Zürich: Characterization and performance of a new extraction system. *Nuclear Instruments and Methods in Physics Research Section B: Beam Interactions with Materials and Atoms*, 457:30–36.

Lupker, M., Lavé, J., France-Lanord, C., Christl, M., Bourlès, D., Carcaillet, J., Maden, C., Wieler, R., Rahman, M., Bezbaruah, D., and Xiaohan, L. (2017). 10Be systematics in the Tsangpo-Brahmaputra catchment: The cosmogenic nuclide legacy of the eastern Himalayan syntaxis. *Earth Surface Dynamics*, 5(3):429–449.

Mackey, B. H., Scheingross, J. S., Lamb, M. P., and Farley, K. A. (2014). Knickpoint formation, rapid propagation, and landscape response following coastal cliff retreat at the last interglacial sea-level highstand: Kaua'i, Hawai'i. *Bulletin of the Geological Society of America*, 126(7-8):925–942.

Mason, R. J. and Polvi, L. E. (2023). Unravelling fluvial versus glacial legacy controls on boulder-bed river geomorphology for semi-alluvial rivers in Fennoscandia. *Earth Surface Processes and Landforms*, 48(14):2900–2919.

Masselink, G., Russell, P., Rennie, A., Brooks, S., and Spencer, T. (2020). Impacts of climate change on coastal geomorphology and coastal erosion relevant to the coastal and marine environment around the UK. *MCCIP Science Review*, pages 158–189.

Matthews, B., Naylor, M., Sinclair, H., Black, A., Williams, R., Cuthill, C., Gervais, M., Dietze, M., and Smith, A. (2024). Sounding out the river: Seismic and hydroacoustic monitoring of bedload transport. *Earth Surface Processes and Landforms*.

Messager, M. L., Lehner, B., Grill, G., Nedeva, I., and Schmitt, O. (2016). Estimating the volume and age of water stored in global lakes using a geo-statistical approach. *Nature Communications*, 7:1–11.

Miazza, R., Pascal, I., and Ancey, C. (2024). Automated grain sizing from uncrewed aerial vehicles imagery of a gravel-bed river: Benchmarking of three object-based methods. *Earth Surface Processes and Landforms*.

Montgomery, D. R. and Buffington, J. M. (1997). Channel-reach morphology in mountain drainage basins. *GSA Bulletin*, 109(5):596–611.

Moussavi-Harami, R., Mahboubi, A., and Khanehbad, M. (2004). Analysis of controls on downstream fining along three gravel-bed rivers in the Band-e-Golestan drainage basin NE Iran. *Geomorphology*, 61(1):143–153.

Mudd, S., Clubb, F., Grieve, S., Milodowski, D., Gailleton, B., Hurst, M., Valters, D., Wickert, A., and Hutton, E. (2023). LSDtopotools/LSDTopoTools2: LSDTopoTools2 v0.8.

Mudd, S. M. (2017). Detection of transience in eroding landscapes. *Earth Surface Processes and Landforms*, 42(1):24–41.

Mudd, S. M., Attal, M., Milodowski, D. T., Grieve, S. W., and Valters, D. A. (2014). A statistical framework to quantify spatial variation in channel gradients using the integral method of channel profile analysis. *Journal of Geophysical Research: Earth Surface*, 119(2):138–152.

Mudd, S. M., Harel, M. A., Hurst, M. D., Grieve, S. W., and Marrero, S. M. (2016). The CAIRN method: Automated, reproducible calculation of catchment-averaged denudation rates from cosmogenic nuclide concentrations. *Earth Surface Dynamics*, 4(3):655–674.

Mueller, E. R. and Pitlick, J. (2013). Sediment supply and channel morphology in mountain river systems: 1. Relative importance of lithology, topography, and climate. *Journal of Geophysical Research: Earth Surface*, 118(4):2325–2342.

Mueller, E. R. and Pitlick, J. (2014). Sediment supply and channel morphology in mountain river systems: 2. Single thread to braided transitions. *Journal of Geophysical Research: Earth Surface*, 119(7):1516–1541.

Mugodo, J., Kennard, M., Liston, P., Nichols, S., Linke, S., Norris, R. H., and Lintermans, M. (2006). Local stream habitat variables predicted from catchment scale characteristics are useful for predicting fish distribution. *Hydrobiologia*, 572(1):59–70.

Nichols, K. A. and Goehring, B. M. (2019). Isolation of quartz for cosmogenic in situ \chem{^{14}C} analysis. *Geochronology*, 1(1):43–52.

Ordnance Survey (2021). OS Terrain 5.

Parker, G. (1991). possible to formulate quantitative theories of downstream fining that rely solely on the mechanism of selective sorting , e . g ., Diegaard (1980) and Di Silvio (1984). In the case of gravel streams the situation is much less clear . The abrasion rate. *Journal of Hydraulic Engineering*, 117(2):131–147.

Perron, J. T. and Royden, L. (2013). An integral approach to bedrock river profile analysis. *Earth surface processes and landforms*, 38(6):570–576.

Prasicek, G., Larsen, I. J., and Montgomery, D. R. (2015). Tectonic control on the persistence of glacially sculpted topography. *Nature Communications*, 6.

Prémaillon, M., Regard, V., Dewez, T. J. B., and Auda, Y. (2018). GlobR2C2 (Global Recession Rates of Coastal Cliffs): a global relational database to investigate coastal rocky cliff erosion rate variations. *Earth Surface Dynamics*, 6(3):651–668.

Purinton, B. and Bookhagen, B. (2019). Introducing PebbleCounts: A grain-sizing tool for photo surveys of dynamic gravel-bed rivers. *Earth Surface Dynamics Discussions*, pages 1–33.

Purinton, B. and Bookhagen, B. (2021). Tracking downstream variability in large grain-size distributions in the south-central Andes. *Journal of Geophysical Research: Earth Surface*, pages 1–29.

Quinn, N., Bates, P. D., and Siddall, M. (2013). The contribution to future flood risk in the severn estuary from extreme sea level rise due to ice sheet mass loss. *Journal of Geophysical Research: Oceans*, 118(11):5887–5898.

Raven, E. K., Lane, S. N., Ferguson, R. I., and Bracken, L. J. (2009). The spatial and temporal patterns of aggradation in a temperate, upland, gravel-bed river. *Earth Surface Processes and Landforms*, 34(9):1181–1197.

Reid, D. A., Hassan, M. A., and McCleary, R. (2022). Glacial landscape configuration influences channel response to flooding. *Earth Surface Processes and Landforms*, 47(1):209–227.

Reimer, P. J., Austin, W. E., Bard, E., Bayliss, A., Blackwell, P. G., Ramsey, C. B., Butzin, M., Cheng, H., Edwards, R. L., Friedrich, M., et al. (2020). The intcal20 northern hemisphere radiocarbon age calibration curve (0–55 cal kbp). *Radiocarbon*, 62(4):725–757.

Rennie, A. F. and Hansom, J. D. (2011). Sea level trend reversal: Land uplift outpaced by sea level rise on Scotland's coast. *Geomorphology*, 125(1):193–202.

Rice, S. and Church, M. (1998). Grain size along two gravel-bed rivers: Statistical variation, spatial pattern and sedimentary links. *Earth Surface Processes and Landforms*, 23(4):345–363.

Robertson-Rintoul, M. S. (1986). A quantitative soil-stratigraphic approach to the correlation and dating of post-glacial river terraces in Glen Feshie, western Cairngorms. *Earth Surface Processes and Landforms*, 11(6):605–617.

Rosser, N. J., Brain, M. J., Petley, D. N., Lim, M., and Norman, E. C. (2013). Coastline retreat via progressive failure of rocky coastal cliffs. *Geology*, 41(8):939–942.

Rumsby, B. T., Brasington, J., Langham, J. A., McLelland, S. J., Middleton, R., and Rollinson, G. (2008). Monitoring and modelling particle and reach-scale morphological change in gravel-bed rivers: Applications and challenges. *Geomorphology*, 93(1-2):40–54.

Safran, E. B., Bierman, P. R., Aalto, R., Dunne, T., Whipple, K. X., and Caffee, M. (2005). Erosion rates driven by channel network incision in the Bolivian Andes. *Earth Surface Processes and Landforms*, 30(8):1007–1024.

Schaller, M., Ehlers, T. A., Blum, J. D., and Kallenberg, M. A. (2009). Quantifying glacial moraine age, denudation, and soil mixing with cosmogenic nuclide depth profiles. *Journal of Geophysical Research: Earth Surface*, 114(1):1–18.

Scherler, D., Bookhagen, B., and Strecker, M. R. (2014). Tectonic control on 10Be-derived erosion rates in the Garhwal Himalaya, India. *Journal of Geophysical Research: Earth Surface*, 119(2):83–105.

Schiffer, M., Stolz, A., López, D. A., Spanier, R., Herb, S., Müller-Gatermann, C., Heinze, S., Binnie, S., Melchert, J., Kivel, N., Schumann, D., Rethemeyer, J., Dunai, T., and Dewald, A. (2020). Method developments for accelerator mass spectrometry at CologneAMS, 53Mn/3He burial dating and ultra-small 14CO2 samples. *Global and Planetary Change*, 184(May 2019):103053.

Scott, E. M., Naysmith, P., and Cook, G. T. (2018). Why do we need 14C inter-comparisons?: The Glasgow -14C inter-comparison series, a reflection over 30 years. *Quaternary Geochronology*, 43:72–82.

Scott, T., McCarroll, R., Masselink, G., Castelle, B., Dodet, G., Saulter, A., Scaife, A., and Dunstone, N. (2021). Role of atmospheric indices in describing inshore directional wave climate in the united kingdom and ireland. *Earth's Future*, 9(5):e2020EF001625.

Shadrick, J. R., Rood, D. H., Hurst, M. D., Piggott, M. D., Hebditch, B. G., Seal, A. J., and Wilcken, K. M. (2022). Sea-level rise will likely accelerate rock coast cliff retreat rates. *Nature Communications*, 13(1).

Shennan, I., Lambeck, K., Horton, B., Innes, J., Lloyd, J., McArthur, J., Purcell, T., and Rutherford, M. (2000). Late Devensian and Holocene records of relative sea-level changes in northwest Scotland and their implications for glacio-hydro-isostatic modelling. *Quaternary Science Reviews*, 19(11):1103–1135.

Shennan, I., Milne, G., and Bradley, S. (2009). Late Holocene relative land- and sea-level changes: Providing information for stakeholders. *GSA Today*, 19(9):52–53.

Shields, a. (1936). Application of similarity principles and turbulence research for bed-load movement. *Mitteilungen der preussischen Versuchsanstalt fu¨r Wasserbau und Schiffbuar*.

Sissons, J. B. (1974). Late-glacial marine erosion in Scotland. *Boreas*, 3(2):41–48.

Sklar, D. W. (2001). Sediment and rock strength controls on river incision into bedrock. *Geology*, 29(12):1087–1090.

Sklar, L. S. (2024). Grain Size in Landscapes. *Downloaded from www.annualreviews.org. Guest (guest*.

Sklar, L. S. and Dietrich, W. E. (2004). A mechanistic model for river incision into bedrock by saltating bed load. *Water Resources Research*, 40(6):1–22.

Sklar, L. S. and Dietrich, W. E. (2006). The role of sediment in controlling steady-state bedrock channel slope: Implications of the saltation-abrasion incision model. *Geomorphology*, 82(1-2):58–83.

Sklar, L. S., Dietrich, W. E., Foufoula-Georgiou, E., Lashermes, B., and Bellugi, D. (2006). Do gravel bed river size distributions record channel network structure? *Water Resources Research*, 42(SUPPL.):1–22.

Sklar, L. S., Riebe, C. S., Genetti, J., Leclere, S., and Lukens, C. E. (2020). Downvalley fining of hillslope sediment in an alpine catchment: implications for downstream fining of sediment flux in mountain rivers. *Earth Surface Processes and Landforms*, 45(8):1828–1845.

Sklar, L. S., Riebe, C. S., Marshall, J. A., Genetti, J., Leclere, S., Lukens, C. L., and Merces, V. (2017). The problem of predicting the size distribution of sediment supplied by hillslopes to rivers. *Geomorphology*, 277:31–49.

Slater, L. J., Singer, M. B., and Kirchner, J. W. (2015). Hydrologic versus geomorphic drivers of trends in flood hazard. *Geophysical Research Letters*, 42(2):370–376.

Slosson, J. R., Hoke, G. D., and Lifton, N. (2022). Non-Steady-State 14C-10Be and Transient Hillslope Dynamics in Steep High Mountain Catchments. *Geophysical Research Letters*, 49(24):1–10.

Snelder, T. H., Lamouroux, N., and Pella, H. (2011). Empirical modelling of large scale patterns in river bed surface grain size. *Geomorphology*, 127(3-4):189–197.

Snyder, N. P., Whipple, K. X., Tucker, G. E., and Merritts, D. J. (2002). Interactions between onshore bedrock-channel incision and nearshore wave-base erosion forced by eustasy and tectonics. *Basin Research*, 14(2):105–127.

Spratt, R. M. and Lisiecki, L. E. (2016). A Late Pleistocene sea level stack. *Climate of the Past*, 12(4):1079–1092.

Sternberg (1875). Untersuchungen uber langen-und Querprofil geschiebefuhrender flusse. *Zeitshrift fur Bauwesen*, 25:483–506.

Stock, J. D. and Montgomery, D. R. (1999). Geologic constraints on bedrock river incision using the stream power law. *Journal of Geophysical Research: Solid Earth*, 104(B3):4983–4993.

Stockamp, J., Bishop, P., Li, Z., Petrie, E. J., Hansom, J., and Rennie, A. (2016). State-of-the-art in studies of glacial isostatic adjustment for the British Isles: A literature review.

Stone, J. O. (2000). isotope production T , T ,. *Journal of Geophysical Research,*, 105(1):753–759.

Stover, S. C. and Montgomery, D. R. (2001). Channel change and flooding, Skokomish River, Washington. *Journal of Hydrology*, 243(3-4):272–286.

Stübner, K., Balco, G., and Schmeisser, N. (2023). RIVERSAND: A NEW TOOL FOR EFFICIENT COMPUTATION OF CATCHMENTWIDE EROSION RATES. *Radiocarbon*, pages 1–14.

Sunamura, T. (2015). Rocky coast processes: with special reference to the recession of soft rock cliffs. *Proceedings of the Japan Academy, Series B*, 91(9):481–500.

Thapa, S., Sinclair, H. D., Creed, M. J., Mudd, S. M., Attal, M., Borthwick, A. G., Ghimire, B. N., and Watson, C. S. (2024). The impact of sediment flux and calibre on flood risk in the kathmandu valley, nepal. *Earth Surface Processes and Landforms*, 49(2):706–727.

Tolman, H. L. (2009). User manual and system documentation of WAVEWATCH III TM version 3.14. *Technical note, MMAB contribution*, 276(220).

Vermeesch, P. (2007). CosmoCalc: An Excel add-in for cosmogenic nuclide calculations. *Geochemistry, Geophysics, Geosystems*, 8(8):1–14.

von Blanckenburg, F. (2005). The control mechanisms of erosion and weathering at basin scale from cosmogenic nuclides in river sediment. *Earth and Planetary Science Letters*, 237(3-4):462–479.

Wacker, L., Fahrni, S. M., Hajdas, I., Molnár, M., Synal, H., Szidat, S., and Zhang, Y. (2013). A versatile gas interface for routine radiocarbon analysis with a gas ion source. *Nuclear Instruments & Methods in Physics Research Section B-beam Interactions With Materials and Atoms*, 294:315–319.

Wells, T., Hancock, G., and Fryer, J. (2008). Weathering rates of sandstone in a semi-arid environment (Hunter Valley, Australia). *Environmental Geology*, 54(5):1047–1057.

Westoby, M. J., Dunning, S. A., Woodward, J., Hein, A. S., Marrero, S. M., Winter, K., and Sugden, D. E. (2015). Instruments and methods: Sedimentological characterization of Antarctic moraines using uavs and Structure-from-Motion photogrammetry. *Journal of Glaciology*, 61(230):1088–1102.

Whipple, K. X. (2002). Implications of sediment-flux-dependent river incision models for landscape evolution. *Journal of Geophysical Research*, 107(B2).

Whipple, K. X., Snyder, N. P., and Dollenmayer, K. (2000). Rates and processes of bedrock incision by the upper ukak river since the 1912 novarupta ash flow in the valley of ten thousand smokes, alaska. *Geology*, 28(9):835–838.

Whipple, K. X. and Tucker, G. E. (1999). Dynamics of the stream-power river incision model: Implications for height limits of mountain ranges, landscape response timescales, and research needs. *Journal of Geophysical Research: Solid Earth*, 104(B8):17661–17674.

Whitaker, A. C. and Potts, D. F. (2007). Analysis of flow competence in an alluvial gravel bed stream, Dupuyer Creek, Montana. *Water Resources Research*, 43(7):1–16.

Whitbread, K., Jansen, J., Bishop, P., and Attal, M. (2015). Substrate, sediment, and slope controls on bedrock channel geometry in postglacial streams. *Journal of Geophysical Research: Earth Surface*, 120:779–798.

Whittaker, A. C. (2012). How do landscapes record tectonics and climate? *Lithosphere*, 4(2):160–164.

Whittaker, A. C., Attal, M., and Allen, P. A. (2010). Characterising the origin, nature and fate of sediment exported from catchments perturbed by active tectonics. *Basin Research*, 22(6):809–828.

Williams, R. D., Lamy, M. L., Maniatis, G., and Stott, E. (2020). Three-dimensional reconstruction of fluvial surface sedimentology and topography using personal mobile laser scanning. *Earth Surface Processes and Landforms*, 45(1):251–261.

Williams, R. D., Measures, R., Hicks, D. M., and Brasington, J. (2016). Assessment of a numerical model to reproduce event-scale erosion and deposition distributions in a braided river. *Water Resources Research*, 52(8):6621–6642.

Wittmann, H. and von Blanckenburg, F. (2009). Cosmogenic nuclide budgeting of floodplain sediment transfer. *Geomorphology*, 109(3-4):246–256.

Wittmann, H., von Blanckenburg, F., Kruesmann, T., Norton, K. P., and Kubik, P. W. (2007). Relation between rock uplift and denudation from cosmogenic nuclides in river sediment in the Central Alps of Switzerland. *Journal of Geophysical Research: Earth Surface*, 112(4):1–20.

Wittmann, H., von Blanckenburg, F., Maurice, L., Guyot, J. L., Filizola, N., and Kubik, P. W. (2011). Sediment production and delivery in the Amazon River basin quantified by in situ-produced cosmogenic nuclides and recent river loads. *Bulletin of the Geological Society of America*, 123(5):934–950.

Wobus, C. W., Crosby, B. T., and Whipple, K. X. (2006). Hanging valleys in fluvial systems: Controls on occurrence and implications for landscape evolution. *Journal of Geophysical Research: Earth Surface*, 111(2):1–14.

Wolinsky, M. A. and Murray, A. B. (2009). A unifying framework for shoreline migration: 2. Application to wave-dominated coasts. *Journal of Geophysical Research: Earth Surface*, 114(F1).

Wolman, M. G. (1954). A method of sampling coarse river-bed material. *Eos, Transactions American Geophysical Union*, 35(6):951–956.

Young, J. A. (1975). Ice wastage in glen Feshie, Inverness-shire. *Scottish Geographical Magazine*, 91(2):91–101.

Young, J. A. (1976). The Terraces of Glen Feshie, Inverness-shire. *Earth and Environmental Science Transactions of The Royal Society of Edinburgh*, 69(22).

Zomer, R. J., Xu, J., and Trabucco, A. (2022). Version 3 of the Global Aridity Index and Potential Evapotranspiration Database. *Scientific Data*, 9(1):1–15.